

UNCLASSIFIED

AD NUMBER: AD0885817

LIMITATION CHANGES

TO:

Approved for public release; distribution is unlimited.

FROM:

Distribution authorized to U.S. Gov't. agencies only; Test and Evaluation; 19 Jul 1971. Other requests shall be referred to the Office of Naval Research, Code 468 (Acoustic Programs), Washington, DC 20360. Export Controlled.

AUTHORITY

29 Aug 1973, ONR ltr

SPERRY RAND

20

CB

AD885817

INTERIM REPORT

ANALYSIS OF ACOUSTIC BAFFLES FOR UNDERWATER NOISE REDUCTION

CONTRACT N00014-67-C-0303 ✓

DDDC RECEIVED JUL 10 1971

Reproduction in whole or in part is permitted for any purpose of the United States Government.

AD No. \_\_\_\_\_ DDC FILE COPY

Prepared for

OFFICE OF NAVAL RESEARCH DEPARTMENT OF THE NAVY WASHINGTON, D.C. 20360

Distribution limited to U.S. Govt. agencies only; Test and Evaluation; 19 JUL 1971 Other requests for this document must be referred to

This document is subject to special export controls and each transmittal to foreign governments or foreign nationals may be made only with prior approval of Office of Naval Research, Acoustics Program (Code 400), Washington, D.C. 20360

SPERRY CYROSCOPE DIVISION GREAT NECK, NEW YORK 11080

SGD-4230-0430 JUNE 1971

ARL, VA-22219

80

INTERIM REPORT

ANALYSIS OF ACOUSTIC BAFFLES  
FOR  
UNDERWATER NOISE REDUCTION

CONTRACT N00014-67-C-0303

Reproduction in whole or in part is permitted for any purpose of the United States Government.

Prepared for

OFFICE OF NAVAL RESEARCH  
DEPARTMENT OF THE NAVY  
WASHINGTON, D.C. 20360

~~This document is subject to special export controls and each transmittal to foreign governments or foreign nationals may be made only with prior approval of Office of Naval Research, Acoustics Program (Code 468), Washington, D.C. 20360~~

SGD-4230 - 0430  
JUNE 1971

SPERRY GYROSCOPE DIVISION  
GREAT NECK, NEW YORK 11020

Distribution limited to U.S. Govt. agencies only. For test and evaluation use only. Other requests for this document must be referred to ARL/Va 22217 19 JUL 1971

UNCLASSIFIED

Security Classification

DOCUMENT CONTROL DATA - R & D		
<i>(Security classification of title, body of abstract and indexing annotation must be entered when the overall report is classified)</i>		
1. ORIGINATING ACTIVITY (Corporate author) Sperry Gyroscope Division Sperry Rand Corporation Great Neck, N.Y., 11020		2a. REPORT SECURITY CLASSIFICATION Unclassified
		2b. GROUP None
3. REPORT TITLE  ANALYSIS OF ACOUSTIC BAFFLES FOR UNDERWATER NOISE REDUCTION		
4. DESCRIPTIVE NOTES (Type of report and inclusive dates) Research Report		
5. AUTHOR(S) (First name, middle initial, last name)  Brian E. Owens, George Rand, Barry Schwartz		
6. REPORT DATE June 1971	7a. TOTAL NO. OF PAGES 69	7b. NO. OF REFS 5
8a. CONTRACT OR GRANT NO. N00014-67-C-0303 ✓	8b. ORIGINATOR'S REPORT NUMBER(S) SGD-4230-0430	
8c. PROJECT NO.	8d. OTHER REPORT NO(S) (Any other numbers that may be assigned this report)	
10. DISTRIBUTION STATEMENT This document is subject to special export controls and each transmittal to foreign governments or foreign persons is made only with the approval of Office of Naval Research, Acoustics Program, Washington, D.C. 20360		
11. SUPPLEMENTARY NOTES	12. SPONSORING MILITARY ACTIVITY Department of the Navy Office of Naval Research Acoustics Programs (Code 468) Washington, D.C. 20360	
13. ABSTRACT  This is an interim report on the study of underwater noise reduction techniques being conducted by the Sperry Division, for the Office of Naval Research, Acoustics Programs, under Contract No. N00014-67-C-0303. Included in this report is a description of the work being done on various types of acoustic baffles. The theoretical analysis of a multilayer cylindrical baffle is given; spring-mass type baffles are analyzed using a lumped-parameter approach. For both of these baffles, good agreement is obtained between analytical and experimental data. Also presented are both theoretical and experimental results of a new baffle material, Sonite, which shows promise of operating at deep depths without the need for pressure compensation.		

UNCLASSIFIED  
Security Classification

KEY WORDS	LINK A		LINK B		LINK C	
	ROLE	WT	ROLE	WT	ROLE	WT
Acoustic baffles Waterborne noise reduction						

DD FORM 1 NOV 68 1473 (BACK)  
(PAGE 2)

UNCLASSIFIED  
Security Classification

## FOREWORD

This is an interim report on the study of underwater noise reduction techniques being conducted by the Sperry Division for the Office of Naval Research, Acoustics Programs, under Contract No. N00014-67-C-0303. Included in this report is a description of the work being done on various types of acoustic baffles. The theoretical analysis of a multilayer cylindrical baffle is given; spring-mass type baffles are analyzed using a lumped-parameter approach. For both of these baffles, good agreement is obtained between analytical and experimental data. Also presented are both theoretical and experimental results of a new baffle material, Sonite, which shows promise of operating at deep depths without the need for pressure compensation.

## TABLE OF CONTENTS

<u>Section</u>		<u>Page</u>
1	INTRODUCTION	1-1
2	MULTILAYER CYLINDRICAL BAFFLES	2-1
	2.1 Introduction	2-1
	2.2 Basic Solutions to the Wave Equation	2-1
	2.3 Boundary Conditions	2-3
	2.4 Numerical Methods	2-5
	2.5 Computer Program	2-7
	2.6 Correlation with Experimental Data	2-12
	2.7 Symbols	2-12
3	SPRING-MASS BAFFLES	3-1
	3.1 Introduction	3-1
	3.2 Transmission Loss Computation	3-2
	3.3 Experimental Data	3-7
4	SONITE	4-1
	4.1 Introduction	4-1
	4.2 Theoretical Considerations	4-1
	4.3 Experimental Investigation	4-3
5	SUMMARY	5-1
6	REFERENCES	6-1

## LIST OF ILLUSTRATIONS

<u>Figure</u>		<u>Page</u>
2-1	Structure of Three-Layer Cylindrical Baffle	2-14
2-2	Structure of Boundary Condition Matrix for a Three-Layer Baffle	2-15
2-3	Comparison of Predicted and Experimental Results of Two-Layer Cylindrical Baffle	2-16
2-4	Predicted and Experimental Hydrophone/Baffle Azimuthal Response at 2500 Hz	2-17
2-5	Predicted and Experimental Hydrophone/Baffle Azimuthal Response at 4500 Hz	2-18
3-1	Insertion Loss Versus Frequency for Various Air Layer Thicknesses	3-8
3-2	Response of a Hydrophone 1.5 Inches in Front of an Air Layer	3-9
3-3	Response of a Hydrophone 1.5 Inches in Front of a Steel Layer	3-10
3-4	Insertion Loss Versus Frequency of Various Steel Layer Thicknesses	3-11
3-5	Response of a Hydrophone 1.5 Inches in Front of a Combined Air/Steel Baffle	3-12
3-6	Spring-Mass Baffle Configuration Under Hydrostatic Pressure	3-13
3-7	Lumped Parameter Model and Equivalent Circuit of Spring-Mass Baffle	3-14
3-8	Converted Equivalent Circuit for Spring-Mass Baffle	3-15
3-9	Plots of Transmission Loss Versus Frequency for Various Spring Constants and Damping Values (3 Sheets)	3-16
3-10	Arrangement of Test Hydrophones	3-19

LIST OF ILLUSTRATIONS (Cont'd)

<u>Figure</u>		<u>Page</u>
3-11	Directivity Pattern of Hydrophone 1 at 2.5 kHz	3-20
3-12	Directivity Pattern of Hydrophone 2 at 2.5 kHz	3-21
3-13	Directivity Pattern of Hydrophone 3 at 2.5 kHz	3-22
3-14	Directivity Pattern of Hydrophone 4 at 2.5 kHz	3-23
3-15	Directivity Pattern of Hydrophone 5 at 2.5 kHz	3-24
3-16	Directivity Pattern of Hydrophone 6 at 2.5 kHz	3-25
3-17	Zero-Degree Beam Pattern, Hydrophones 1 through 6 at 1 kHz	3-26
3-18	Zero-Degree Beam Pattern, Hydrophones 1 through 6 at 2.5 kHz	3-27
3-19	Zero-Degree Beam Pattern, Hydrophones 1 through 6 at 3.5 kHz	3-28
3-20	30-Degree Beam Pattern, Hydrophones 1 through 6 at 2.5 kHz With No Shading	3-29
3-21	30-Degree Beam Pattern, Hydrophones 1 through 6 at 2.5 kHz with 20 dB Shading	3-30
3-22	30-Degree Beam Pattern, Hydrophones 1 through 6 at 2.5 kHz with 30 dB Shading	3-31
3-23	45-Degree Beam Pattern, Hydrophones 1 through 6 at 2.5 kHz With No Shading	3-32
3-24	45-Degree Beam Pattern, Hydrophones 1 through 6 at 2.5 kHz with 20 dB Shading	3-33
4-1	Sonite Test Configuration	4-4
4-2	Relative Hydrophone Response in Presence of Sonite Baffle, Spacing 1-5/8 Inches	4-5
4-3	Relative Hydrophone Response in Presence of Sonite Baffle, Spacing 3-1/4 Inches	4-6
4-4	Comparative Response of Sonite Baffle	4-7

## SECTION 1

### INTRODUCTION

The effectiveness of the acoustic baffle is often a determining factor in the maximum capability of a sonar system. Basically, the baffle is a structure, placed between an unwanted signal or noise source and a sensor, to shield the sensor from the unwanted source. To achieve an array gain consistent with the directivity index of the array, efficient baffle structures must be provided. A further purpose of the baffle is to provide a desired response characteristic for the hydrophone array. Thus, the acoustic baffle is a primary tool for underwater noise reduction and directivity pattern control in sonar arrays.

The transmission of acoustic energy in water can be impeded by a compliant baffle. To be effective, such a baffle must be sufficiently stiff to withstand hydrostatic pressures yet it should be dynamically soft to perform as a highly reflective structure.

A reflective characteristic is acceptable for the side of the baffle facing the interfering noise source, but the portion facing the hydrophone presents a major design challenge. Unless this side is nonreflective, the interaction between the incident signal and the reflected signal from the baffle can alter the hydrophone array's response, often seriously degrading it.

Under the current program, the Sperry Division has developed a set of analytical models for predicting the reflectivity, transmittivity, and other acoustic parameters of planar multilayered baffle structures. This capability extends to the prediction of directivity pattern and response for line hydrophones at any steering angle, including end fire.

The analytical models have been incorporated into a FORTRAN IV computer program which has been described, together with its implementation and built-in plotting routines, in previous interim reports (references 1 and 2). Empirical and theoretical data have been successfully correlated with the results of the computer trials.

Several aspects of baffle technology are discussed in this report. First, the analysis of a multilayer planar baffle was extended to a multilayer cylindrical baffle. As in the planar case, the cylindrical baffle consists of random layers of fluid and elastic media. Secondly, baffle designs based on the use of mechanical springs coupled to masses, which represent a compliant steel plate structure, were also investigated. Lumped parameter models were developed, which were used to calculate insertion loss. Results of studies on a new particulate, fiber-reinforced, ceramic baffle material are presented in Section 4. This material can be fabricated into intricate shapes with conventional techniques and shows promise of operating as an effective baffle at high pressures without requiring pressure compensation.

## SECTION 2

### MULTILAYER CYLINDRICAL BAFFLES

#### 2.1 INTRODUCTION

The analysis of cylindrical baffles is a natural extension of the work done on planar baffles during previous phases of this program. In this section an infinitely long cylinder, with wall composed of layers of various materials, is taken to represent the baffle configuration. A plane wave, parallel to the cylindrical axis, is the excitation (see figure 2-1). An analysis was performed to determine the acoustic pressure at any point outside of the cylinder. With this information, the response of a hydrophone placed outside the baffle, as well as the transmission loss through the baffle, can be computed.

Solution of the wave equation, consistent with the boundary conditions imposed by the multilayer cylinder, forms the basis of the analysis. The fundamental equations for this approach are contained in Section 2.2 of reference 3.

A description of a computer program, which calculates the response of a hydrophone outside the cylindrical baffle, is presented in this section following the theoretical analysis. The results of the program are compared to experimental measurements and are also presented. A list of symbols is included at the end of the section (paragraph 2.7).

#### 2.2 BASIC SOLUTIONS TO THE WAVE EQUATION

The equation of motion for a homogeneous isotropic elastic medium is

$$\rho \ddot{\underline{u}} = (\lambda + 2\mu) \text{grad div } \underline{u} - \mu \text{curl curl } \underline{u} \quad (1)$$

where  $\underline{u}$  is the particle displacement vector,  $\lambda$  and  $\mu$  are constants characteristic of the medium, and  $\rho$  is the density. It can be shown that the most general solution of (1) has the form

$$\underline{u} = \text{grad } P + \text{curl } \underline{Q} \quad (2)$$

where the scalar  $P$  and the vector  $\underline{Q}$  satisfy

$$\rho \ddot{P} = (\lambda + 2\mu) \nabla^2 P \quad (3.1)$$

$$\rho \ddot{\underline{Q}} = \mu \nabla^2 \underline{Q} \quad (3.2)$$

In the case of a fluid,  $\mu$  is set equal to 0 and  $\lambda$  is replaced by the bulk modulus  $k$ .

For the present application, equations (3) may be specialized in two ways. First, motion at a single frequency will be assumed; the components of  $\underline{u}$  will then be complex numbers representing the phase and amplitude of the displacement components along the coordinate axes. The actual physical displacement vector is the real part of  $\underline{u} \exp(-i\omega t)$ . Second, it will be assumed that all components of  $\underline{u}$  are independent of  $z$ , and that the  $z$ -component vanishes identically. These are natural assumptions when considering normal incidence on an infinite cylinder. One may then write

$$\underline{Q} = S \hat{z} \quad (4)$$

$$\text{curl } \underline{Q} = \text{grad } S \times \hat{z}$$

where  $\hat{z}$  is the unit vector in the  $z$  direction. Equations (3) now take the form

$$\nabla^2 P + n^2 P = 0 \quad (5.1)$$

$$\nabla^2 S + m^2 S = 0 \quad (5.2)$$

where the compressional and rotational wave numbers  $n$  and  $m$  are given by

$$n^2 (\lambda + 2\mu) = \omega^2 \rho = m^2 \mu \quad (6)$$

The multilayer cylindrical baffle, with the  $z$  coordinate suppressed, becomes in effect a set of concentric rings. Solutions to equations (5), valid for specific values of  $m$  and  $n$ , can only apply to the zone between two circular boundaries. To facilitate matching the solutions on opposite sides of a boundary, so that continuity of stress and displacement can be maintained, the use of polar coordinates is indicated. Solutions of the form  $P = BR$ , where  $B$  is a function of bearing  $b$  only, and  $R$  depends only on range  $r$ , will be especially useful. Transforming the operator  $\nabla^2$  into polar coordinates, equation (5.1) gives

$$B''/r^2 B + R'/rR + R''/R = -n^2 \quad (7)$$

as the condition for  $B$  and  $R$ .

Since  $B''/B$  in (7) can be expressed as a function of  $r$  only, while in fact it is a function of  $b$  only, it must be a constant. Hence  $B$  must be a linear combination of  $\sin pb$  and  $\cos pb$  for some number  $p$ . Furthermore, when the bearing  $b$  increases by  $2\pi$ , the values of  $B$  must repeat. Thus,  $p$  must be an integer. The condition for  $R$  is then

$$R'' + R'/r + \left[ n^2 - (p/r)^2 \right] R = 0 \quad (8)$$

which requires  $R$  to be a linear combination of  $J_p(nr)$  and  $H_p(nr)$ ; by  $J_p$  is denoted the Bessel function of the first kind, and by  $H_p$  the Hankel function  $H_p(1)$ .

Replacing  $n$  by  $m$  provides solutions  $S$  to equation (5.2). The next step is to form more complex solutions, for both  $P$  and  $S$ , by combining the basic solutions. For instance, letting  $B_p(b)$  denote a linear combination of  $\sin pb$  and  $\cos pb$ , and using  $R_p(x)$  to indicate a linear combination of  $J_p(x)$  and  $H_p(x)$ , the series

$$\sum_{p=0}^{\infty} B_p(b) R_p(kr) \quad (9)$$

will provide a general solution for  $P$  when  $k = n$  and for  $S$  when  $k = m$ .

A solution of the form (9) is required for each zone of constant  $n$  and  $m$ . The constants used in forming the linear combinations  $B_p$  and  $R_p$  must be adjusted to make the solutions match at the boundaries between zones. Section 2.3 discusses how the matching is done.

### 2.3 BOUNDARY CONDITIONS

At the boundaries separating regions of different wave velocities, two types of conditions must be met. First, the stress vector must be continuous across the boundary. Second, the displacement normal to the boundary must be continuous as the boundary is crossed; and in the case of a solid-solid boundary, the tangential displacement must also be continuous (assuming secure bonding of the surfaces).

The stress vector  $\underline{t}$  acting on a surface may be expressed in terms of the displacements by the formula

$$\underline{t} = \underline{a} \cdot \text{div } \underline{u} + \mu \underline{a} \cdot (\nabla \underline{u} + \underline{u} \nabla) \quad (10)$$

where  $\underline{a}$  is the unit normal to the surface. Using polar coordinates and setting  $\underline{a}$  equal to  $\underline{r}$  (the unit vector in the range direction), the stress components normal and tangential to the boundary are

$$\left. \begin{aligned} t_r &= \lambda \text{div } \underline{u} + 2\mu \partial u_r / \partial r \\ t_b &= \mu \left[ (1/r) \partial u_r / \partial b - u_b / r + \partial u_b / \partial r \right] \end{aligned} \right\} \quad (11)$$

where  $u_r$  and  $u_b$  are the displacements normal and tangential to the boundary, respectively.

At the outer boundary, the displacements and stresses must be compatible with the assumed input conditions. In this analysis, an incident plane wave parallel to the cylinder axis is assumed. The displacements in the fluid surrounding the cylinder are thus the sum of an incident plane wave and waves scattered from the cylinder. Assuming that axis  $b=0$  points toward the source of the incident wave, it may be described as

$$\begin{aligned} P_{01} &= \exp(-inr \cos b) \\ &= \sum_0^{\infty} \epsilon_p (-i)^p J_p(nr) \cos pb \end{aligned} \quad (12)$$

where  $\epsilon_p$  equals 2 for positive  $p$  and 1 for  $p=0$ . The scattered waves may be written

$$P_{02} = \sum_0^{\infty} c_p H_p(nr) \cos pb \quad (13)$$

where the coefficients  $c_p$  are to be determined. Note that the scattered waves do not make use of a fully general expansion in the form (9). The function  $R_p$  is restricted to a pure Hankel function so that, for large  $r$ , each term of (13) will correspond to an outgoing circular wave. The function  $B_p$  is restricted to the cosine for symmetry reasons: with the incident wave coming in along the  $b=0$  axis, displacement and stresses normal to the circular boundaries will be even functions of  $b$ , and displacements and stresses tangent to the boundaries will be odd functions of  $b$ . The relations

$$\left. \begin{aligned} u_r &= \partial P / \partial r + (1/r) \partial S / \partial b \\ u_b &= (1/r) \partial P / \partial b - \partial S / \partial r \end{aligned} \right\} \quad (14)$$

and also equation (11), indicate that the functions  $P$  must have even symmetry in  $b$ , while the functions  $S$  must have odd symmetry. In short, the expansions of form (9) for  $P$  and  $S$  have predetermined choices of  $B_p$ ; only  $R_p$  is open to selection. Except for the restriction on the scattered waves, one may generally choose  $R_p$  freely; however, in the innermost zone one must select pure Bessel functions to avoid a pole at the origin.

The entire process of matching displacements and stresses at the boundaries must be carried out separately for each  $p$ , until the terms in (12) become negligible. For a given  $p$ , let  $F$  and  $G$  denote the choices for  $R_p$  in the expansions of  $P$  and  $S$ , respectively; then

$$\left. \begin{aligned} F(r) &= C_{11} J_p(nr) + C_{12} H_p(nr) \\ G(r) &= C_{21} J_p(nr) + C_{22} H_p(nr) \end{aligned} \right\} \quad (15)$$

Substituting  $P = F \cos pb$  and  $S = G \sin pb$  into (14) and (11), and noting that  $\text{div } \underline{u} = -n^2 P$ , gives the  $p^{\text{th}}$  terms in the sine or cosine series for the displacement and stress components. Using capital letters to denote the series coefficients, so that, for instance

$$u_r = \sum_0^{\infty} U_{rp} \cos pb$$

one finds directly that

$$\left. \begin{aligned} U_{rp} &= F' + (p/r) G \\ U_{bp} &= - \left[ G' + (p/r) F \right] \end{aligned} \right\} (16)$$

Some additional calculation shows that the coefficients in the expansions for the stress components are

$$T_{rp} = -\lambda n^2 F + 2\mu F'' + 2\mu (p/r^2) (rG' - G) \quad (17.1)$$

$$T_{bp} = -\mu m^2 G - 2\mu G'' - 2\mu (p/r^2) (rF' - F) \quad (17.2)$$

where (8) has been used to modify equation (17.2).

It is the quantities given in (16) and (17) which must show continuity at the boundaries, with the exception of  $U_{bp}$  in the fluid/solid case. The next step is to represent these displacement and stress coefficients explicitly as linear functions of the constants  $C_{ij}$  appearing in equations (15). This will be done in Section 2.4, where the procedure for solving the equations is discussed.

## 2.4 NUMERICAL METHODS

Upon substituting (15) into (16) and (17) the following explicit formulas are obtained giving the Fourier coefficients of the displacement and stress components. The symbols  $x$  and  $y$  are used for  $nr$  and  $mr$ , respectively.

$$rU_{rp} = x J_p'(x) C_{11} + x H_p'(x) C_{12} + p J_p(y) C_{21} + p H_p(y) C_{22} \quad (18.1)$$

$$-rU_{bp} = p J_p(x) C_{11} + p H_p(x) C_{12} + y J_p'(y) C_{21} + y H_p'(y) C_{22} \quad (18.2)$$

$$\begin{aligned} r^2 T_{rp} &= x^2 \left[ 2\mu J_p''(x) - \lambda J_p(x) \right] C_{11} \\ &+ x^2 \left[ 2\mu H_p''(x) - \lambda H_p(x) \right] C_{12} \\ &+ 2\mu p \left[ y J_p'(y) - J_p(y) \right] C_{21} \\ &+ 2\mu p \left[ y H_p'(y) - H_p(y) \right] C_{22} \end{aligned} \quad (18.3)$$

$$\begin{aligned}
-r^2 T_{bp} &= 2 \mu p \left[ x J_p'(x) - J_p(x) \right] C_{11} \\
&+ 2 \mu p \left[ x H_p'(x) - H_p(x) \right] C_{12} \\
&+ \mu y^2 \left[ 2 J_p''(y) + J_p(y) \right] C_{21} \\
&+ \mu y^2 \left[ 2 H_p''(y) + H_p(y) \right] C_{22}
\end{aligned} \tag{18.4}$$

As previously stated, all the quantities (18) except (18.2) must show continuity at every boundary, and at a solid/solid boundary (18.2) also must show continuity. The meaning of this is that if a quantity such as (18.3) is evaluated on the outer side of a boundary  $r = r_0$  using the physical constants  $\lambda^I, \mu^I, n^I, m^I, x^I = n^I r_0$  and  $y^I = m^I r_0$  pertaining to the outer medium, and the values  $C_{ij}^I$  describing the wave in the outer medium, then the resultant value of (18.3) will be the same as that found on the inner side of the boundary using the physical constants  $\lambda^{II}, \mu^{II}, n^{II}, m^{II}, x^{II} = n^{II} r_0$  and  $y^{II} = m^{II} r_0$  pertaining to the inner medium and the values  $C_{ij}^{II}$  describing the wave in the inner medium.

Thus, at each boundary a set of equations may be set up, expressing the requirements of continuity. The equations may be written

$$\left. \begin{aligned}
(r U_{rp})^I - (r U_{rp})^{II} &= 0 \\
(-r U_{bp})^I - (-r U_{bp})^{II} &= 0 \\
(r^2 T_{rp})^I - (r^2 T_{rp})^{II} &= 0 \\
(-r^2 T_{bp})^I - (-r^2 T_{bp})^{II} &= 0
\end{aligned} \right\} \tag{19}$$

where superscripts I and II indicate evaluation in the outer and the inner medium, respectively. It must be noted, however, that not all the equations are required at every boundary. At a fluid/fluid boundary, only the first and third equations are needed, since the fourth is satisfied automatically when  $\mu = 0$  in both media. At a fluid/solid boundary all but the second are needed, and all are needed at a solid/solid boundary. The number of equations (19) needed to express the continuity requirements can thus be two, three, or four, depending on the type of boundary.

When the continuity equations have been written for all the boundaries, one has a number of simultaneous linear equations. The unknowns are the various  $C_{ij}$  which describe the waves within the various zones of constant velocity. There will always be just enough equations to allow a solution to be found, based on the given values of  $C_{11}$  in the outermost zone. When the equations have been solved for the value of  $C_{12}$  in the outermost zone, all this being for a particular value of  $p$ , the  $p$ th coefficient in the expansion (13) has been calculated. When sufficient coefficients have been determined, the overall displacement potential in the outermost medium may be calculated from

$$P = P_{01} + P_{02}$$

where the notations  $P_{01}$  and  $P_{02}$  refer to (12) and (13), respectively.

The actual rms pressure in the outermost medium equals  $\omega^2 \rho$  times  $0.707 |P|$ .

## 2.5 COMPUTER PROGRAM

This subsection contains an annotated listing of CYLBAF, a program to calculate the response of a multilayer cylindrical baffle to normally incident waves. The program language employed is time sharing FORTRAN.

The principal function of the program is to find the coefficients in the scattered-wave expansion, equation (13). These coefficients form a one-dimensional array C02 in the program: one value for each azimuth harmonic used in the incident-wave expansion, equation (12). (The order of the harmonic is indicated by N in the program, instead of the symbol  $p$  used in the equations.)

To find the scattered-wave coefficient for any N, it is necessary to set up the matrix A showing the combined boundary conditions (18) for all the boundaries present. The structure of the matrix for a baffle of three layers is illustrated in figure 2-2. Each boundary is assigned a number (NCON in the program) of rows, involving the parameters of two adjacent zones. Blocks marked "I" involve the parameters of the zone on the inner side of the boundary, while blocks marked "II" involve the zone on the outer side. Each zone is assigned NCOE columns. Unmarked blocks are zero-filled.

For each marked block, sufficient Bessel functions are computed to allow the coefficients of equation (18) to be calculated. Then, depending on the type of boundary, the proper coefficient values are put into the matrix. When the entire matrix has been filled in this way, it is solved for the scattered-wave coefficient.

Finally, the coefficients are stored on a disc-file. Also, the pressure at various points of interest is calculated and stored on a separate file. Thus, immediate results are available, but also, the stored coefficients may be used to obtain further results at a later time.

## ANNOTATED LISTING OF COMPUTER PROGRAM

```

*CYLBAF: PROGRAM TO CALCULATE RESPONSE OF MULTILAYER CYLINDRICAL
BAFFLE TO NORMALLY-INCIDENT PLANE WAVE. CAN HANDLE UP TO 5 LAYERS.
  DIMENSION IDENT(4),TH(7),D(7),C(7),B(7),LA(7),MU(7),TMU(7),
& NC0E(7),NC0N(6),XSQ(6,2),X(6,2),YSQ(6,2),Y(6,2),BF(5,12,4),
& BV(2,3,4),BVC(3,4),A(23,24),C02(50)
  REAL LA,MU
  COMPLEX BVC,A,C02,C01
  EQUIVALENCE (BV,BVC)
*USE OF BV FACILITATES HANDLING REAL AND IMAGINARY PARTS OF BVC.
  CALL OPENF(1,"CYLDAT")
*'CYLDAT' CONTAINS PHYSICAL PARAMETERS DESCRIBING BAFFLE AND INCIDENT
WAVE. FIRST READ RUN IDENTIFICATION AND NUMBER OF CONSTANT-VELOCITY
ZONES, INCLUDING CORE AND EXTERNAL ZONES.
  READ(1,500) IDENT,NZ0N
  SOOF0RMA(4A3,2X11)
  NBDD= NZ0N-1
*NBDD IS THE NUMBER OF INTERZONE BOUNDARIES. NEXT READ PARAMETERS
FOR EACH ZONE: TH= LAYER THICKNESS (DUMMY VALUE REQUIRED FOR CORE
AND EXTERNAL ZONES), D= DENSITY, C= COMPRESSONAL-WAVE SPEED,
B= ROTATIONAL-WAVE SPEED.
  DO 5 K=1,NZ0N
  READ(1,) T1,T2,T3,T4
*FREE-FIELD F0RMA
  TH(K)= T1
  D(K)= T2
  C(K)= T3
  SB(K)= T4
*READ 0UTER RADIUS OF CYLINDER. READ INCIDENT-WAVE FREQUENCY AND
CONVERT TO RADIANS/SEC.
  READ(1,) R,T1
  0MEGA= FPI(2*T1)
*FOR EACH ZONE COMPUTE LAME PARAMETERS LA AND MU, AND NC0E= NUMBER
OF COEFFICIENTS NEEDED. FOR EACH BOUNDARY COMPUTE SPECIAL SYMBOLS
X AND Y, AND NC0N= NUMBER OF 0ONTINUITY CONDITIONS (EQS 18).
  T2= R
  NC0N(NBDD)= 1
  DO 10 L=1,NZ0N
  K= NZ0N-L+1
  LA(K)= D(K)*C(K)**2 - TMU(K)= 2*MU(K)= D(K)*B(K)**2
  IF(L.EQ.1)GOTO 10
  T1= 0MEGA*T2
  XSQ(K,2)= (X(K,2)= T1/C(K+1))**2
  YSQ(K,2)= (Y(K,2)= T1/B(K+1))**2
*SECOND SUBSCRIPT = 2 FOR 0UTER MEDIUM, = 1 FOR INNER
  XSQ(K,1)= (X(K,1)= T1/C(K))**2
  YSQ(K,1)= (Y(K,1)= T1/B(K))**2

```

```

NC0E(K)= 4
IF(B(K).EQ.0) NC0E(K)= 2
NC0N(K)= NC0N(K) + NC0E(K)/2
*THIS IS INNER-MEDIUM CONTRIBUTION TO NC0N. NOW MAKE OUTER-MEDIUM
CONTRIBUTION FOR NEXT BOUNDARY, AND UPDATE RADIUS.
IF(K.EQ.1)GOTO 10
NC0N(K-1)= NC0E(K)/2
T2= T2-TH(K)
10CONTINUE
*ADJUST NC0E(1) FOR LACK OF HANKEL FUNCTIONS IN CORE ZONE.
NC0E(1)= NC0E(1)/2
*FOR EACH ORDER N, WILL NOW WRITE MATRIX A FOR CONTINUITY CONDITIONS.
FIRST MAKE SURE UNSPECIFIED A-VALUES ARE ZERO.
D0 12 I=1,23
D0 12 J=1,24
12A(I,J)= 0
C01= 1
*CO1 IS COEFFICIENT IN INCIDENT-WAVE EXPANSION (EQ 12).
N= -1
15N= N+1
19M= -1
I0= J0= 1
*I0 AND J0 INDEX UPPER-LEFT ELEMENT OF MATRIX BLOCK. II WILL INDEX
BOUNDARIES, JJ ZONES.
D0 70 II=1,NBDD
D0 65 LL=1,2
*LL= 1 FOR INNER MEDIUM, = 2 FOR OUTER MEDIUM.
JJ= II+LL-1
KK= 2*II+LL-2
*KK IS INDEX FOR BESSEL-FUNCTION VALUES.
IF(N.GT.0)GOTO 30
*FOR N=0 COMPUTE BESSEL FUNCTIONS OF ORDER -2 THROUGH 2.
D0 20 K=3,5
CALL BESS(BF(K,KK,1),BF(K,KK,2),K-3,X(II,LL))
20CALL BESS(BF(K,KK,3),BF(K,KK,4),K-3,Y(II,LL))
D0 25 K=1,4
BF(1,KK,K)= BF(5,KK,K)
25BF(2,KK,K)= -BF(4,KK,K)
GOTO 40
*IF N>0, SHIFT OVER OLD BESSEL FUNCTION VALUES AND COMPUTE NEW
FUNCTIONS, OF ORDER N+2.
30D0 35 K=1,4
D0 35 L=1,4
35BF(K,KK,L)= BF(K+1,KK,L)
CALL BESS(BF(5,KK,1),BF(5,KK,2),N+2,X(II,LL))
CALL BESS(BF(5,KK,3),BF(5,KK,4),N+2,Y(II,LL))

```

```

40SIGN= 3-2*LL
*THIS IS THE CENTRAL (MINUS) SIGN IN EQS 19. NOW FORM SIGNED J- AND
H-FUNCTIONS, TOGETHER WITH FIRST AND SECOND DERIVATIVES, FROM
THE J- AND Y- FUNCTION VALUES BF.
D0 50 K=2,4,2
D0 45 L=1,2
*HANKEL FUNCTIONS FIRST.
I= K+L-2
BV(L,1,K)= SIGN*BF(3,KK,1)
BV(L,2,K)= .5*SIGN*(BF(2,KK,1)-BF(4,KK,1))
45BV(L,3,K)= .25*SIGN*(BF(1,KK,1)-2*BF(3,KK,1)+BF(5,KK,1))
*THEN J-FUNCTIONS.
D0 50 J=1,3
50BVC(J,K-1)= BV(1,J,K)
*NOW FILL IN A MATRIX BLOCK. IBM= 1 FOR II= LL= 1, WHEN H-FUNCTIONS
FORBIDDEN. AFTER THAT IBM STAYS = 2.
IBM= (IBM+3)/2
D0 55 IB=1,IBM
*IB= 1 FOR J-FUNCTION COEFFICIENT, = 2 FOR H-FUNCTION COEFFICIENT.
J= JO+IB-1
*COMPRESSIONAL-WAVE COEFFICIENTS, EQS 18.1 AND 18.3:
A(IO,J)= X(II,LL)*BVC(2,IB)
A(IO+1,J)= XSQ(II,LL)*(TMU(JJ)*BVC(3,IB)-LA(JJ)*BVC(1,IB))
IF(NC0N(II).EQ.2)G0T055
*COMPRESSIONAL-WAVE COEFFICIENTS, EQ 18.4:
A(IO+2,J)= TMU(JJ)*N*(X(II,LL)*BVC(2,IB)-BVC(1,IB))
IF(NC0N(II).EQ.3)G0T0 55
*COMPRESSIONAL-WAVE COEFFICIENTS, EQ 18.2:
A(IO+3,J)= N*BVC(1,IB)
55CONTINUE
IF(B(JJ).EQ.0)G0T0 65
*NOW ROTATIONAL-WAVE COEFFICIENTS, IF ANY.
D0 60 IB=1,IBM
J= JO+IB-1+IBM
*EQS 18.1 AND 18.3:
A(IO,J)= N*BVC(1,IB+2)
A(IO+1,J)= TMU(JJ)*N*(Y(II,LL)*BVC(2,IB+2)-BVC(1,IB+2))
IF(NC0N(II).EQ.2)G0T0 60
*EQ 18.4:
A(IO+2,J)= YSQ(II,LL)*(TMU(JJ)*BVC(3,IB+2)+MU(JJ)*BVC(1,IB+2))
IF(NC0N(II).EQ.3)G0T0 60
*EQ 18.2:
A(IO+3,J)= Y(II,LL)*BVC(2,IB+2)
60CONTINUE
*UPDATE JO IN PASSING FROM INNER TO OUTER MEDIUM.
65JO= JO + (2-LL)*NC0E(II)
70IO= IO + NC0N(II)

```

```

*ALL MATRIX ENTRIES HAVE BEEN COMPUTED. INTERCHANGE LAST TWO
COLUMNS OF A, AND MULTIPLY (NEW) LAST COLUMN BY -C01.
  KK= 10-NC0N(NBDD)
  LL= 10-1
  D0 75 I=KK,LL
  @1= A(I,J0-1)
  A(I,J0-1)= -C01*A(I,J0-2)
  75A(I,J0-2)= @1
*NOW SOLVE MATRIX FOR SCATTERED-WAVE COEFFICIENT C02 (EQ 13).
  CALL SOLV(A,I0-1,C02(N+1))
*UPDATE C01 AND TEST FOR EXHAUSTION OF INCIDENT-WAVE EXPANSION.
  IF(N.GT.0)G0T0 80
  C01= 2
  80C01= C01*CMPLX(0.,-1.)
  IF(ABS(BF(3,2*NBDD,1))+ABS(BF(4,2*NBDD,1))+ABS(BF(5,2*NBDD,1))
&.GT.1E-5)G0T0 15
*CALCULATION OF SCATTERED-WAVE COEFFICIENTS COMPLETE. STORE THEM
FOR FUTURE USE.
  CALL OPENF(2,"CYLC0E")
  I= N+1
  WRITE(2,505) IDENT,I
  505FORMAT(4A3,":",I4," COEFFICIENTS")
  D0 85 J=1,I
  @1= C02(J)
  85WRITE(2,510) @1
  510FORMAT(2E17.10)
*IF IMMEDIATE PRESSURE READINGS ARE DESIRED, TAKE LOCATIONS FOR
READINGS FROM "CYLL0C" AND PUT VALUES INTO "CYLVAL".
  CALL OPENF(3,"CYLL0C")
  CALL OPENF(4,"CYLVAL")
  FACT0R= SQRT(.5)*D(NZ0N)*@MEGA**2
  WRITE(4,515) IDENT
  515FORMAT("VALUES FOR ",4A3)
  90READ(3,,END=999) GAP,ANGLE
  T1= (R+GAP)*@MEGA/C(NZ0N)
  T2= FPI(ANGLE/180)
  T3= -T1*C0S(T2)
*INCIDENT-WAVE POTENTIAL:
  @1= CMPLX(C0S(T3),SIN(T3))
*ADD TERMS OF SCATTERED-WAVE POTENTIAL TO GET TOTAL POTENTIAL.
  D0 95 J=0,N
  CALL BESS(T3,T4,J,T1)
  95@1= @1 + C02(J+1)*CMPLX(T3,T4)*C0S(J*T2)
*COMPUTE AND STORE PRESSURE VALUE.
  T1= FACT0R*CABS(@1)
  WRITE(4,520) GAP,ANGLE,T1
  520FORMAT(F7.2,F6.0,E14.6)
*GO BACK AND READ NEXT LOCATION.
  G0T0 90

*DESCRIPTION OF SUBROUTINES:
SUBROUTINE BESS(B1,B2,K,X) COMPUTES BESSEL FUNCTION B1 OF FIRST KIND
AND B2 OF SECOND KIND FOR ARGUMENT X AND ORDER K.
SUBROUTINE SOLV(A,K,X) TAKES THE FIRST K ROWS AND K+1 COLUMNS OF A
AND APPLIES ROW OPERATIONS TO MAKE A(I,J)=0 FOR I>J AND A(I,I)=1.
THEN X= A(K,K+1).
  999END

```

## 2.6 CORRELATION WITH EXPERIMENTAL DATA

Figure 2-3 shows a comparison between the computer program prediction and experimental results on a two-layer cylindrical baffle consisting of 5/8-inch thick steel and 1/2-inch thick RAL. Good agreement exists between 2 and 8 kHz; below 2 kHz, the theory deviates from the experimental results but this is believed due to limitations in certain subroutines of the program which will be improved in the future.

Figures 2-4 and 2-5 show the predicted and experimental azimuthal responses of a hydrophone in front of the same baffle as in figure 2-3 for frequencies of 2500 Hz and 4500 Hz, respectively. The correlation is excellent. Additional comparisons of this type are necessary, however, before a proper evaluation of the program can be made.

## 2.7 SYMBOLS

$\underline{a}$	Unit vector normal to a surface
$b$	Bearing coordinate in polar system $r, b, z$
$B, B_p$	Function of $b$ only
$c_p$	Coefficient in scattered-wave expansion
$C_{11}, C_{12}, C_{21}, C_{22}$	Coefficients in expansion of $F$ and $G$ (equation 15)
$F$	Choice of $R_p$ for compressional waves
$G$	Choice of $R_p$ for rotational waves
$H_p = H_p^{(1)}$	Hankel function of order $p$
$J_p$	Bessel function of first kind and order $p$
$k$	Bulk modulus
$\lambda, \mu$	Lame elastic constants
$m$	Rotational wave number
$n$	Compressional wave number
$\omega$	Angular frequency of sound wave
$P$	Compressional-wave potential
$P_{01}, P_{02}$	Incident and scattered wave potentials
$\underline{Q}$	Vector potential for rotational waves
$r$	Range coordinate in polar system $r, b, z$
$\hat{r}$	Unit vector in range direction
$R, R_p$	Function of $r$ only
$\rho$	Density

$S$	Scalar potential for rotational waves
$t$	Time
$\underline{t}$	Stress vector
$t_r, t_b$	Stress components in radial and tangential directions
$T_{rp}, T_{bp}$	Fourier coefficients of $t_r$ and $t_b$
$\underline{u}$	Displacement vector
$u_r, u_b$	Displacement components in radial and tangential directions
$U_{rp}, U_{bp}$	Fourier coefficients of $u_r$ and $u_b$
$x = nr$	
$y = mr$	
$Z$	Axial coordinate in polar system $r, b, z$
$\hat{Z}$	Unit vector in axial direction

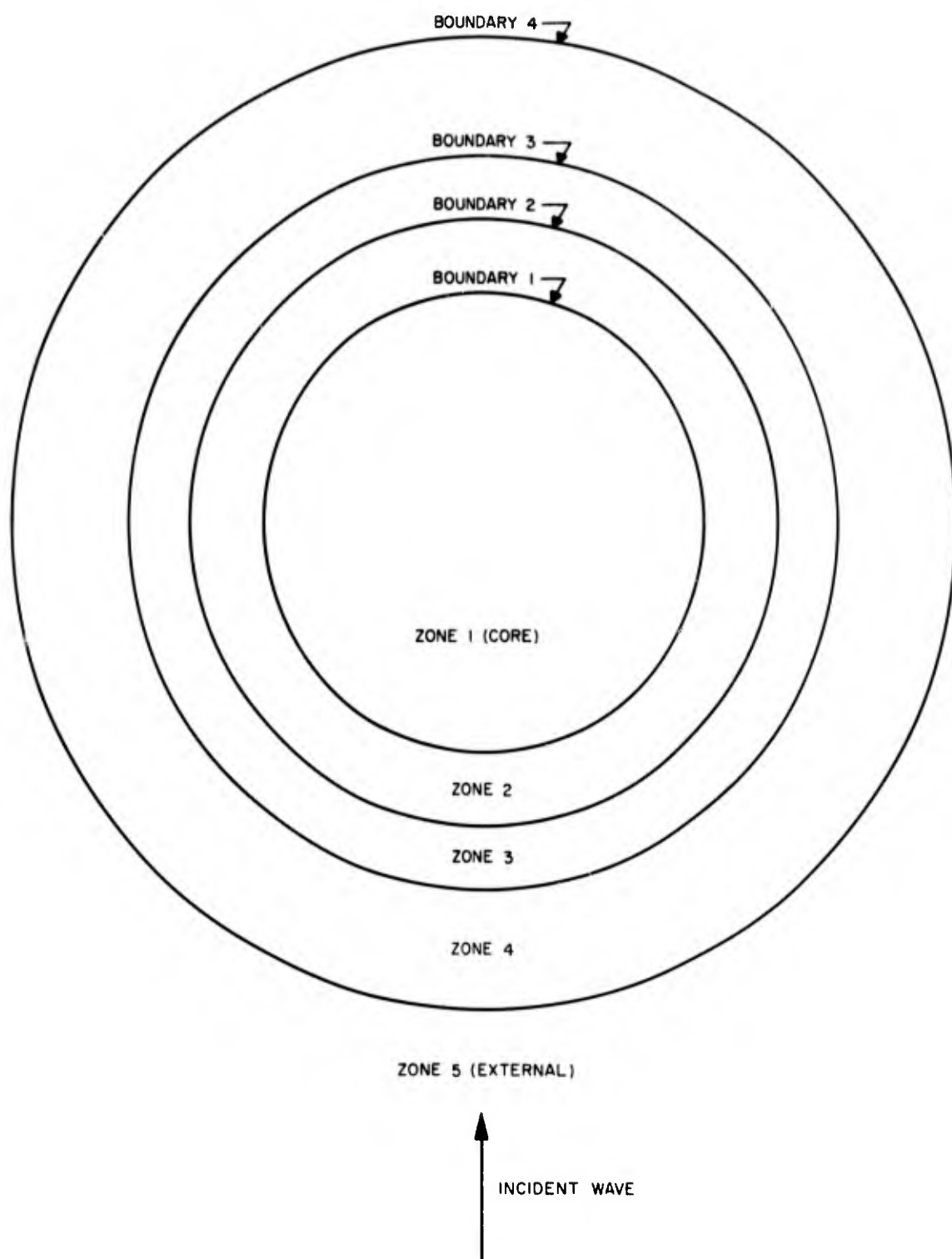


Figure 2-1. Structure of Three-Layer Cylindrical Baffle

	ZONE 1	ZONE 2	ZONE 3	ZONE 4	ZONE 5
BOUNDARY 1	I	H			
BOUNDARY 2		I	H		
BOUNDARY 3			I	H	
BOUNDARY 4				I	H

Figure 2-2. Structure of Boundary Condition Matrix for a Three-Layer Baffle

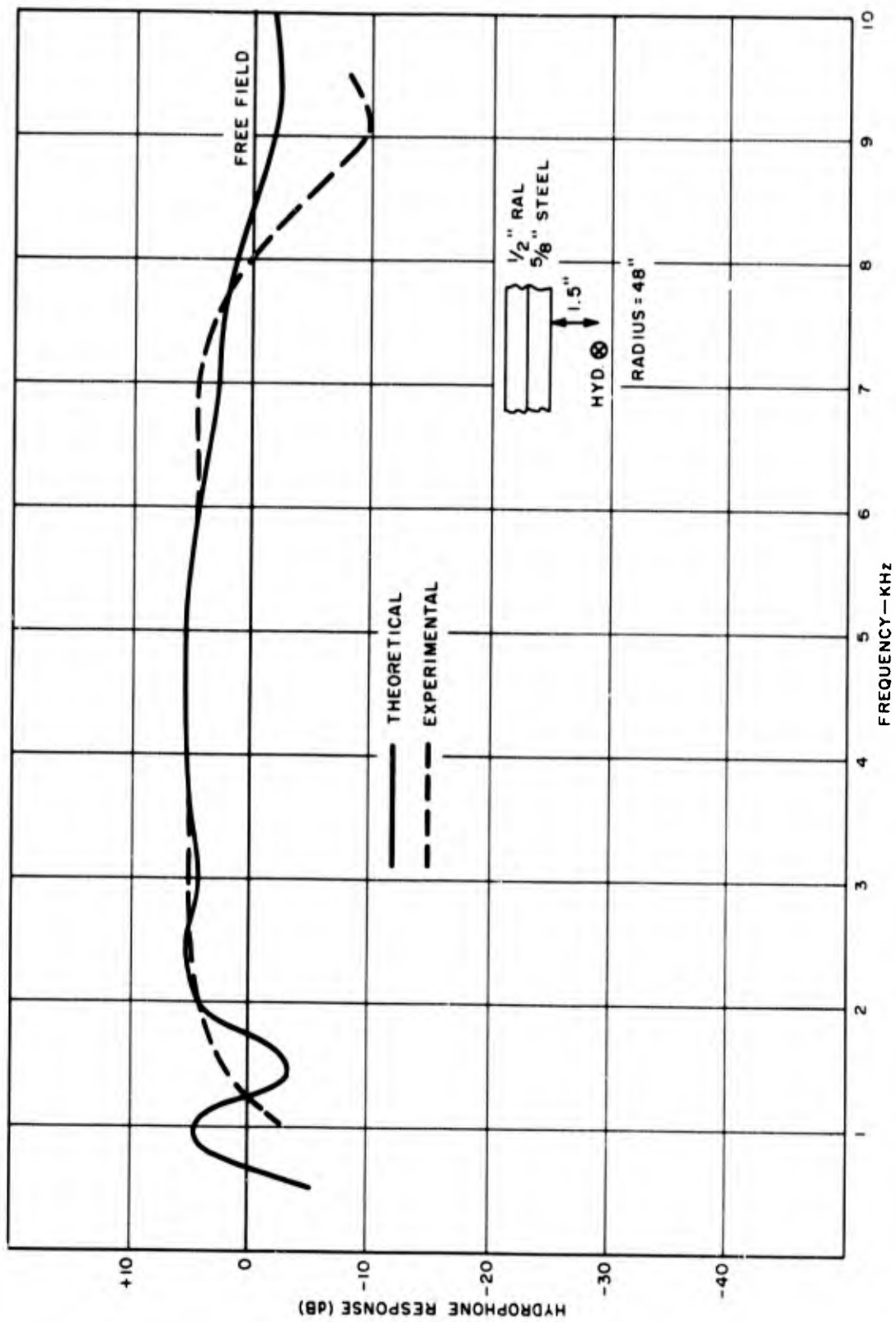
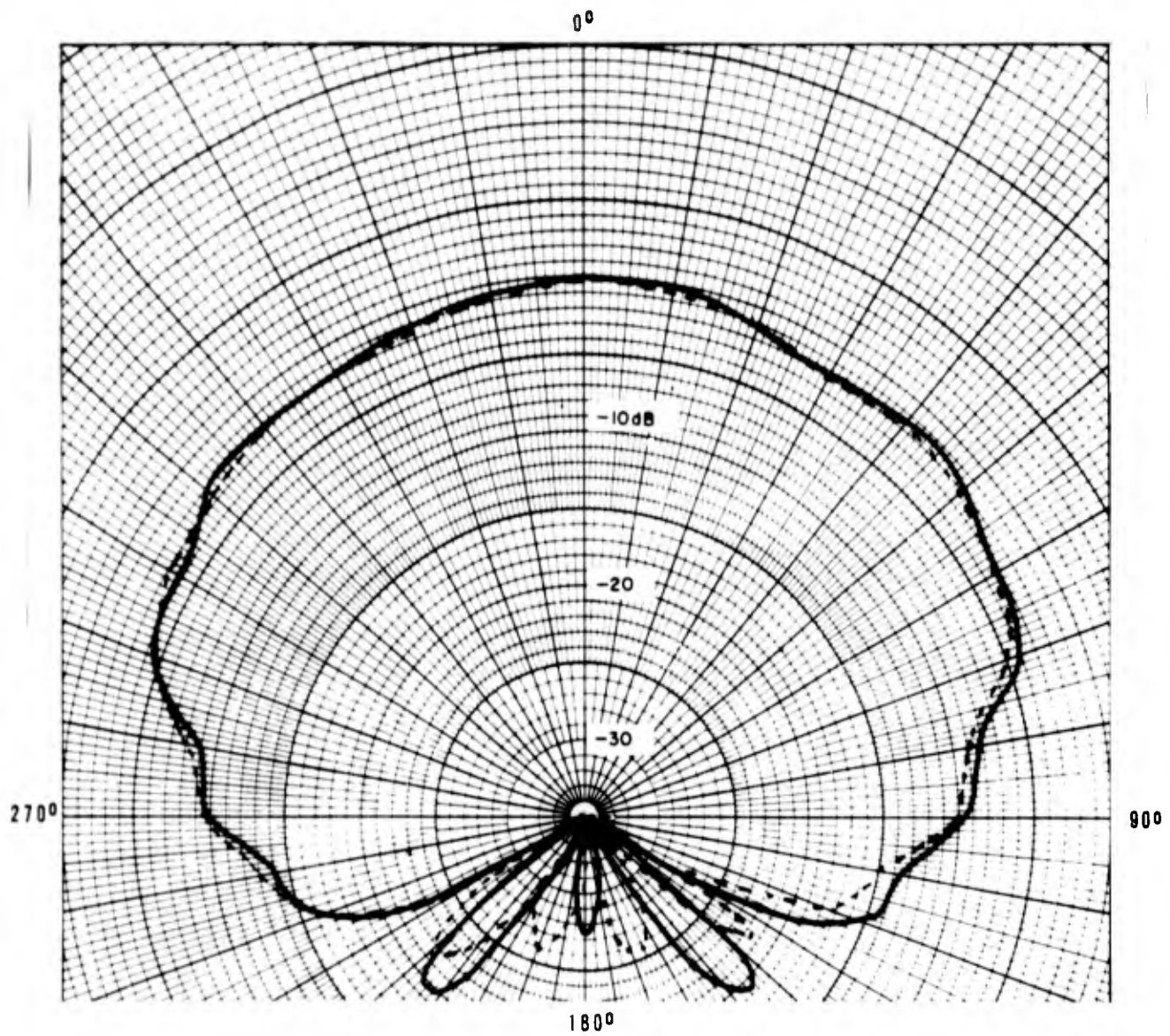


Figure 2-3. Comparison of Predicted and Experimental Results of Two-Layer Cylindrical Baffle



$f = 2500 \text{ Hz}$

**BAFFLE**

RADIUS = 48"

$\frac{5}{8}$ " STEEL OUTSIDE

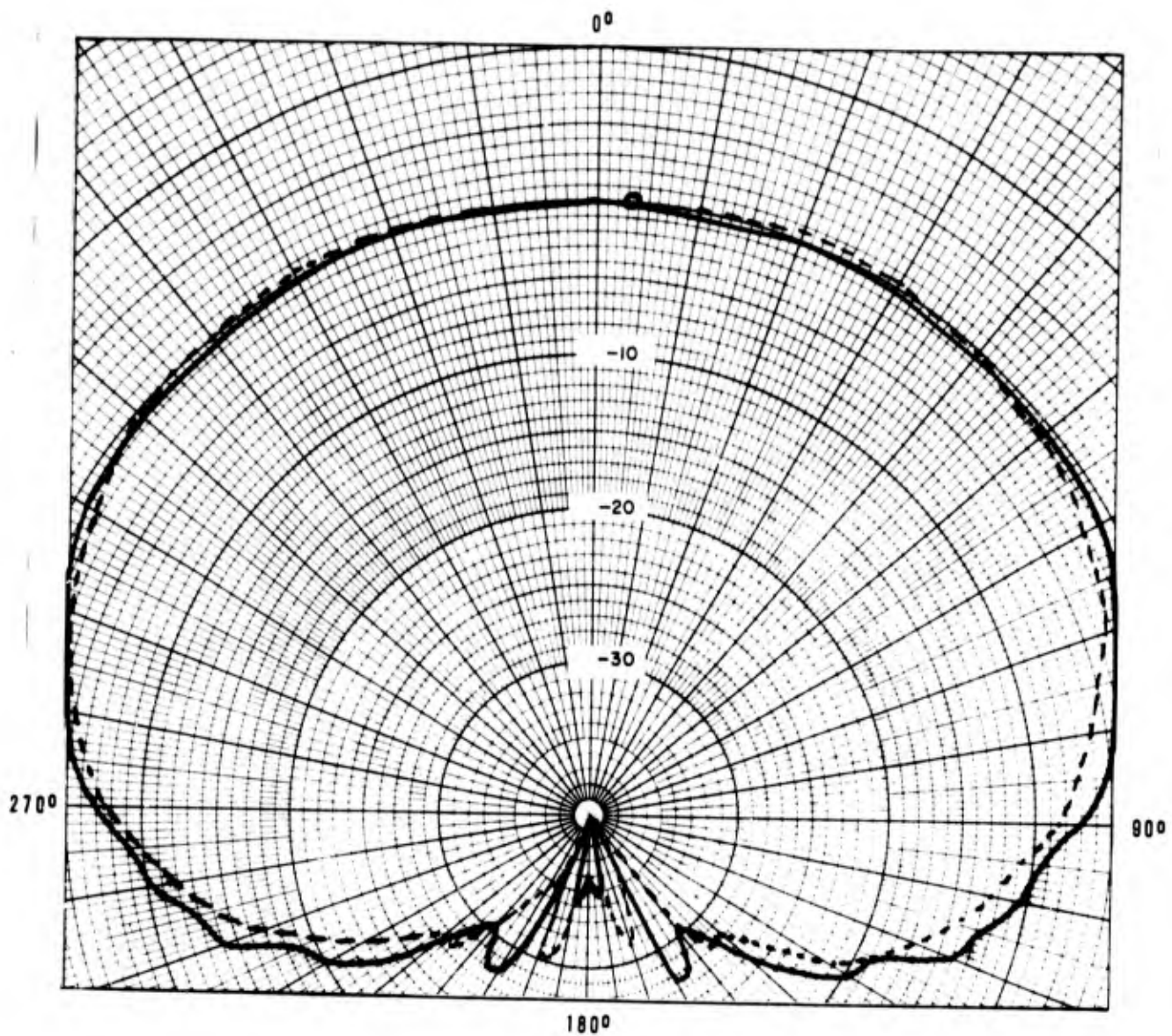
$\frac{1}{2}$ " RAL INSIDE

$1\frac{1}{2}$ " HYDROPHONE SPACING

————— THEORY

----- EXPERIMENT

Figure 2-4. Predicted and Experimental Hydrophone/Baffle Azimuthal Response at 2500 Hz



$f = 4500 \text{ Hz}$   
**BAFFLE**  
 RADIUS = 48"  
 5/8" STEEL OUTSIDE  
 1/2" RAL INSIDE  
 1 1/2" HYDROPHONE SPACING

——— THEORY  
 - - - - EXPERIMENT

Figure 2-5. Predicted and Experimental Hydrophone/Baffle Azimuthal Response at 4500 Hz

## SECTION 3

### SPRING-MASS BAFFLES

#### 3.1 INTRODUCTION

An efficient approach to preventing transfer of acoustic energy from one point in water to another point is to use a layer of material which is more compliant than water. Air is an excellent material for this purpose, as shown in figure 3-1, where the insertion loss as a function of frequency for various air thicknesses is plotted. The curve shows maximum insertion loss at  $\lambda/4$ , while complete transmission corresponds to multiples of a half wavelength of thickness.

The response of a hydrophone in front of this compliant layer must also be considered. Figure 3-2 shows the response of a hydrophone 1.5-inches in front of an air layer. A severe loss in response, compared to free field, occurs in the important frequency band of 1 to 3 kHz due to the 180 degree phase shift when sound is reflected from the compliant layer. One solution to this problem is to place a stiff material, such as steel, between the baffle and the hydrophone. When steel is used alone, as shown in figure 3-3, the hydrophone response improves considerably. However, the insertion loss of steel alone is low, as shown in figure 3-4. The combination of compliant baffle and the steel has only a small affect on the response as shown in figure 3-5, while still providing a high insertion loss.

In practice, an air layer by itself cannot be used as an acoustic baffle for sonar applications because of the pressure requirements. On a submarine the air layer would compress at a moderate depth and would then be useless. It is possible to build a pressure-compensated air baffle in which an arrangement is made to keep the air inside at the same pressure as the water outside; however, such designs are usually complex and unreliable. The goal is to build a baffle which is statically stiff so that it can withstand the hydrostatic pressure and yet dynamically soft so that it provides the required insertion loss.

A promising approach is through the use of spring-mass baffles which consist of a sealed assembly of plates simulating springs with the outside plates behaving as masses. This section reviews spring-mass baffle design parameters and presents the results of experimental investigations utilizing full scale baffle samples.

### 3.2 TRANSMISSION LOSS COMPUTATION

The configuration of an uncompensated spring-mass baffle developed by Sperry is shown in figure 3-6. The assembly utilizes two hardened steel inner plates in a diaphragm mode as springs to provide high compliance. A matrix of steel pins, located on each side of the two inner plates in a staggered orientation, transforms water pressure loads from the outer plates into concentrated loads on the inner plates. This arrangement produces diaphragm-type inner plate deflections in the form of contiguous circles in each inner plate. Each circle is the result of the load from a pin on one side of one of these plates being resisted by the pins on the opposite side of the same plate. The pins, held in place by square rubber pads, fit tightly into undersized holes in the pads, which are cemented to the steel plates. The top outer plate is supported from the bottom outer plate by a perimeter rubber gasket cemented to these plates.

Under increasing static pressure, the inner and outer plates deflect; the outer plate deflections are at least an order of magnitude smaller than the inner plate deflections, both because the outer plates receive a distributed pressure load as compared to the concentrated loads from the pins on the inner plates, and because the outer plates are 1/4-inch thick as compared to the 1/8-inch thick inner plates.

The lumped-parameter model of the spring-mass baffle is shown in figure 3-7(a). In this figure, the transmitted pressure is denoted by  $P_T$  and the total pressure at the incident face is denoted by  $P_O$ . The total pressure is composed of the incident pressure  $P_I$  and the reflected pressure  $P_R$ ; as follows:

$$P_O = P_I + P_R$$

All pressures and velocities are assumed to have a complex exponential time dependence. Thus, for example, the actual physical incident-wave pressure is the real part of  $P_I e^{-i\omega t}$ , where  $\omega$  is the angular frequency of the incident wave.

Let  $v_1$ ,  $v_2$ , and  $v_3$  denote the velocities of the left-hand, center and right-hand masses in figure 3-7(a). The equations of motion are

$$-i\omega M v_1 = P_O + iK (v_2 - v_1)/\omega$$

$$-i\omega m v_2 = iK (v_1 - 2v_2 + v_3)/\omega$$

$$-i\omega M v_3 = iK (v_2 - v_3)/\omega - P_T$$

where  $M$  and  $m$  are the masses per unit area of the outer and inner plates, respectively, and  $K$  is the slope of the baffle pressure/displacement curve. By interpreting pressure as voltage and velocity as current, the equations of motion may be viewed as describing an electrical circuit equivalent in behavior to the mechanical system.

The equivalent circuit for the baffle model is shown in figure 3-7(b). The impedances are given by

$$Z_M = -j\omega M$$

$$Z_m = -j\omega m$$

$$Z_K = jK/\omega$$

The effect of damping in the springs and rubber pads of the baffle may be recognized by using complex values of  $K$ , or more explicitly, by

$$Z_K = L + jK/\omega$$

where  $L$  is the effective viscosity of the spring/pad combination.

By converting the interior  $\pi$ -section of figure 3-7(b) into an equivalent T-section, the equivalent circuit for the baffle is converted into the form shown in figure 3-8(a), where

$$Z_A = Z_M + Z_m Z_K / (Z_m + 2 Z_K)$$

$$Z_B = (Z_K)^2 / (Z_m + 2 Z_K)$$

When the baffle is immersed in water and subjected to an incident wave of pressure  $P_I$ , the pressure/velocity relations for plane progressive waves incident upon and/or radiated from the baffle surfaces must be included. At the right-hand surface pure radiation exists, for which

$$P = P_T e^{i\omega x/c}$$

where  $c$  is the speed of sound in water and  $x$  is measured from the right-hand surface.

At the left-hand surface, both incident and reflected waves exist, so that

$$P = P_I e^{i\omega x/c} + P_R e^{-i\omega x/c}$$

where  $x$  is measured from the left-hand surface.

A water particle is subject to the general law of motion

$$\partial P / \partial x = -\rho \partial v / \partial t$$

which implies that  $P = \rho cv$  for waves moving to the right and  $P = -\rho cv$  for waves moving to the left. The quantity  $\rho c$  is the characteristic impedance of water. Hence,  $P_T$  may be eliminated from the equations of motion by the substitution

$$P_T = \rho cv_3 \quad (20)$$

On the left-hand surface, the following exists

$$\rho cv = P_I e^{i\omega x/c} - P_R e^{-i\omega x/c}$$

so that by setting  $x = 0$  in the equations for the left-hand surface, the following is obtained:

$$P_O = P_I + P_R$$

$$\rho cv_1 = P_I - P_R$$

from which is obtained

$$P_O = 2P_I - \rho cv_1 \quad (21)$$

Adjoining (20) and (21) to the equations of motion shows that the operation is equivalent to the circuit shown in figure 3-8(b), where  $Z_C$  is the characteristic impedance of water.

Simple circuit-analysis techniques show that the transmission loss is given by

$$TL = 20 \log |P_I/P_T|$$

where

$$P_I/P_T = (Z_A + Z_C)(Z_A + 2Z_B + Z_C)/(2Z_B Z_C)$$

Once appropriate values of  $M$ ,  $m$ ,  $K$  and  $L$  have been chosen, computer program BAF, which is listed on the following pages, plots TL against frequency.

For the Sperry baffle,  $M$  and  $m$  are 0.00022 and 0.000072 mass units/in<sup>2</sup>, respectively.  $K$  varies from 100 lb/in<sup>3</sup> at shallow depths to about 3000 lb/in<sup>3</sup> at 700 feet, while  $L$  lies in the range 0.2 to 0.4 lb-sec/in<sup>3</sup>. Figure 3-9 (Sheets 1 through 3) show TL versus frequency for a number of spring constants and damping values ( $A\phi M = M$ ,  $AIM = m$ ,  $AK = K$ ,  $AL = L$ ).

Experimental data on a spring-mass type of baffle has shown good agreement with the theoretical calculations over the low frequency band (approximately 0.5 to 3 kHz). At higher frequencies, the theory predicts larger transmission loss than measured. Also, the measurements show a peak and a null in the transmission loss curve which is an indication that the baffle thickness becomes equivalent to one-quarter and one-half wavelength at certain frequencies. When this occurs, a distributed parameter model is required. The spring-mass type of baffle becomes an appreciable part of a wavelength at even relatively low frequencies because the speed of sound through such a baffle is much lower than that through water. Experimental measurements indicate the velocity through the baffle is only one-sixth that of water.

LISTING OF COMPUTER PROGRAM TO COMPUTE  
TRANSMISSION LOSS OF SPRING-MASS BAFFLES

```

00100 PROGRAM BAF(INPUT,OUTPUT,TAPE1,TAPE6)
00110 DIMENSION DB(70),FMTS(8,2),FORM(5),LINE(72),F(3,2)
00120 DATA PI,RC/3.14159,5.84/
00130 COMPLEX Z1,Z2,Z3
00140 PRINT, *WHAT MODE, MATE*,
00150 READ, MODE
00160 DATA F/1000.,200.,10000.,5.,5.,200./
00170 REWIND 1 $ REWIND 6
00180 WRITE(6,500)
00190 500FORMAT(4H----)
00200 10READ(1,510) A0M,AIM,NUMKL $ IF(EOF,1) 110,15
00210 510FORMAT(4X2F10/4X15)
00220 1500 100 KL=1,NUMKL
00230 READ(1,520) AK,AL
00240 520FORMAT(4X2F10)
00250 I= 1 $ FREQ= F(1,MODE)
00260 20T1= 2.*PI*FREQ
00270 Z1= CMPLX(0.,-T1*AIM)
00280 Z2= CMPLX(AL,AK/T1)
00290 Z3= Z2/(Z1+Z2+Z2)
00300 Z1= CMPLX(0.,-T1*A0M)+Z1*Z3
00310 Z2= Z2*Z3
00320 GOT0(30,40) MODE
00330 30Z1= Z1+RC
00340 DB(I)= -1000.+AINT(1000.5+20.*ALOG10(CABS(Z1*(Z1+Z2+Z2)
00350+ /(2.*RC*Z2))))
00360 GOT0 50
00370 40DB(I)= -1000.+AINT(1000.5+20.*ALOG10(CABS(Z2/(Z1+Z2))))
00380 50I= I+1 $ FREQ= FREQ+F(2,MODE)
00390 IF(FREQ.LT.F(3,MODE)+.5*F(2,MODE)) GOT0 20
00400*WRITE PLOT HEADING
00410 DATA FMTS/
00420+ 50H(///5X30HTRANSMISSION LOSS VS FREQUENCY ),
00430+ 30H(/4H(DB),13,915,7H (KHZ) ),
00440+ 50H(///5X26HVELOCITY GAIN VS FREQUENCY ),
00450+ 30H(/4H(DB),13,815,6H (HZ) )/
00460 ENCODE(50,600,FORM) (FMTS(1,MODE),I=1,5)
00470 600FORMAT(5A10)
00480 WRITE(6,FORM)
00490 WRITE(6,610) A0M,AIM,AK,AL
00500 610FORMAT(/7X,4HA0M=,F8.6,7H AIM=,F8.6,/7X4HAK =,
00510+ F7.0,8H AL =,F7.2)
00520 ENCODE(30,600,FORM) (FMTS(1,MODE),I=6,8)
00530 I= 2-MODE $ J= 190*MODE-180 $ K= 24*MODE-23
00540 WRITE(6,FORM) (L,L=I,J,K)

```

```

00550*FIND DB RANGE
00560     DBMAX= DB(1) $ DBMIN= DB(1)
00570     I= 1.5 + (F(3,MØDE)-F(1,MØDE))/F(2,MØDE)
00580     DØ 60 J=2,I
00590     DBMAX= AMAX1(DBMAX,DB(J))
00600     60DBMIN= AMIN1(DBMIN,DB(J))
00610*PLØT
00620     T1= DBMAX
00630     70LINE(1)= 6H
00640     IF(AMØD(T1,5.).NE.0.) GØTØ 80
00650     ENCØDE(5,620,LINE) T1
00660     620FØRMAT(F5.0)
00670     80DØ 90 J=1,I
00680     LINE(J+1)= 1H
00690     IF(AMØD(T1,5.)*MØD(J+MØDE-2,5).EQ.0.) LINE(J+1)= 1H.
00700     90IF(T1.EQ.DB(J)) LINE(J+1)= 1H*
00710     WRITE(6,640) LINE(1),(LINE(L+1),L=1,I)
00720     640FØRMAT(A6,71A1)
00730     T1= T1-1.
00740     IF(T1.GE.DBMIN) GØTØ 70
00750     100CONTINUE
00760     GØTØ 10
00770     110WRITE(6,650)
00780     650FØRMAT(///4H----)
00790     ENDFILE 6 $ REWIND 6
00800     END

```

### 3.3 EXPERIMENTAL DATA

Data obtained from tests of a spring-mass baffle and associated hydrophone array are presented in this section. The array tested consisted of a 6 by 6 ft, 1-1/2-inch thick, steel plate in which the hydrophones were mounted, a 1-1/2-inch thick rubber sheet bonded to the front of the plate, and the spring-mass baffles placed behind the hydrophones. The test array contained 23 hydrophones located on the steel plate as shown in figure 3-10.

The following tests were performed:

- Single element receiving response
- Single element directivity patterns
- Sum-difference patterns
- Steered beams.

Tests were conducted at depths of 100, 400, and 700 feet. Of the large number of test runs made, some representative samples showing the baffle performance have been selected. Figures 3-11 through 3-16 show the single element directivity patterns of hydrophones 1 through 6 (see figure 3-10), which are located across the array, at 2.5 kHz. It is interesting to observe how the patterns for hydrophones near the center of the array (3 and 4) are symmetrical while those at the edges (1 and 6) show a definite filling in of the pattern. This can be explained by noting that the hydrophones mounted near the array edge do not get the full effect of the baffle. These patterns were taken at a depth of 400 feet and show a front-to-back ratio of 15 to 20 dB.

Figures 3-17 through 3-19 show broadside beam patterns formed by summing the outputs of hydrophones 1 through 6 at 1, 2.5, and 3.5 kHz. The theoretical beam patterns are superimposed on the measured data. Agreement between theory and experiment is excellent in the forward-looking direction. The presence of the baffle reduces the rear response by a factor of better than 20 dB. Depth for these tests was 100 feet.

Figures 3-20 through 3-24 show steered beam patterns at 30 degrees and 45 degrees with and without shading. Hydrophones 1 through 6 were steered using delay lines; shading was added by switching in resistive attenuators; depth was 700 feet. Theoretical patterns, calculated assuming free field hydrophones, are also shown. Agreement is good for the forward looking direction. For the broadside beams, the baffle attenuates the second main beam by more than 20 dB.

The results of these tests indicate that the spring-mass baffle is capable of effective performance over a wide range of frequencies and hydrostatic pressures. These baffles require no external pressure compensation and can be designed to be relatively light and thin. The baffles are highly compliant, thus providing large transmission loss values.

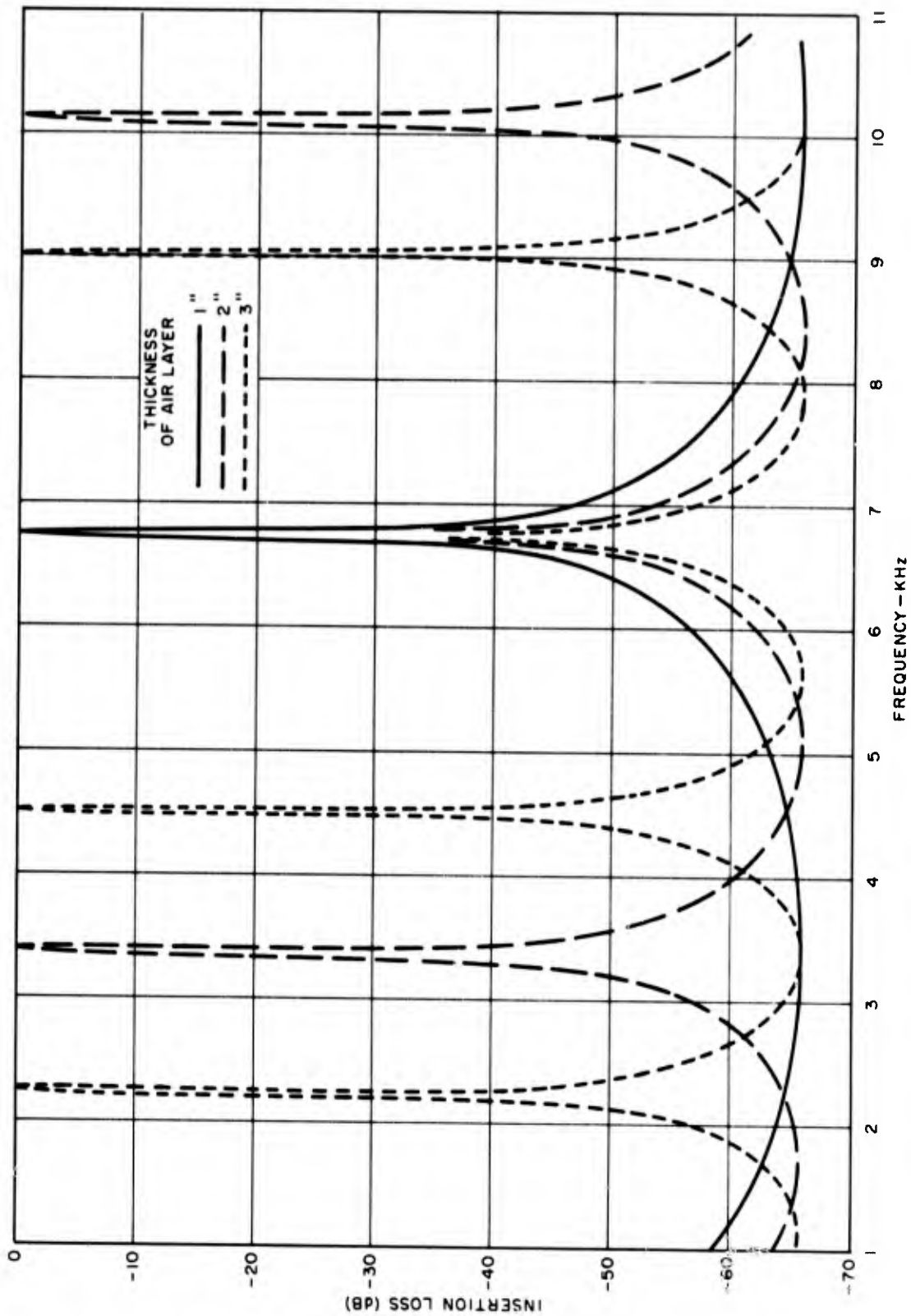


Figure 3-1. Insertion Loss Versus Frequency for Various Air Layer Thicknesses

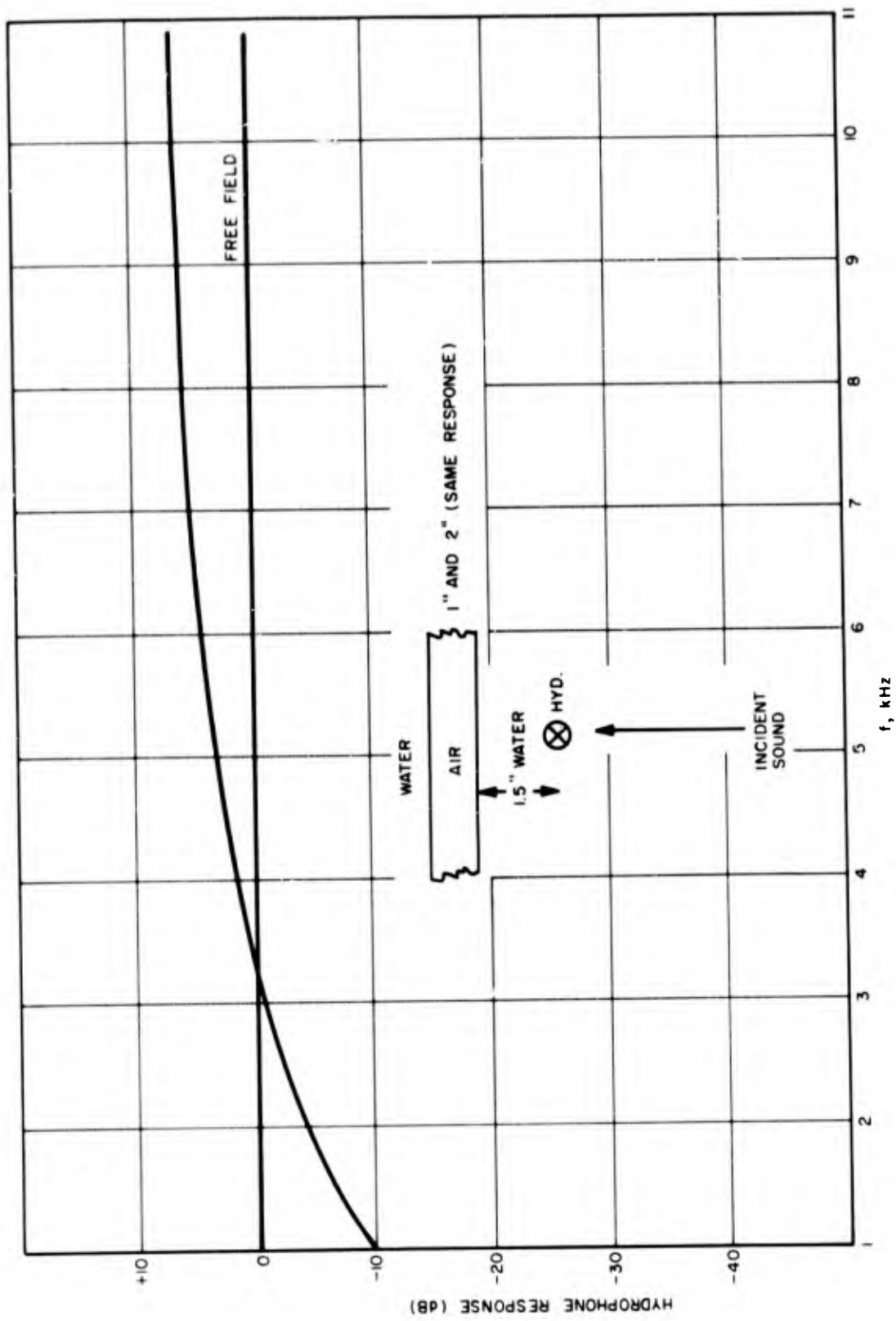


Figure 3-2. Response of a Hydrophone 1.5 Inches in Front of an Air Layer

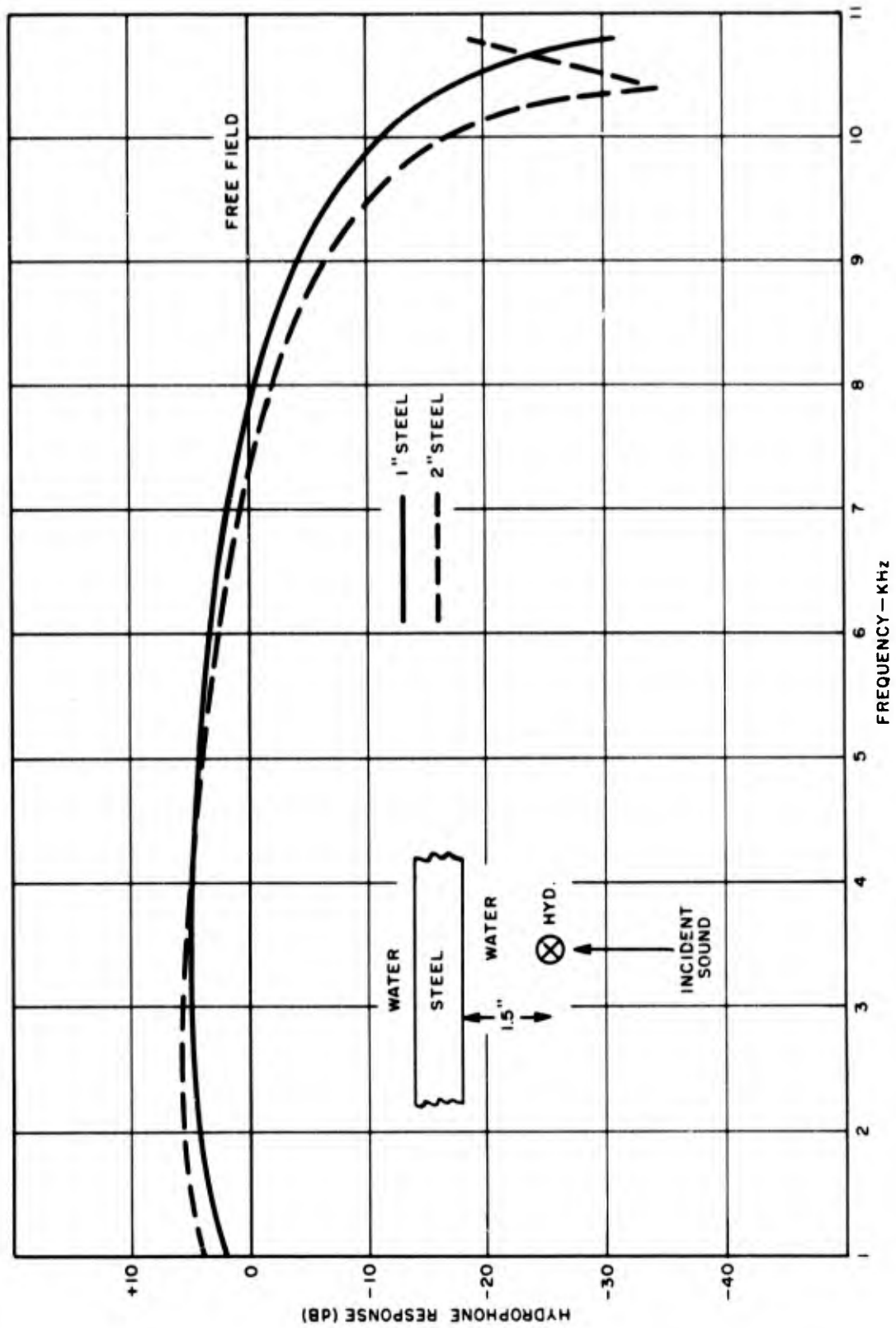


Figure 3-3. Response of a Hydrophone 1.5 Inches in Front of a Steel Layer

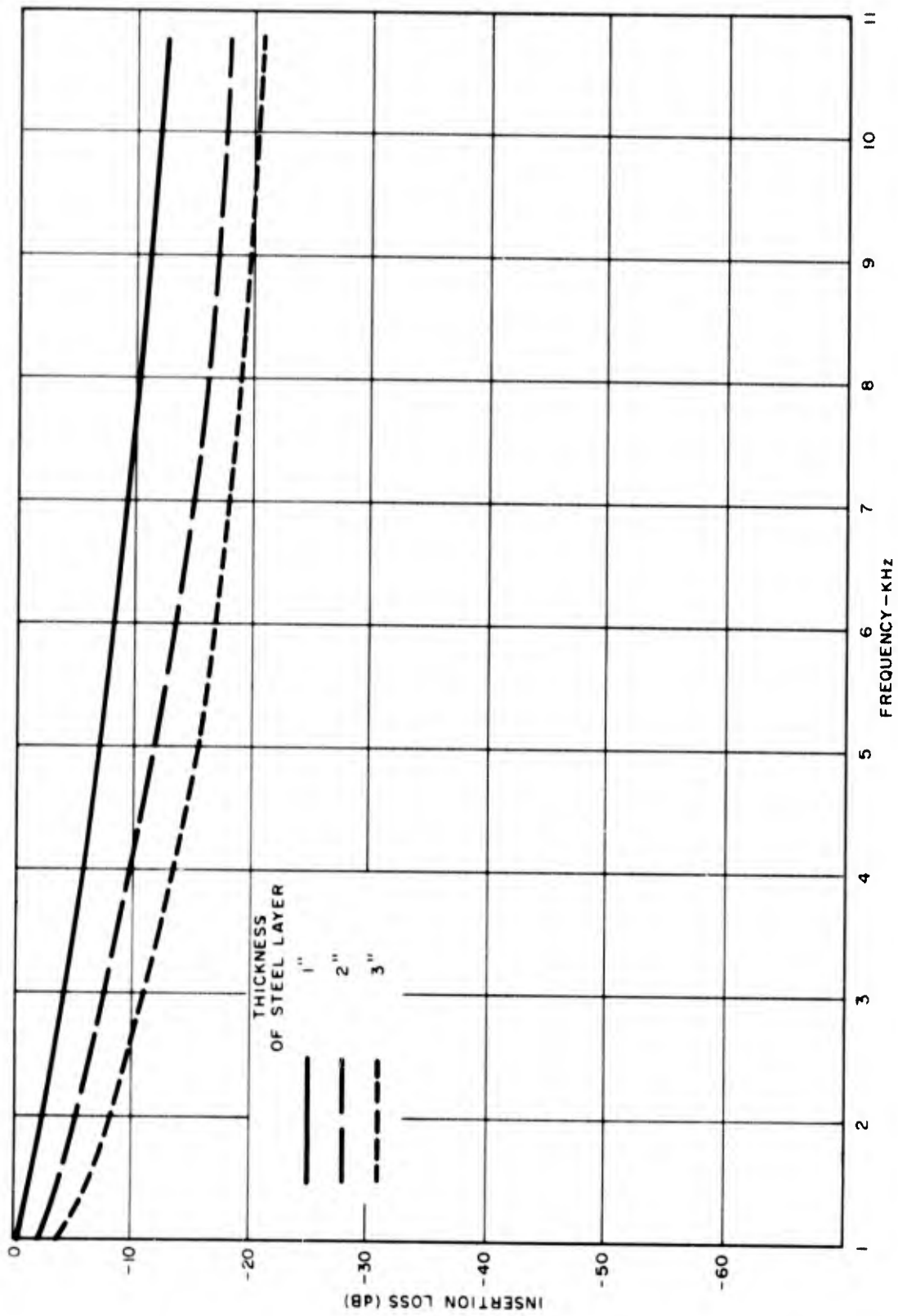


Figure 3-4. Insertion Loss Versus Frequency of Various Steel Layer Thicknesses

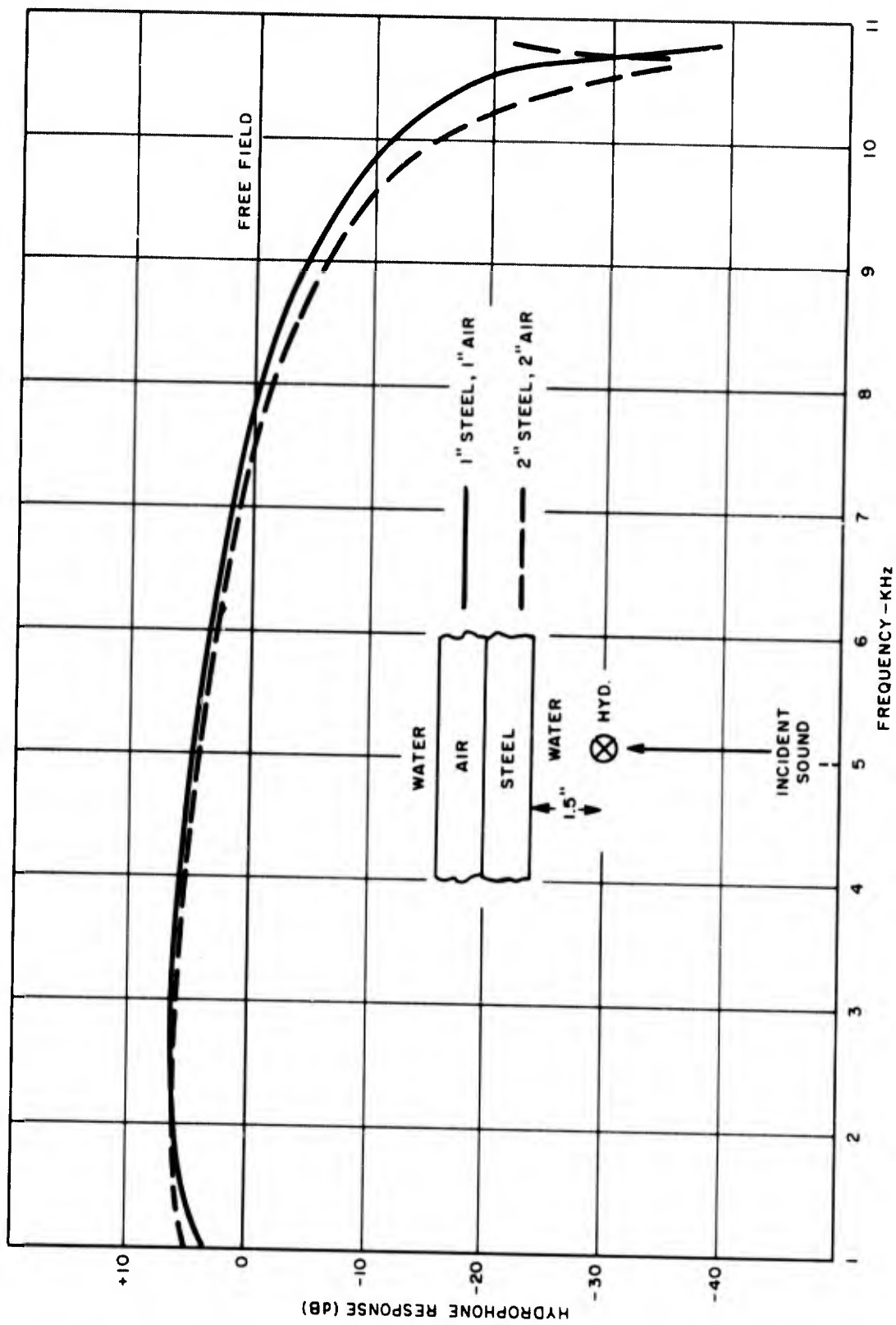


Figure 3-5. Response of a Hydrophone 1.5 Inches in Front of a Combined Air/Steel Baffle

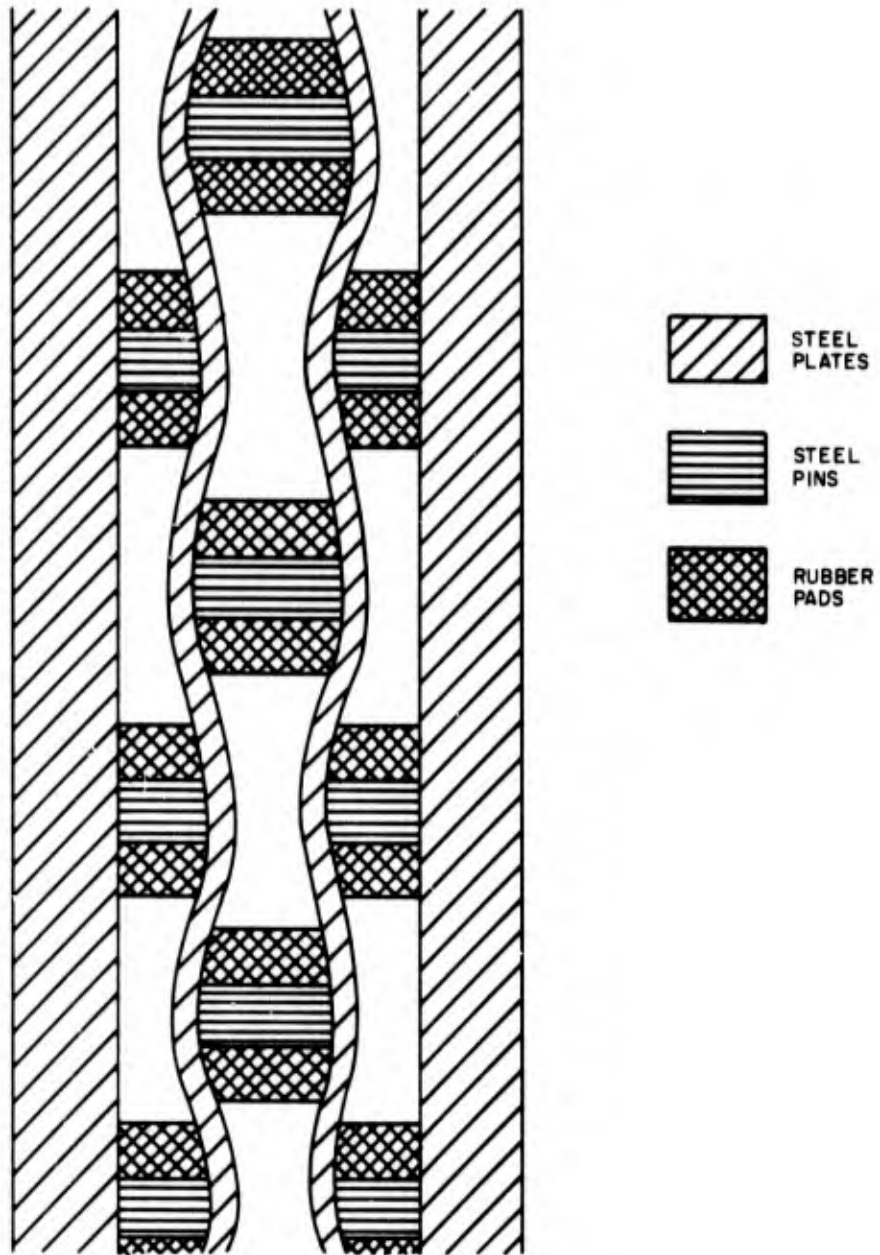
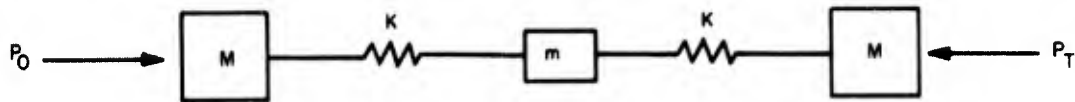
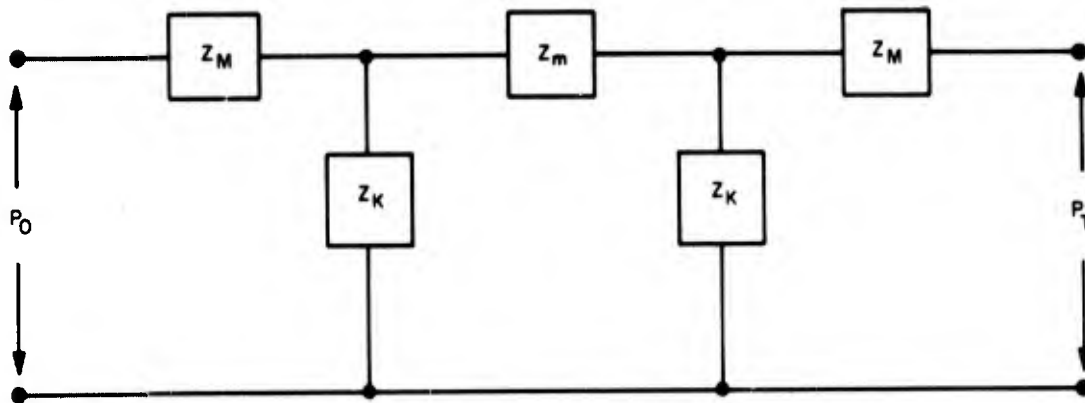


Figure 3-6. Spring-Mass Baffle Configuration Under Hydrostatic Pressure

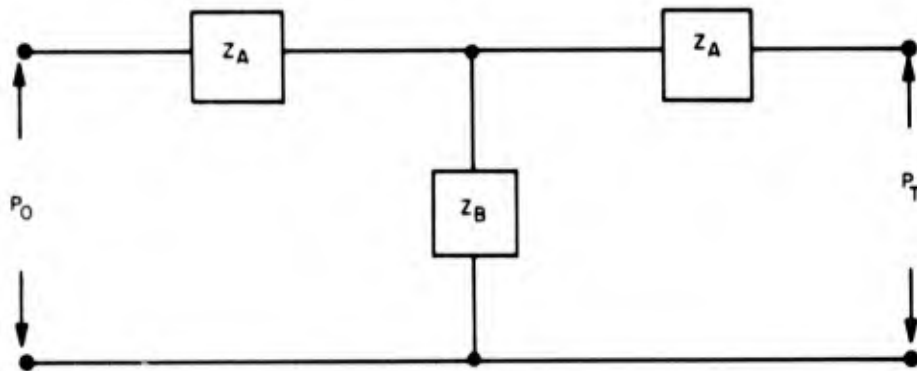


(a) Lumped-Parameter Model of Baffle

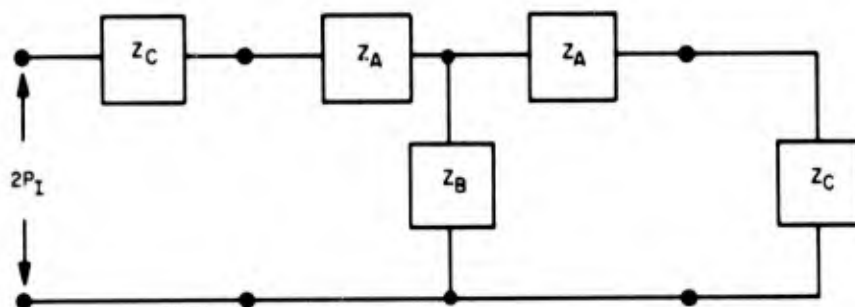


(b) Equivalent Circuit of Baffle

Figure 3-7. Lumped Parameter Model and Equivalent Circuit of Spring-Mass Baffle



(a) Equivalent T Circuit for Baffle

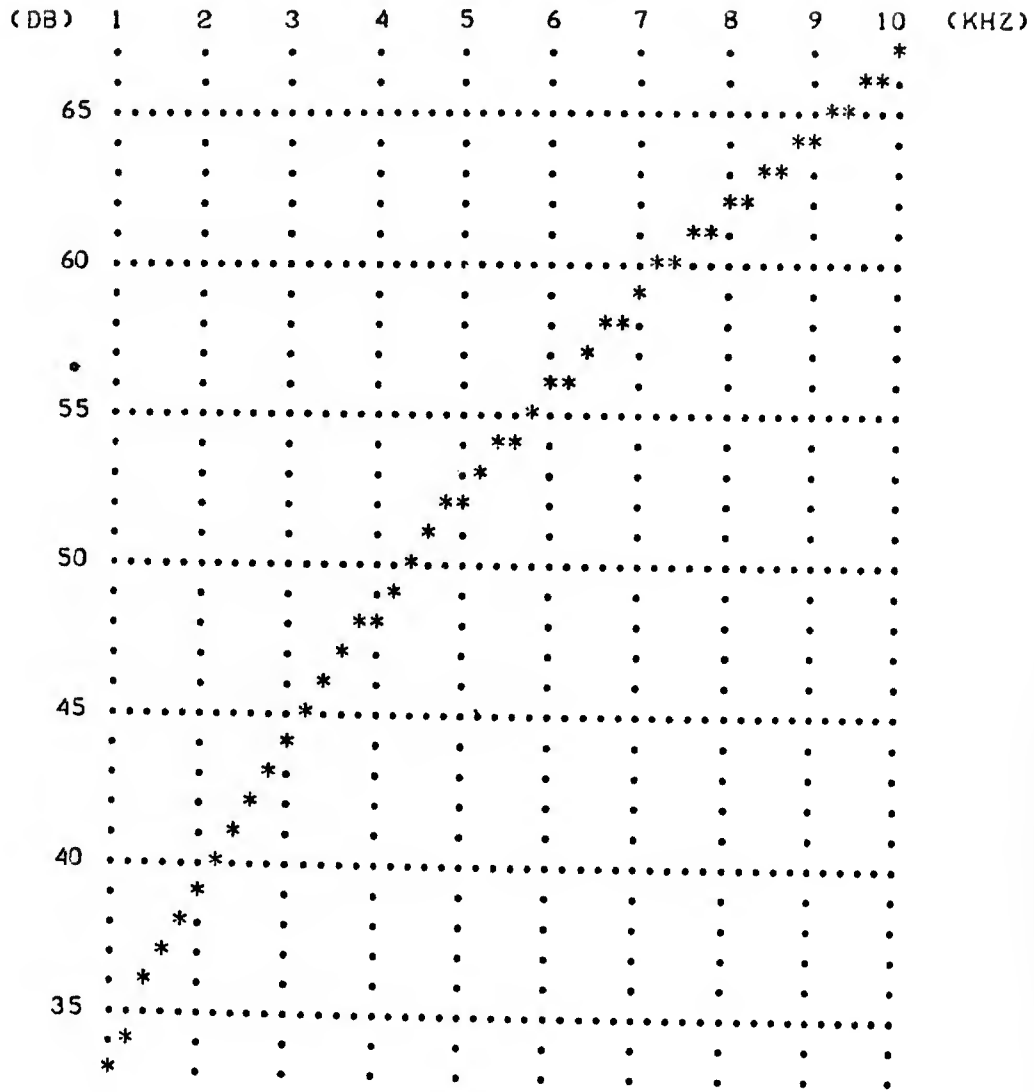


(b) Baffle Circuit in Operation

Figure 3-8. Converted Equivalent Circuit for Spring-Mass Baffle

TRANSMISSION LOSS VS FREQUENCY

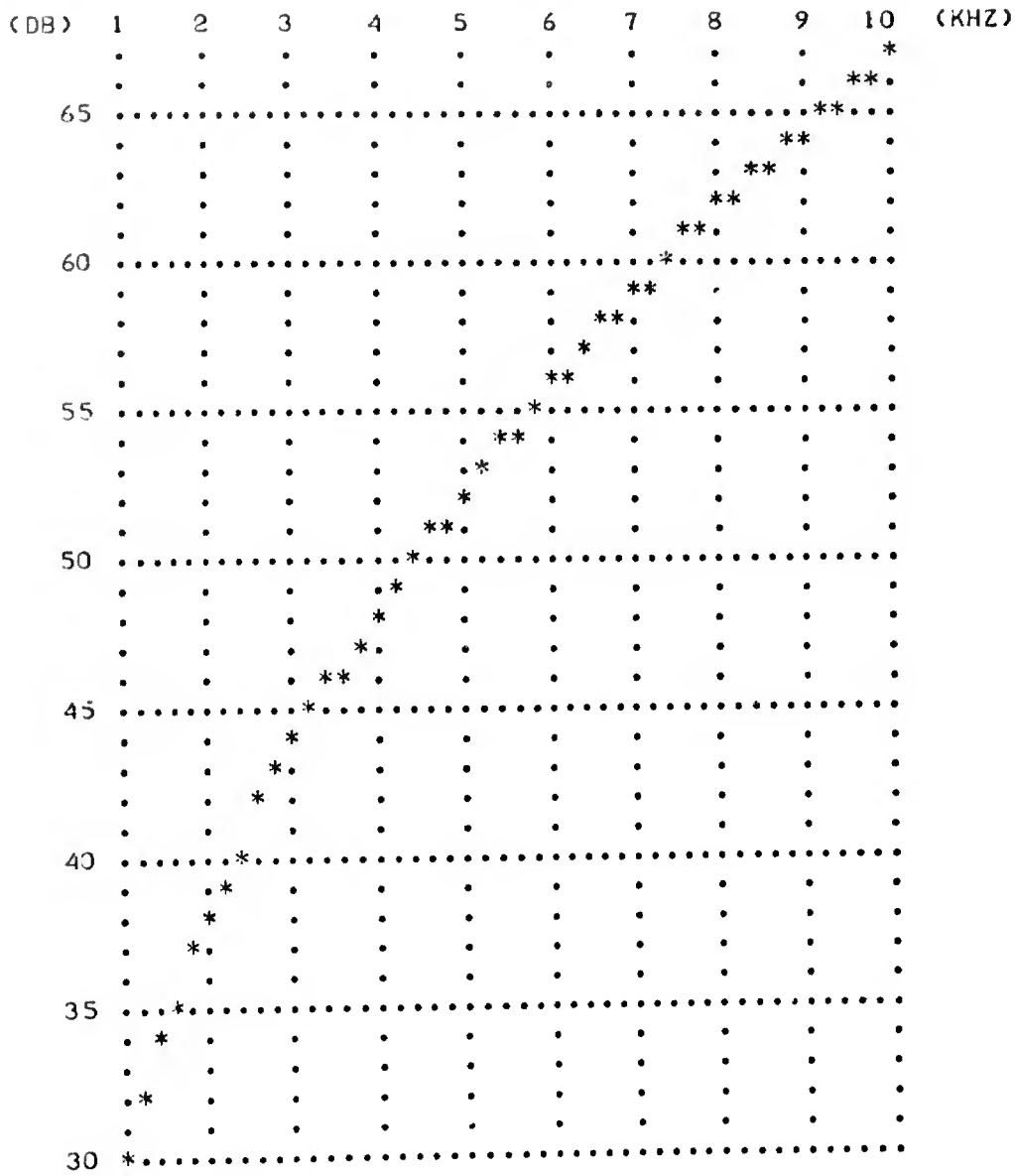
AØM= .000220    AIM= .000072  
 AK =    200    AL =    .20



3-16a

TRANSMISSION LOSS VS FREQUENCY

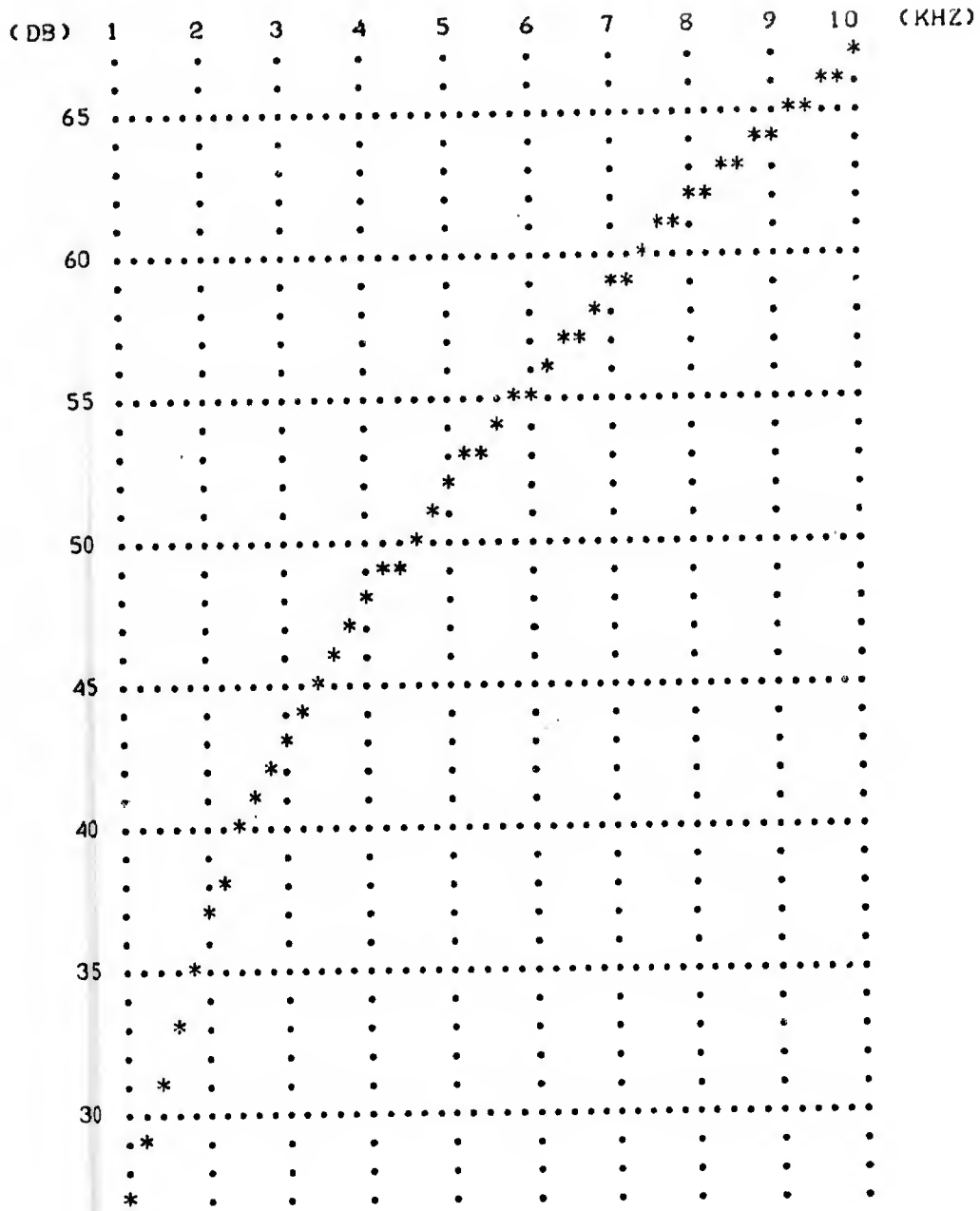
ADM= .000220    AIM= .000072  
 AK =        600    AL =        .20



3-16-h

TRANSMISSION LOSS VS FREQUENCY

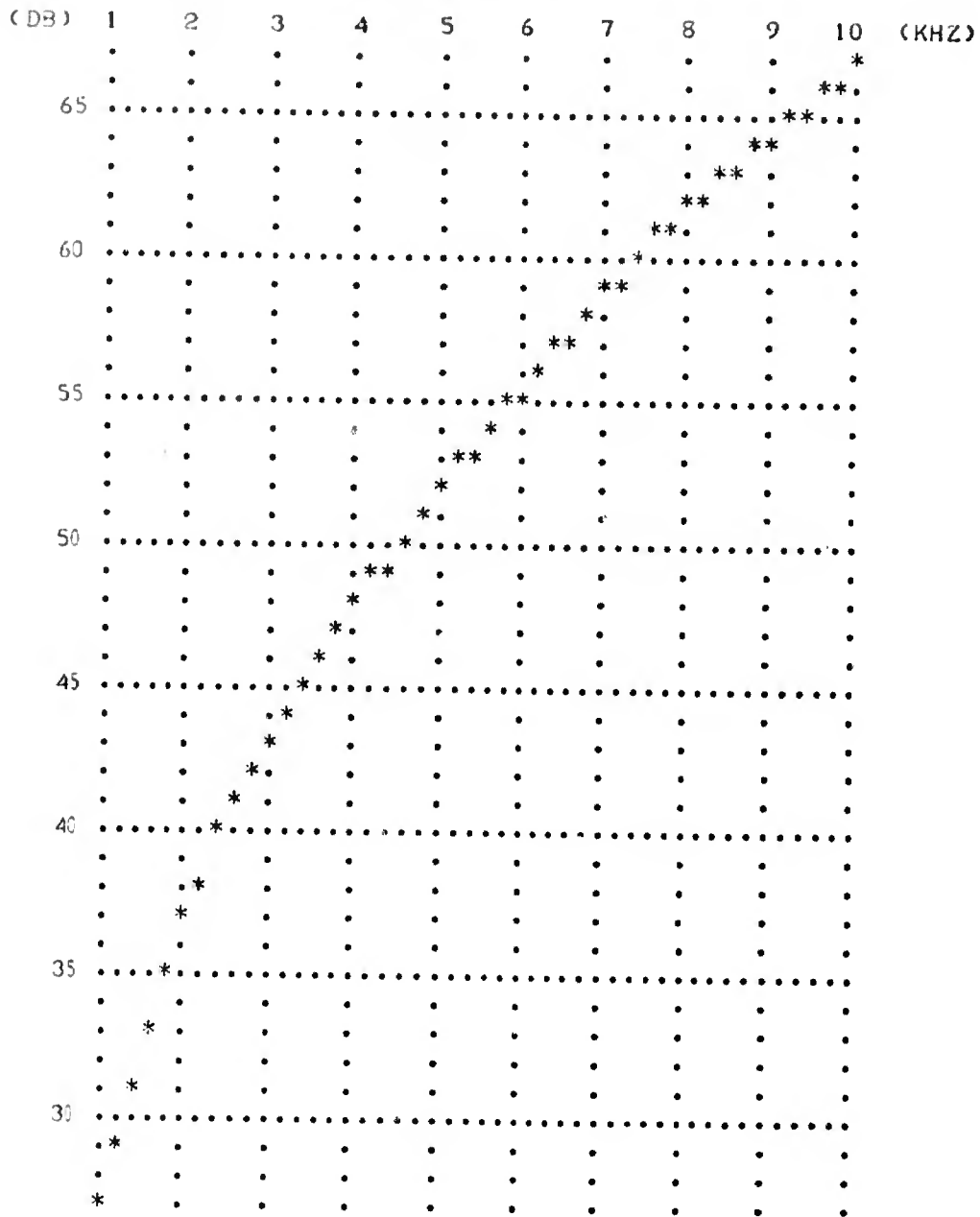
A0M= .000220    AIM= .000072  
 AK = 1000      AL = .20



3-16-c

TRANSMISSION LOSS VS FREQUENCY

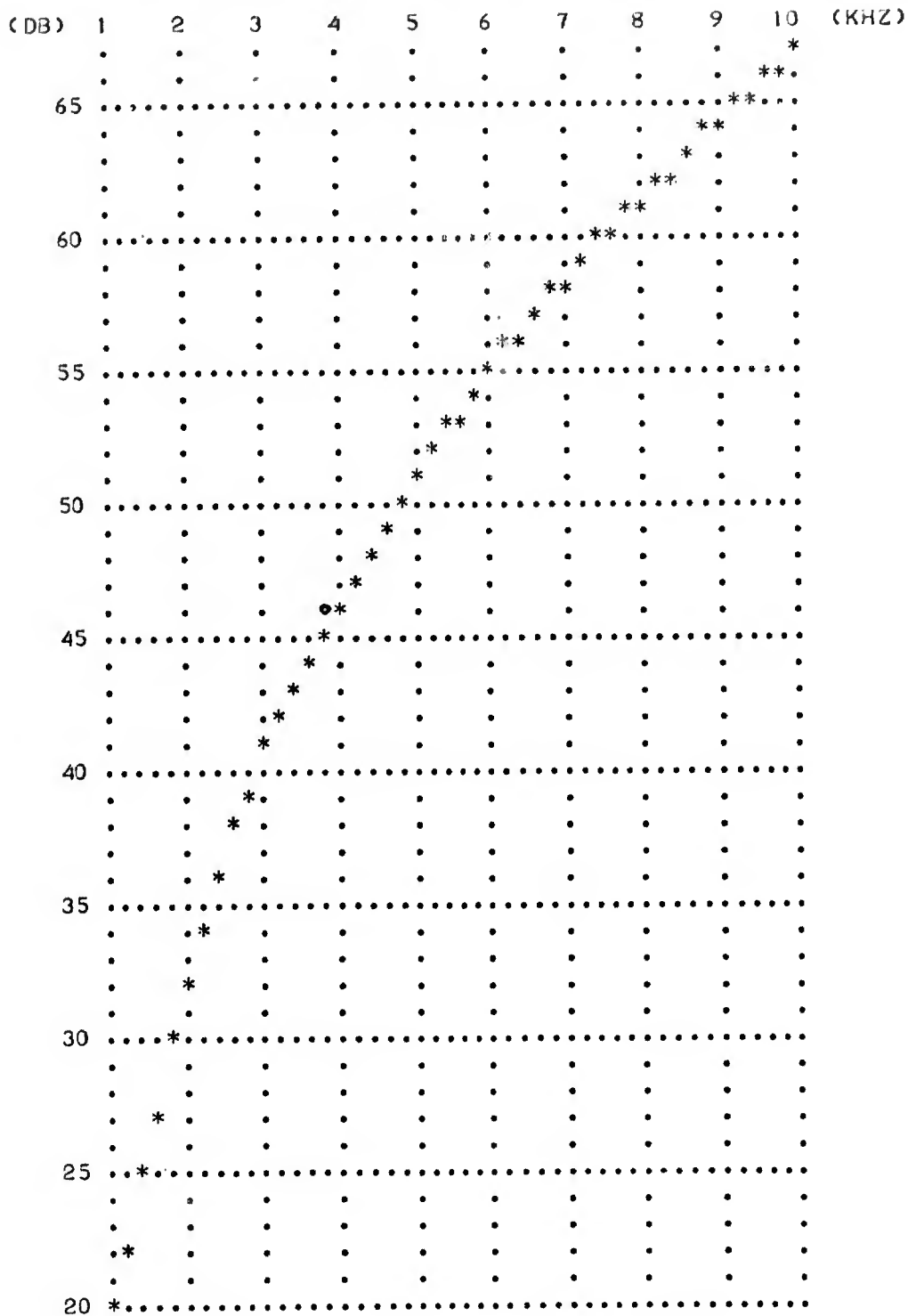
ADM= .000220    AIM= .000072  
 AK = 1000      AL = .20



3-16-C

TRANSMISSION LOSS VS FREQUENCY

A0M= .000220    AIM= .000072  
 AK = 2000      AL = .20



3-16-d

TRANSMISSION LOSS VS FREQUENCY

ADM= .000220    AIM= .000072  
 AK = 3000      AL = .20

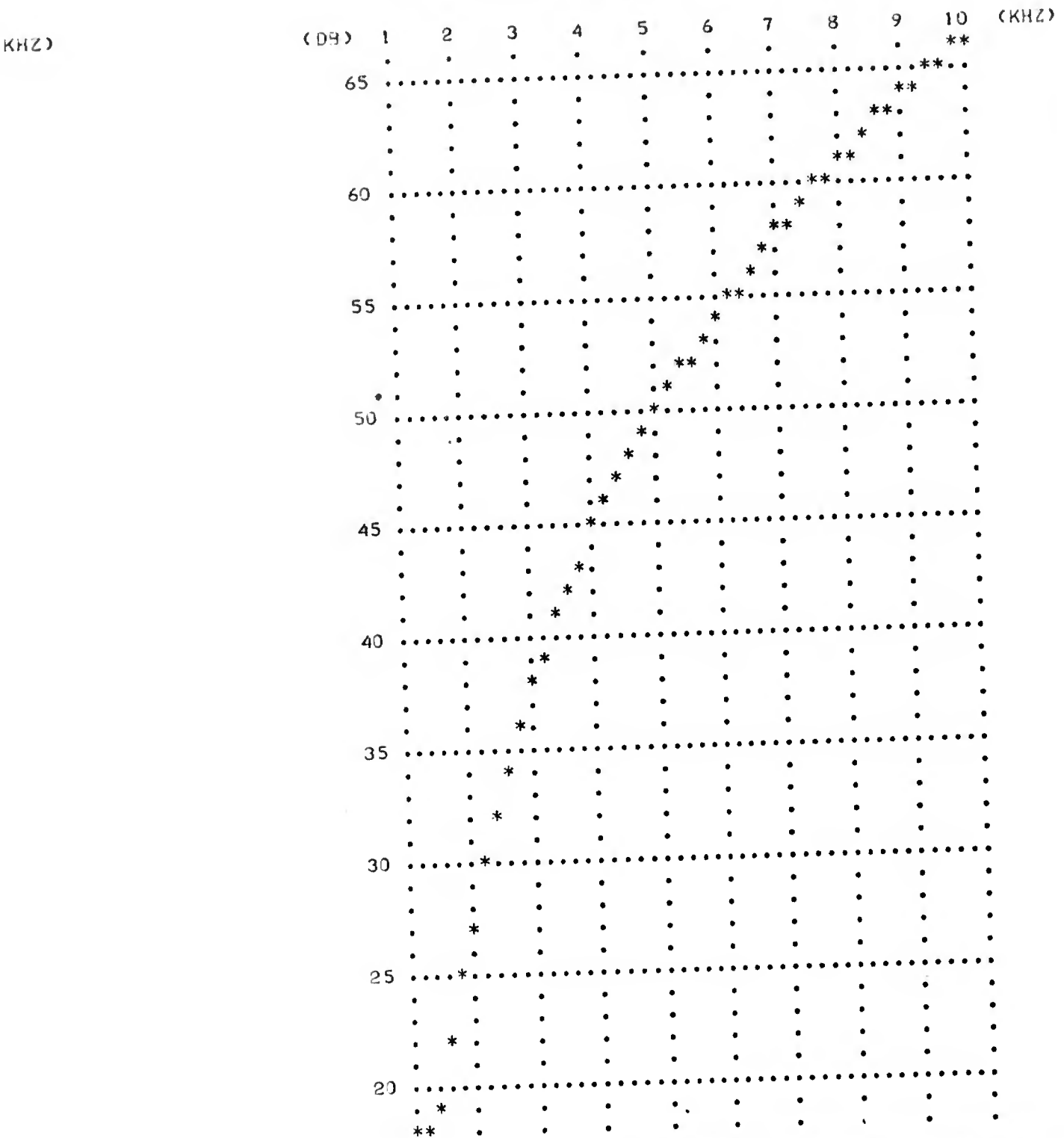
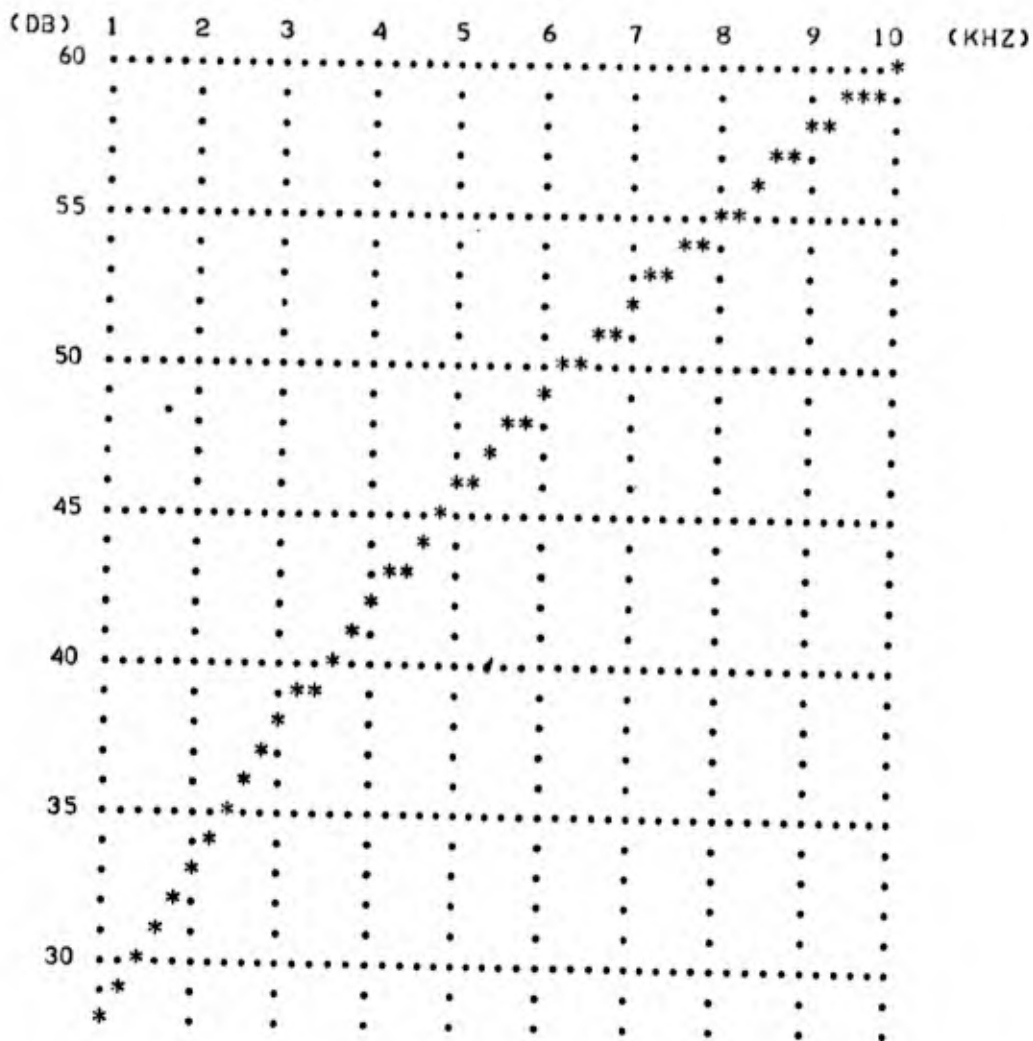


Figure 3-9. Plots of Transmission Loss Versus Frequency for Various Spring Constants and Damping Values (Sheet 1 of 3)

TRANSMISSION LOSS VS FREQUENCY

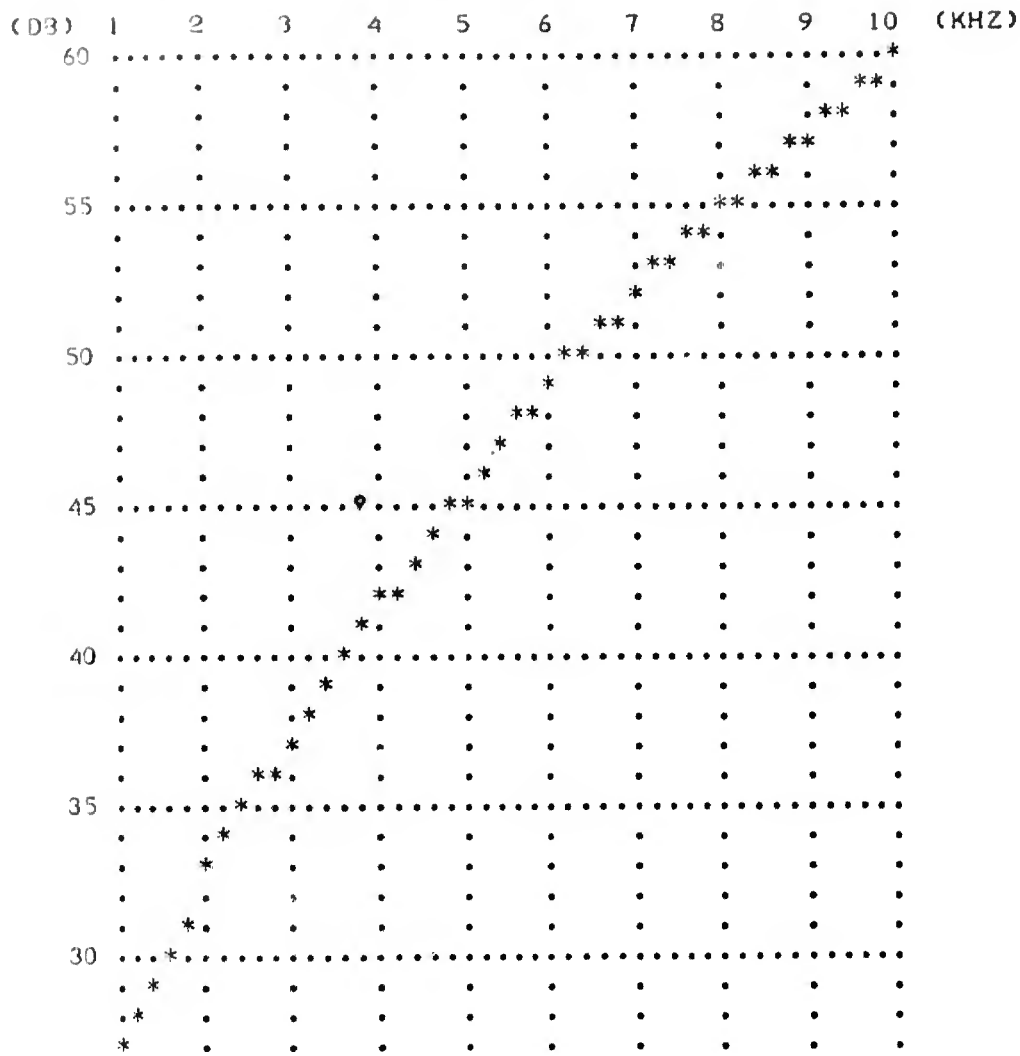
AOM = .000220    AIM = .000072  
 AK = 200        AL = .30



3-17-a

TRANSMISSION LOSS VS FREQUENCY

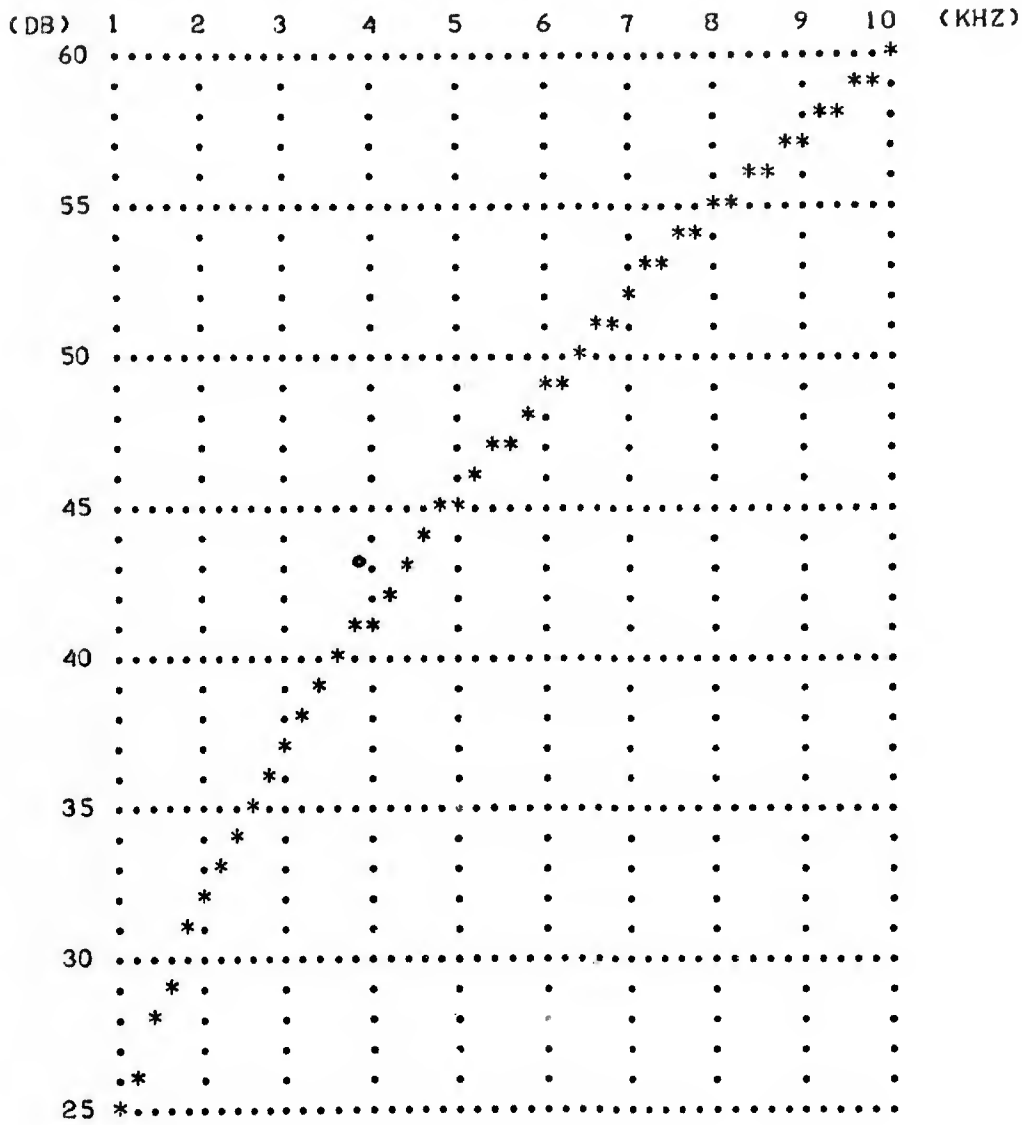
ADM= .000220    AIM= .000072  
 AK =     600     AL =     .30



3-17 k

TRANSMISSION LOSS VS FREQUENCY

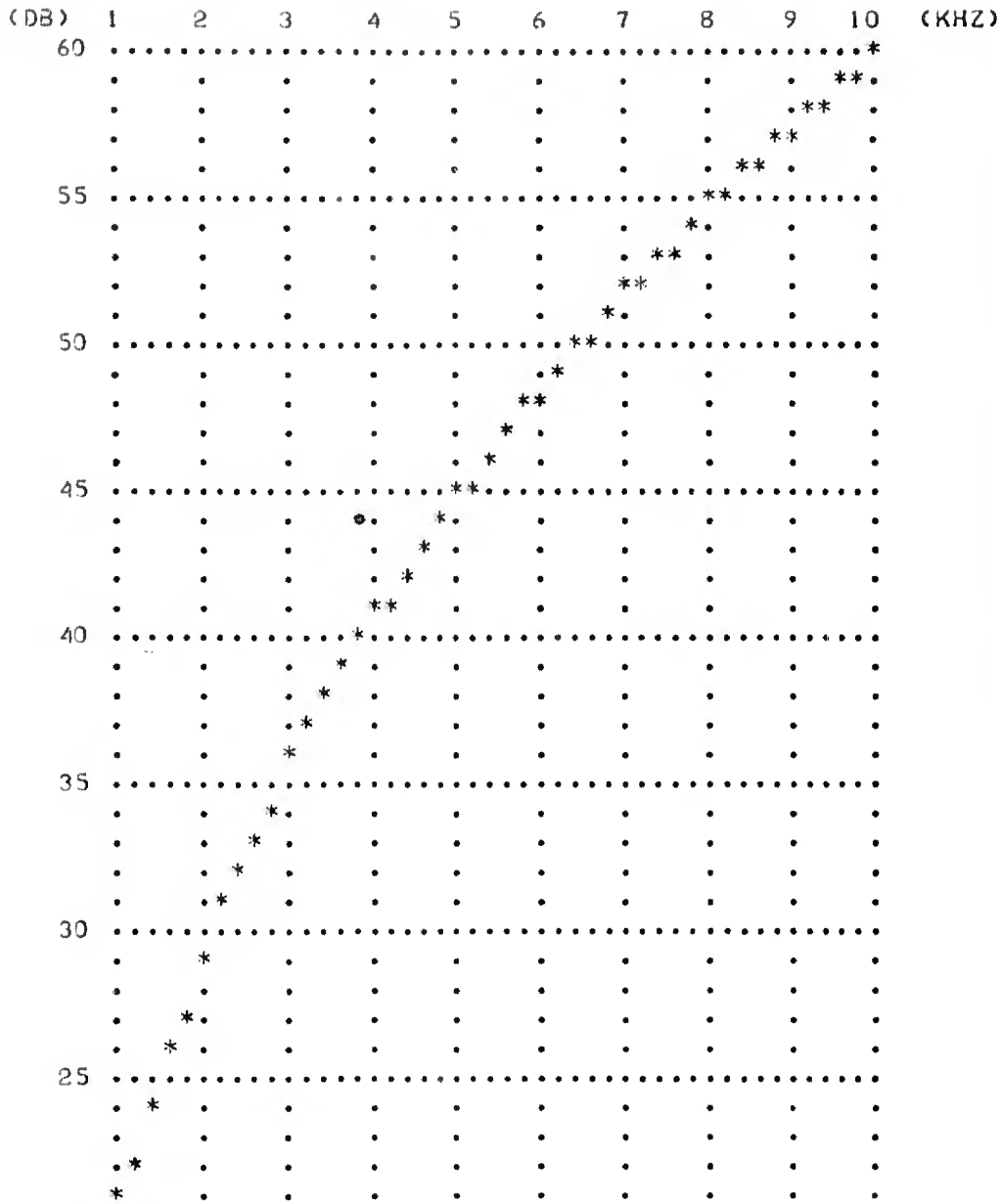
A0M= .000220    AIM= .000072  
 AK = 1000      AL = .30



3-17-C

TRANSMISSION LOSS VS FREQUENCY

A0M= .000220    AIM= .000072  
 AK = 2000      AL = .30



3-17-d

TRANSMISSION LOSS VS FREQUENCY

ADM= .000220    AIM= .000072  
 AK = 3000        AL = .30

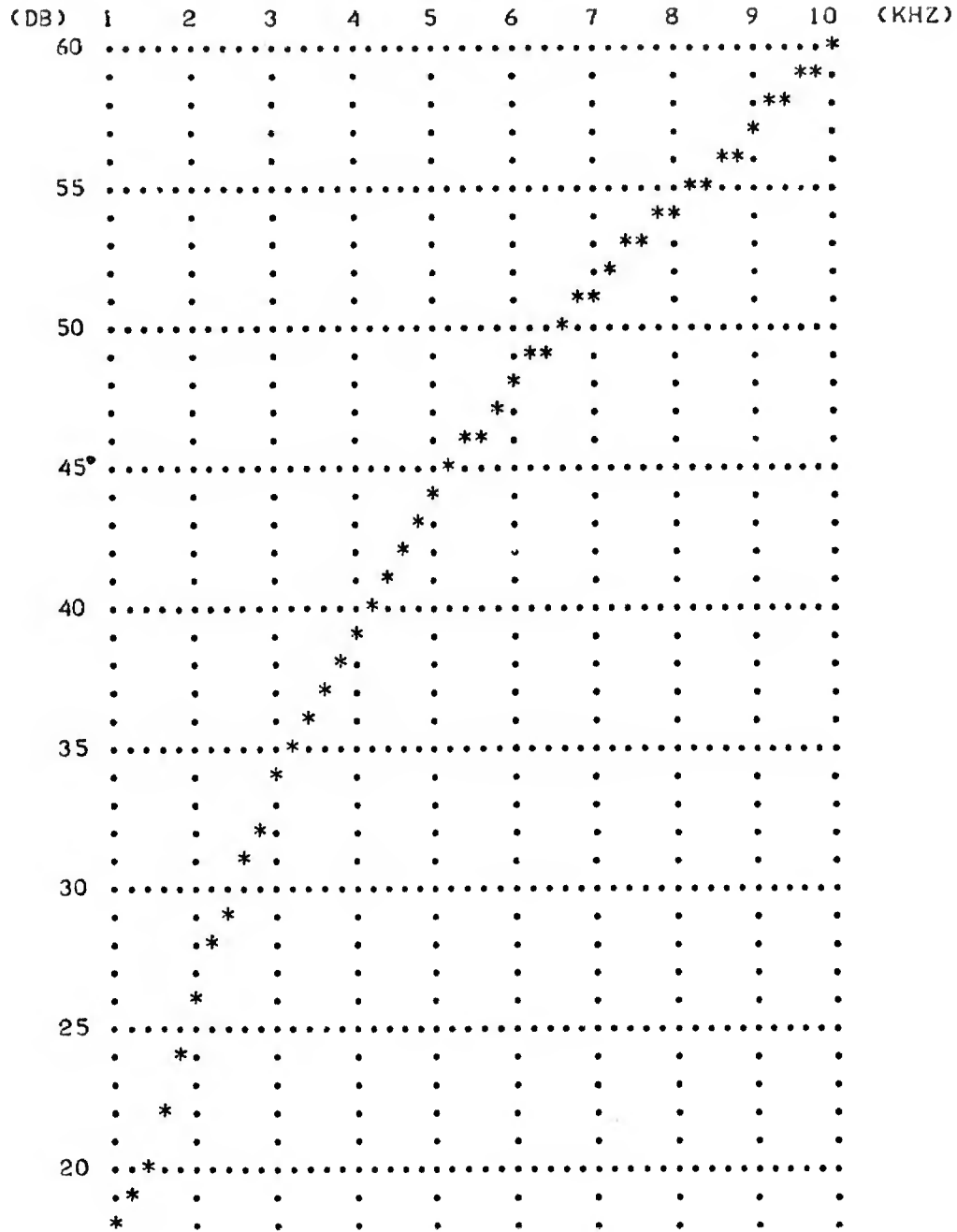
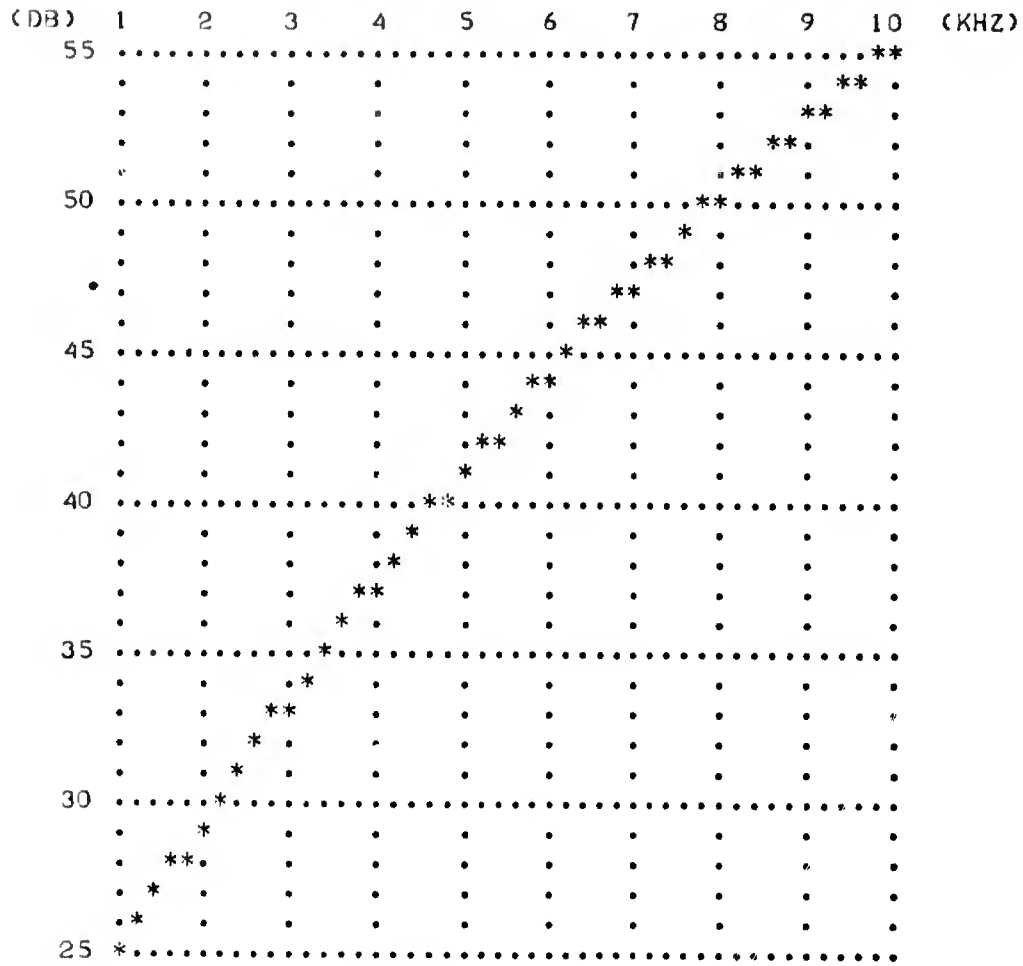


Figure 3-9. Plots of Transmission Loss Versus Frequency for Various Spring Constants and Damping Values (Sheet 2 of 3)

TRANSMISSION LOSS VS FREQUENCY

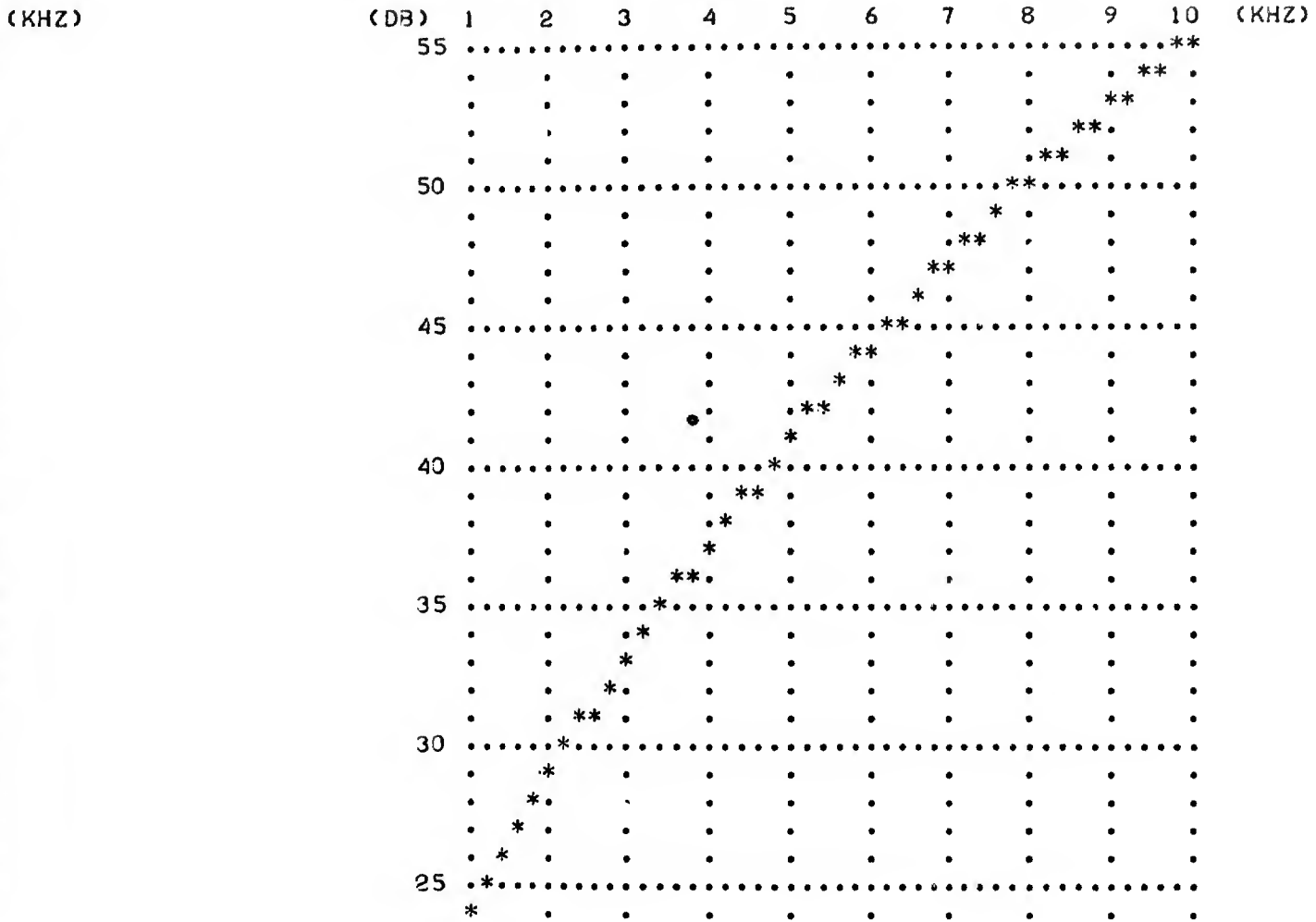
A0M= .000220    AIM= .000072  
 AK =     200    AL =     .40



3-18-A

TRANSMISSION LOSS VS FREQUENCY

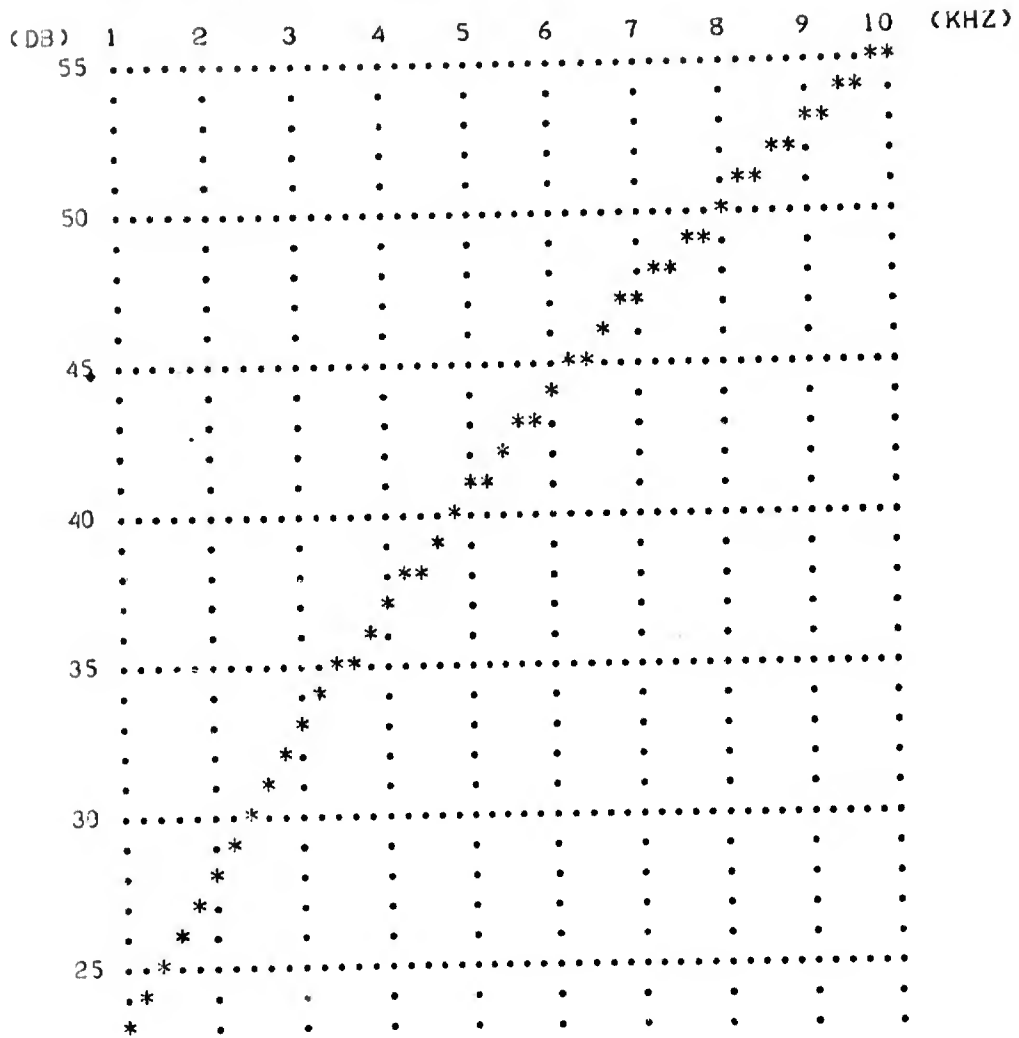
A0M= .000220    AIM= .000072  
 AK =     600    AL =     .40



348.6

TRANSMISSION LOSS VS FREQUENCY

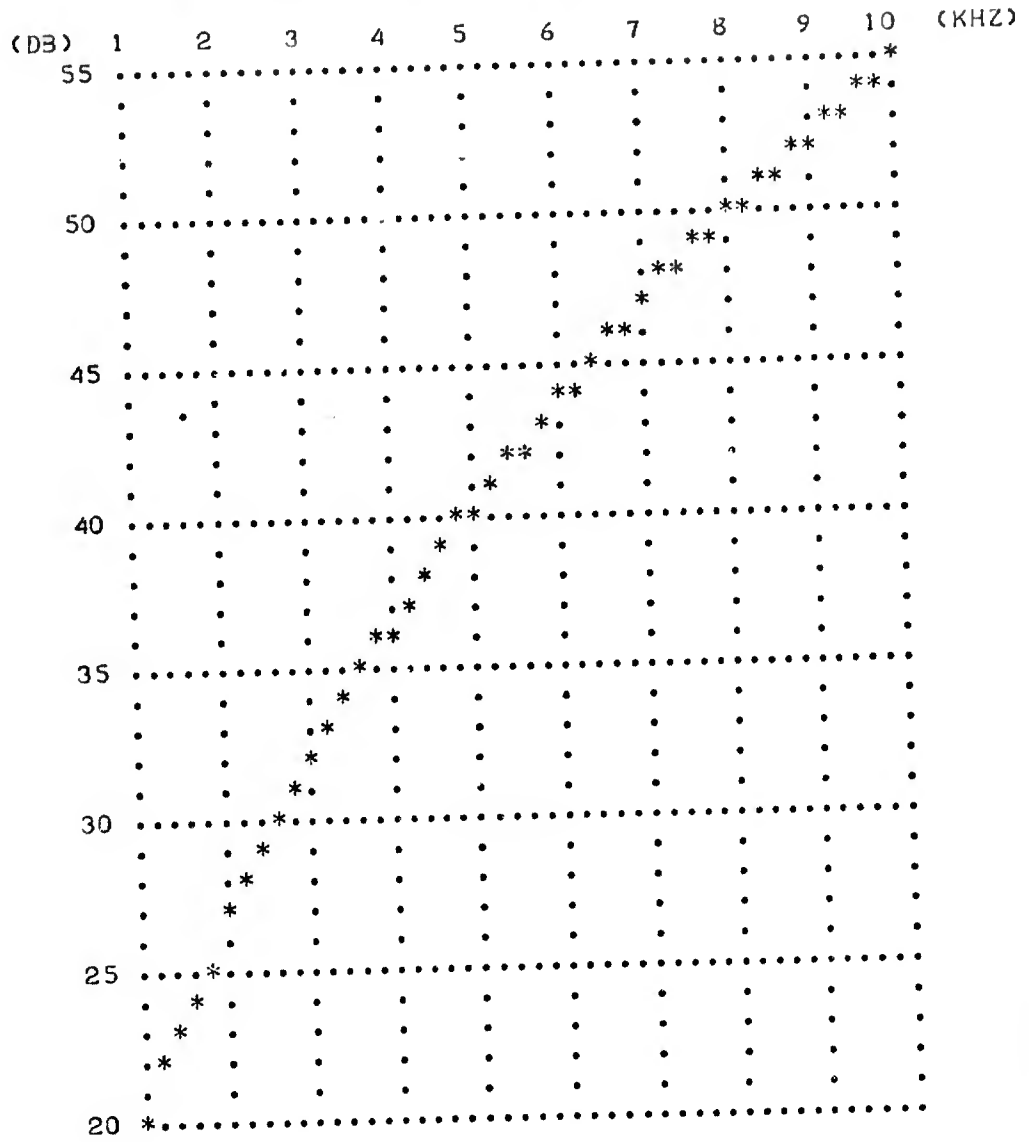
AGM= .000220    AIM= .000072  
 AK = 1000      AL = .40



3-18-C

TRANSMISSION LOSS VS FREQUENCY

AOM = .000220    AIM = .000072  
 AK = 2000        AL = .40



318-d

TRANSMISSION LOSS VS FREQUENCY

ADM= .000220    AIM= .000072  
 AK = 3000      AL = .40

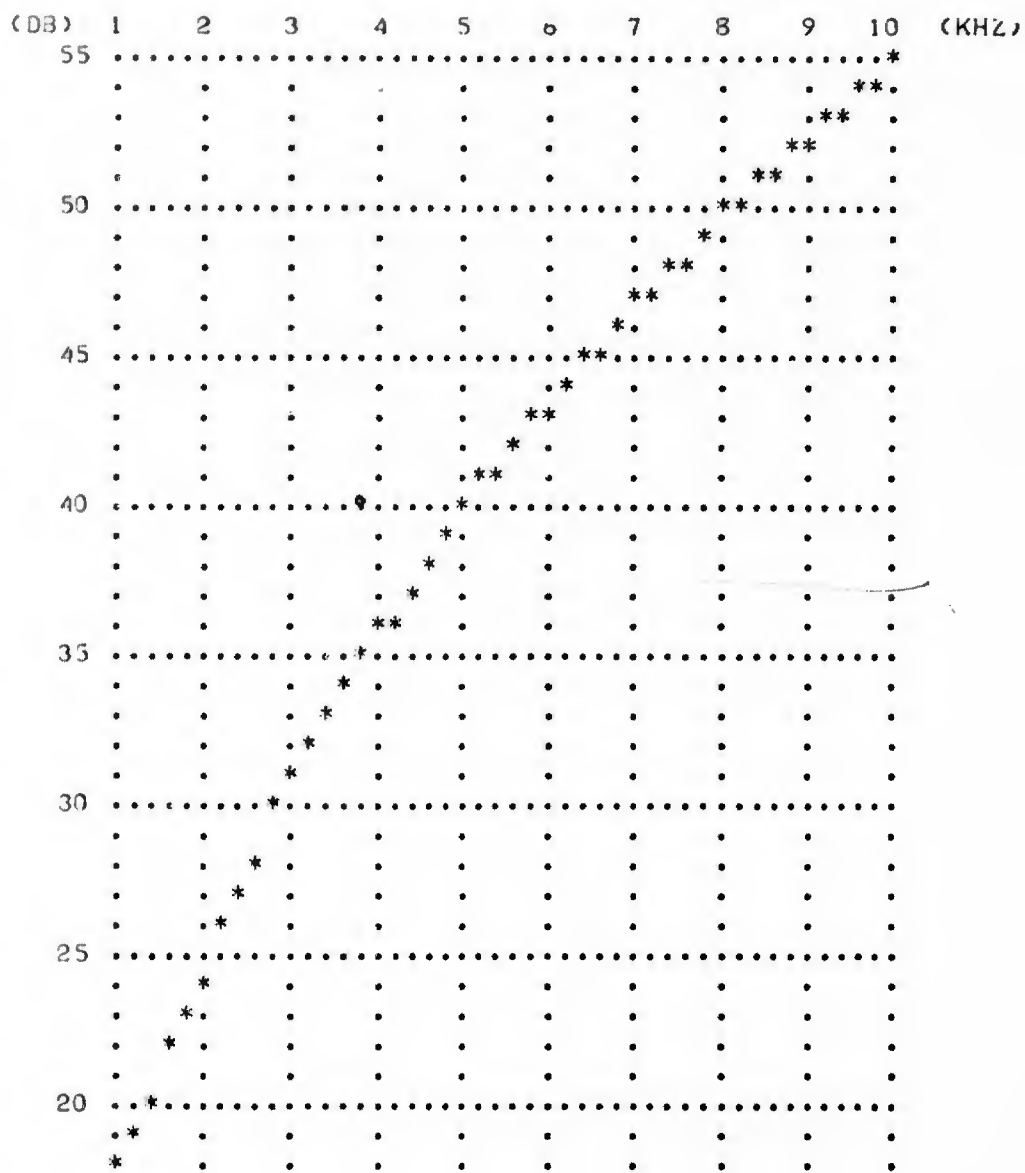


Figure 3-9. Plots of Transmission Loss Versus Frequency for Various Spring Constants and Damping Values (Sheet 3 of 3)

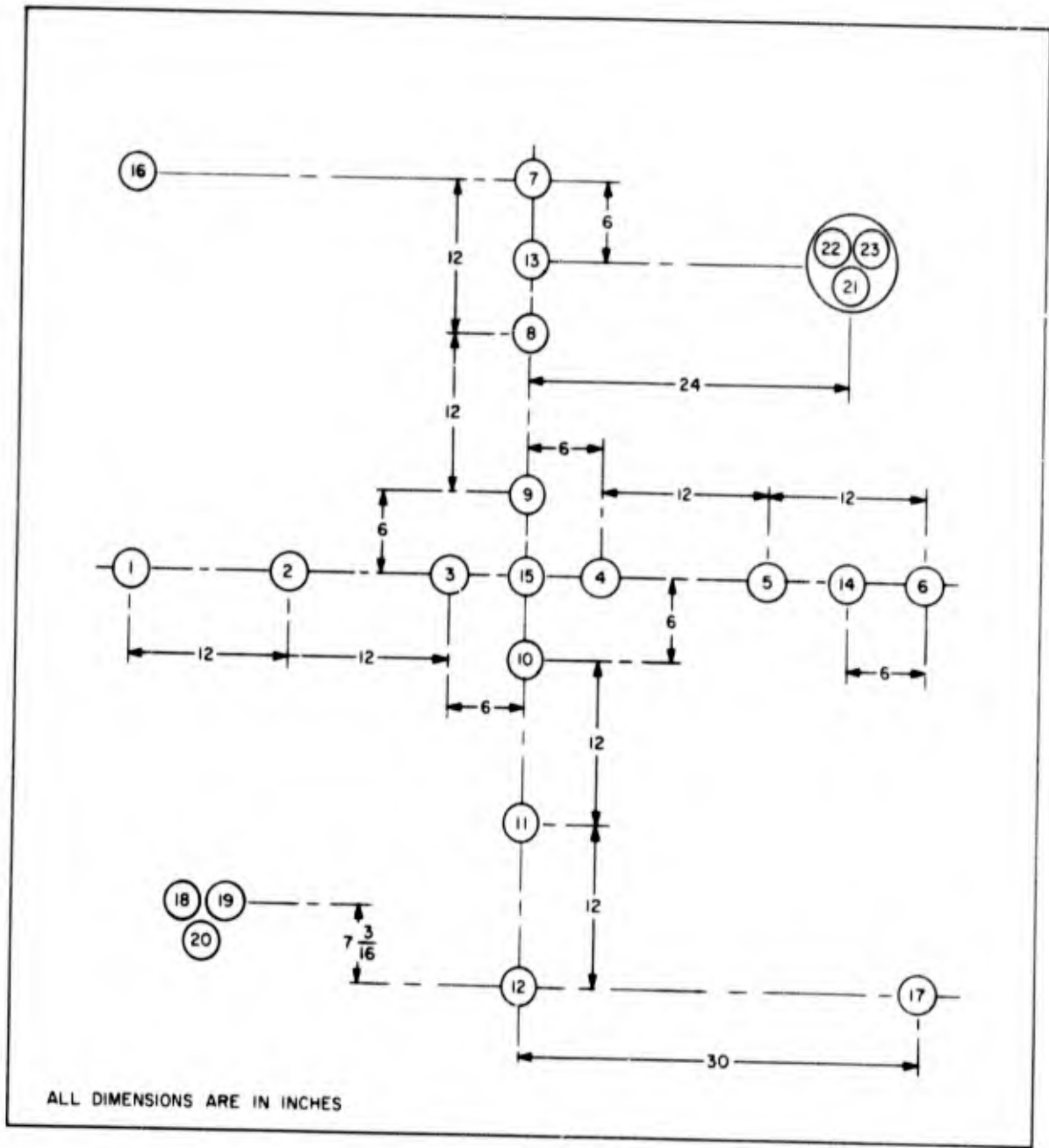


Figure 3-10. Arrangement of Test Hydrophones

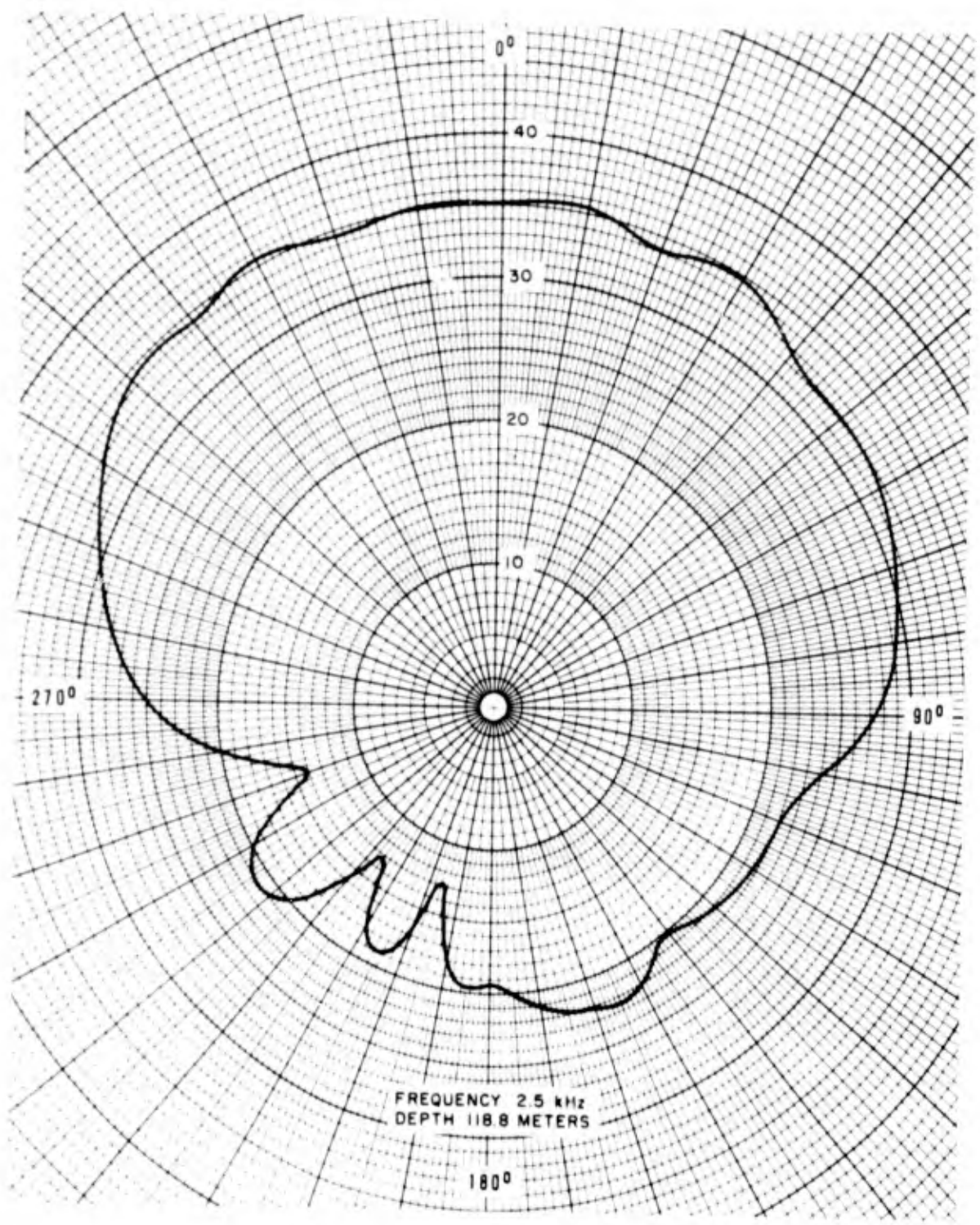


Figure 3-11. Directivity Pattern of Hydrophone 1 at 2.5 kHz

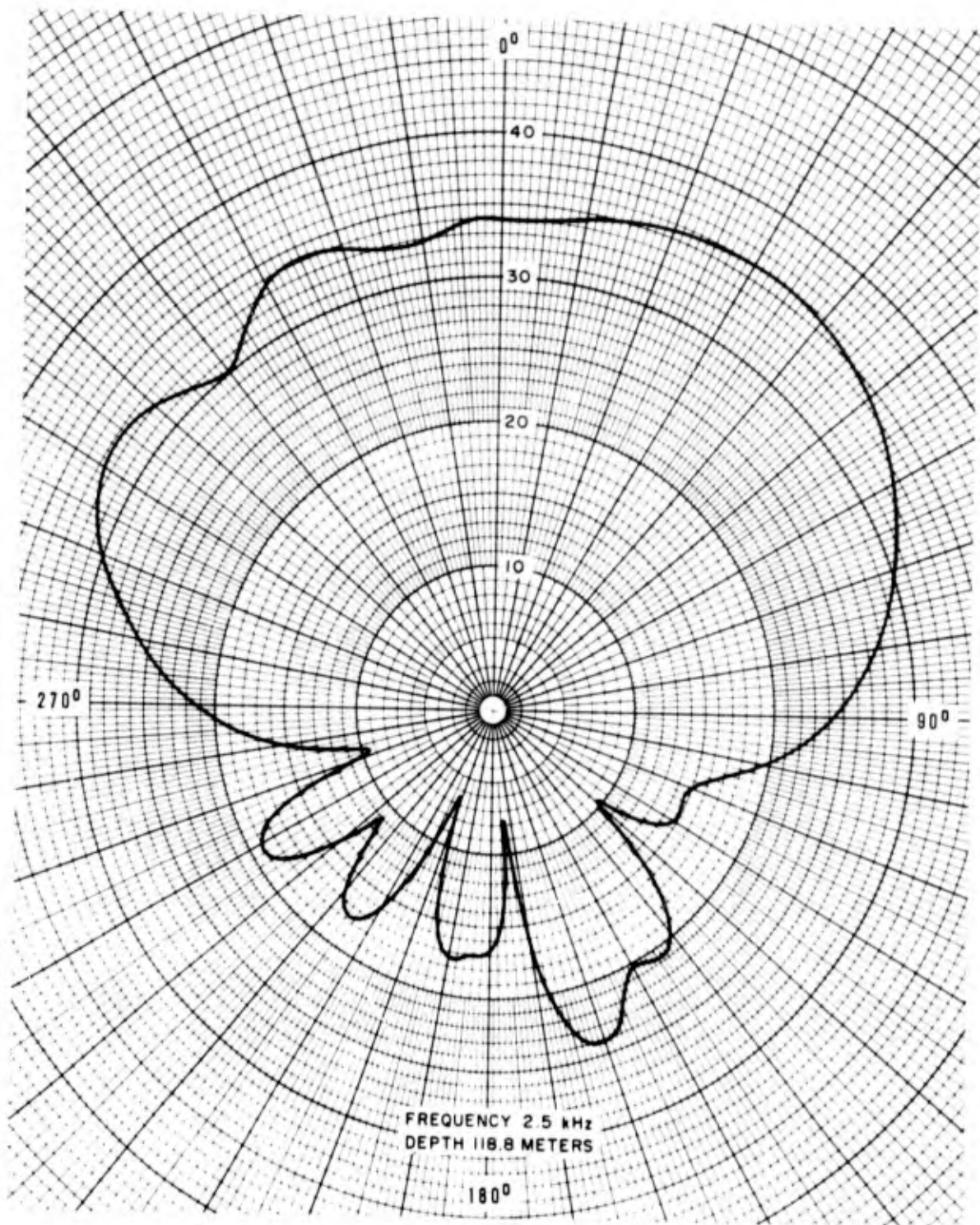


Figure 3-12. Directivity Pattern of Hydrophone 2 at 2.5 kHz

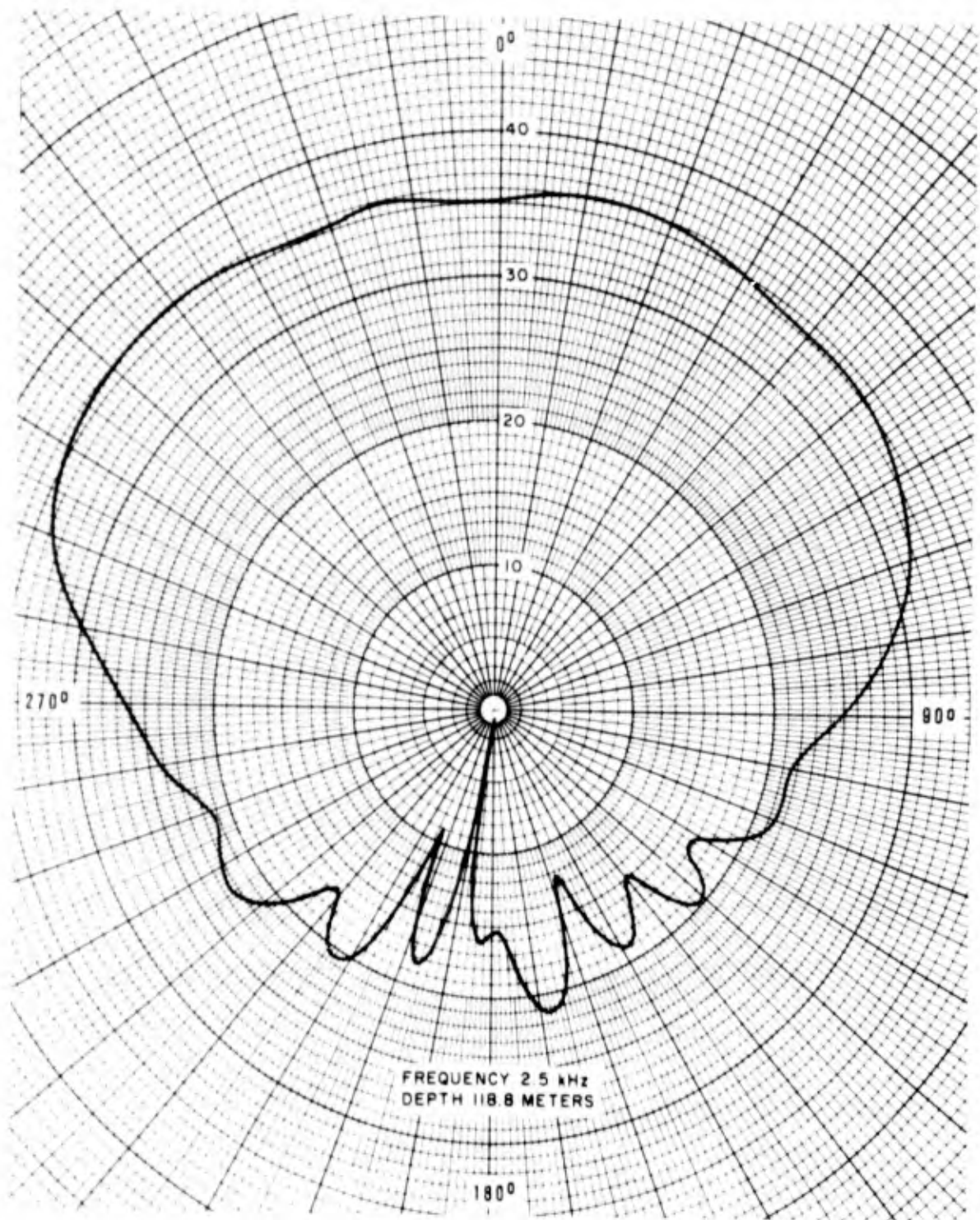


Figure 3-13. Directivity Pattern of Hydrophone 3 at 2.5 kHz

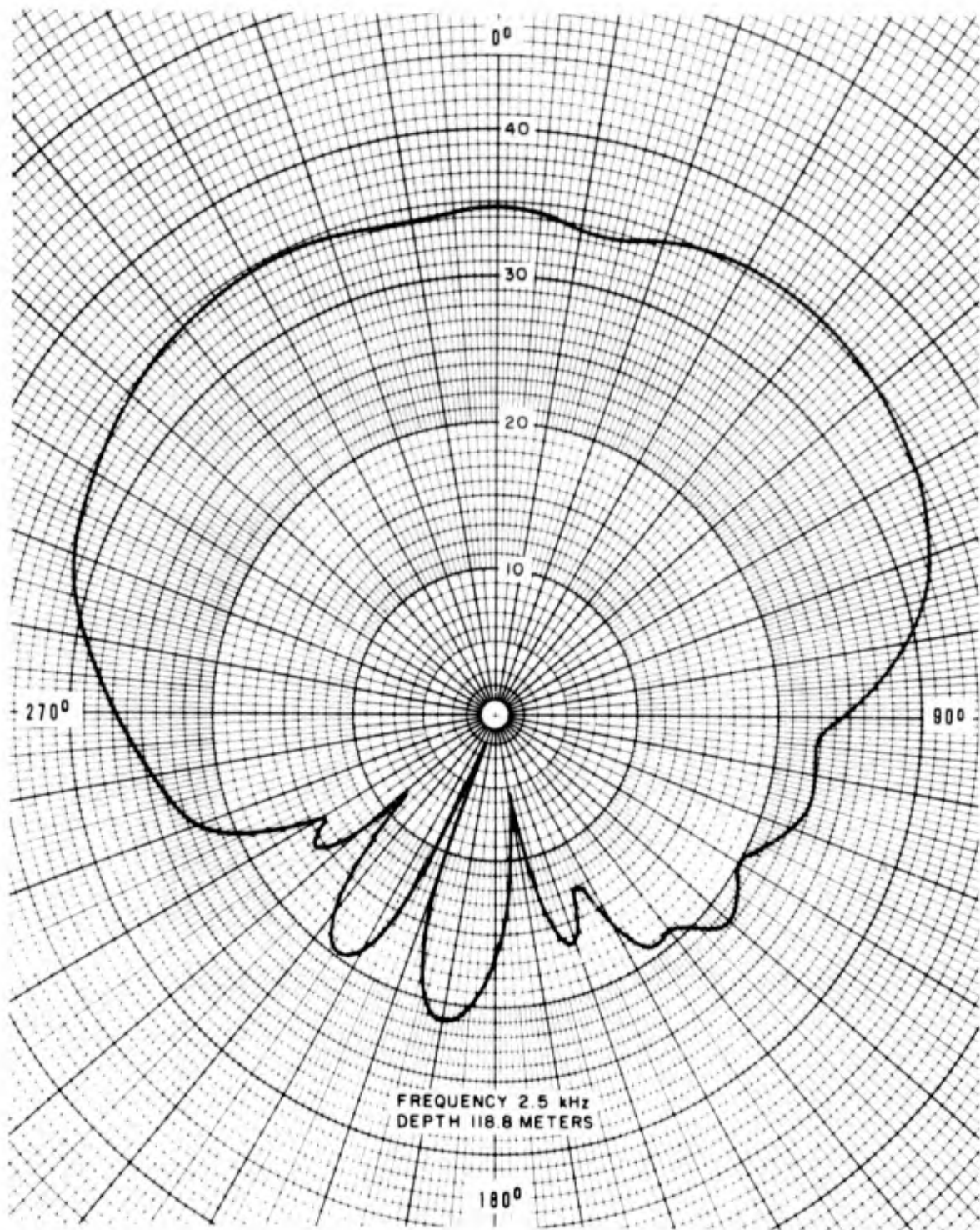


Figure 3-14. Directivity Pattern of Hydrophone 4 at 2.5 kHz

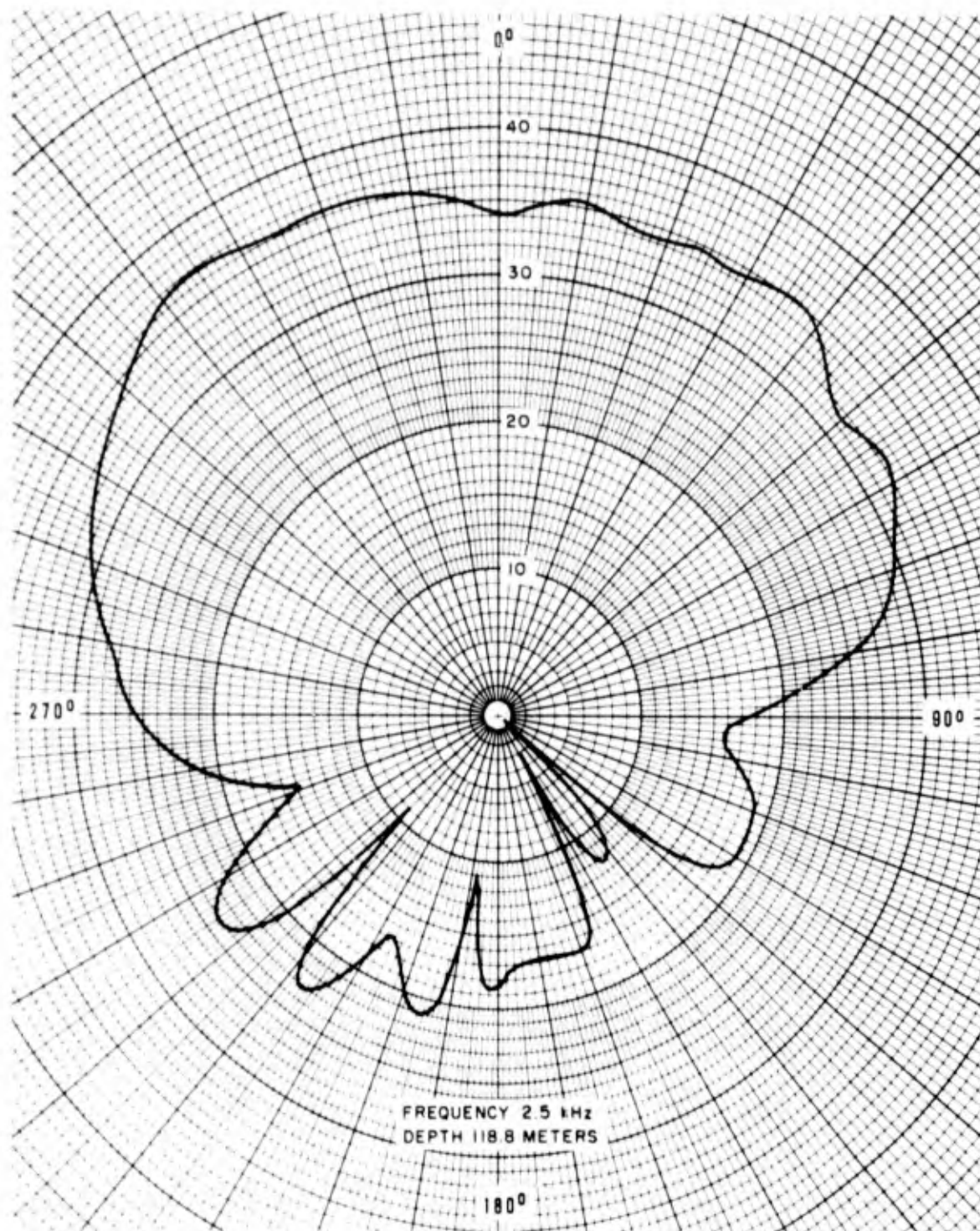


Figure 3-15. Directivity Pattern of Hydrophone 5 at 2.5 kHz

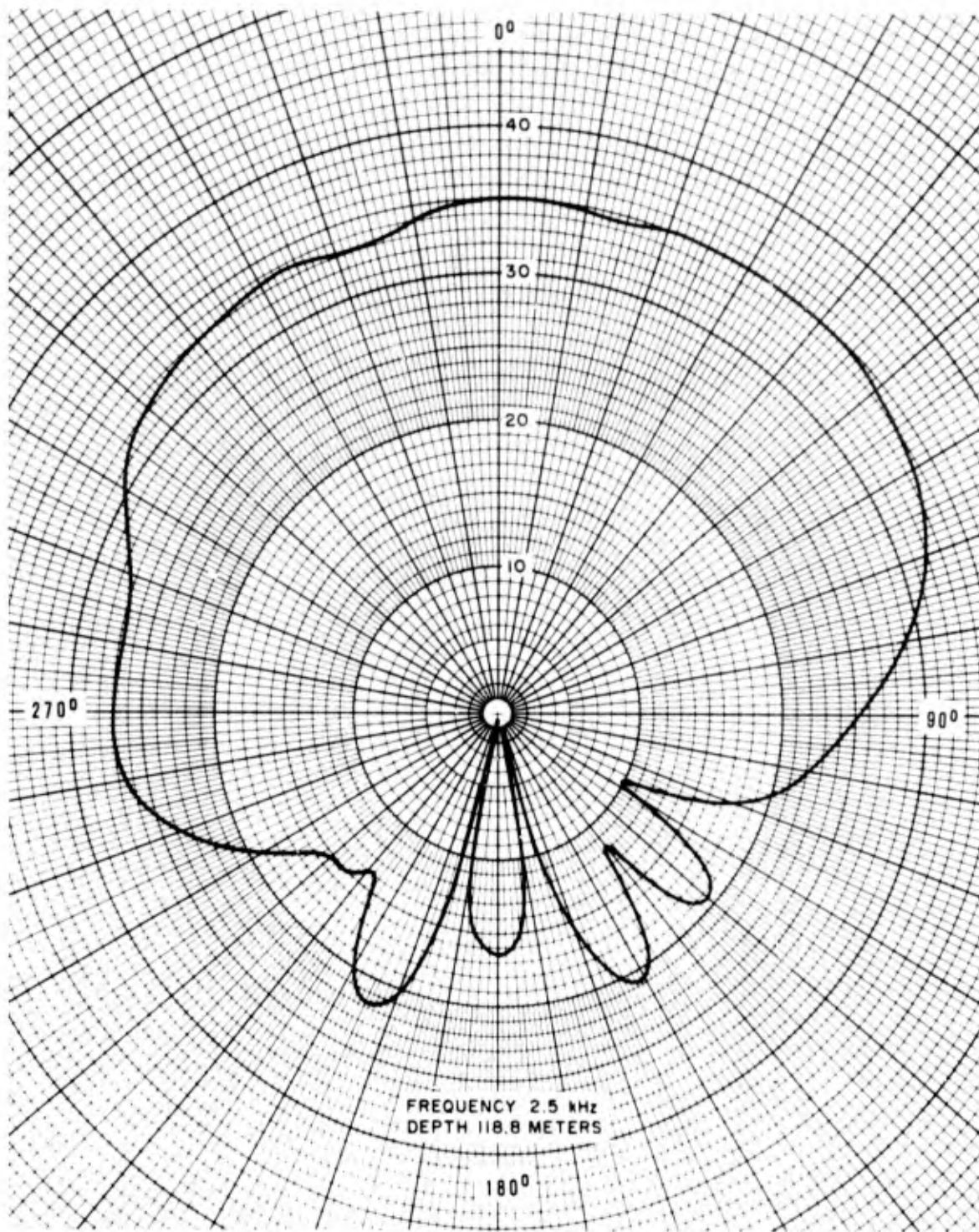


Figure 3-16. Directivity Pattern of Hydrophone 6 at 2.5 kHz

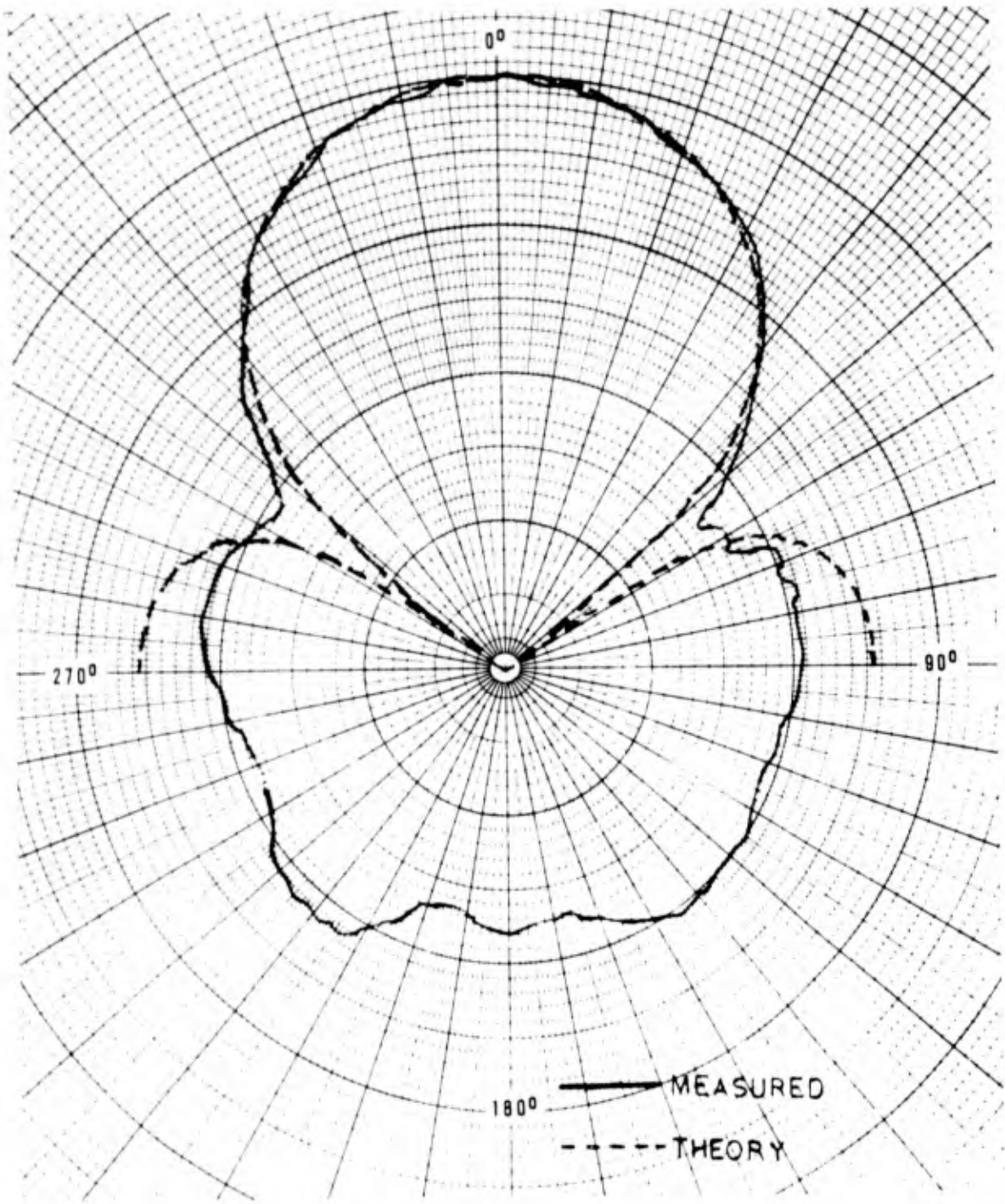


Figure 3-17. Zero-Degree Beam Pattern, Hydrophones 1 Through 6 at 1 kHz

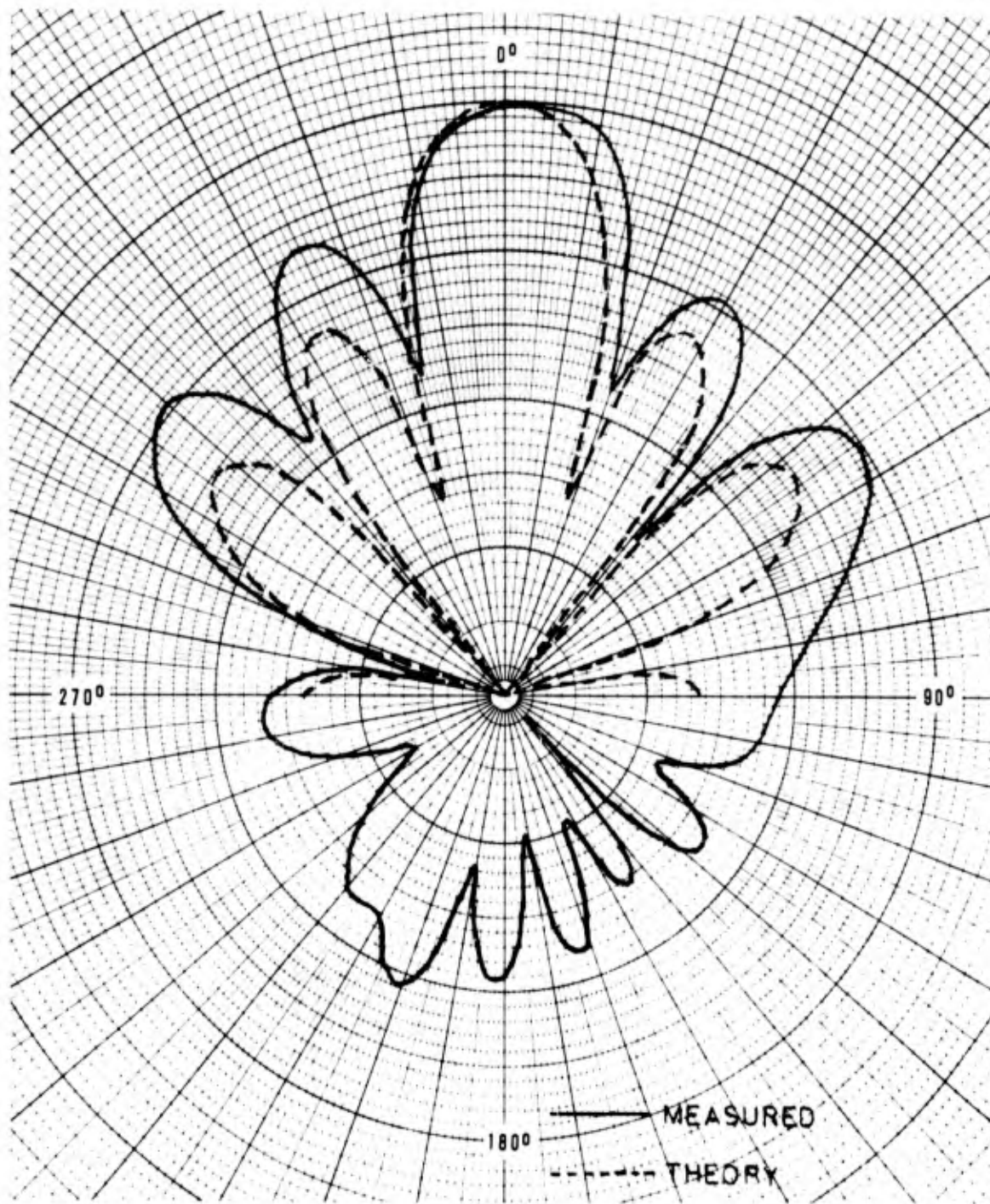


Figure 3-18. Zero-Degree Beam Pattern, Hydrophones 1 Through 6 at 2.5 kHz

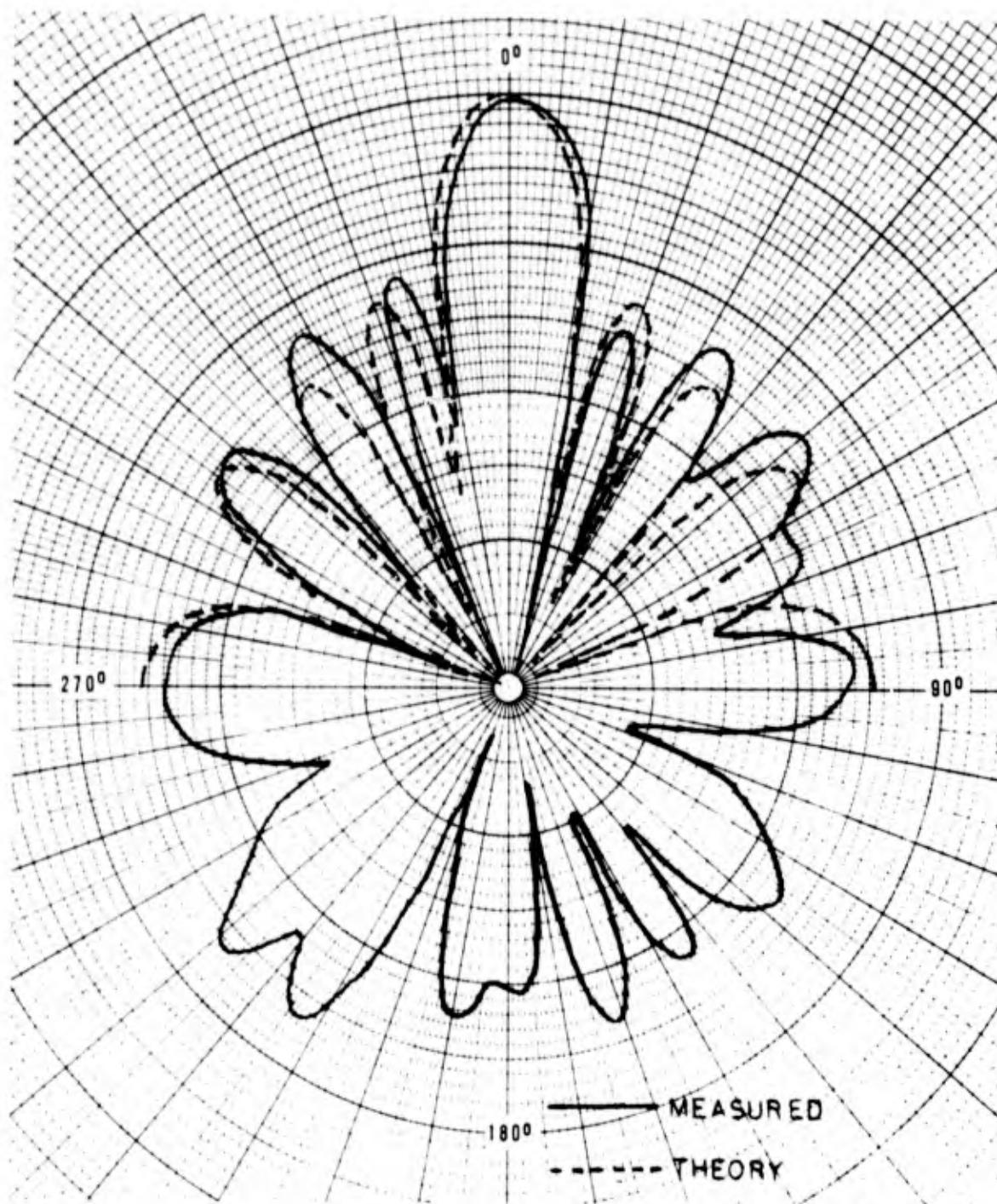


Figure 3-19. Zero-Degree Beam Pattern, Hydrophones 1 Through 6 at 3.5 kHz

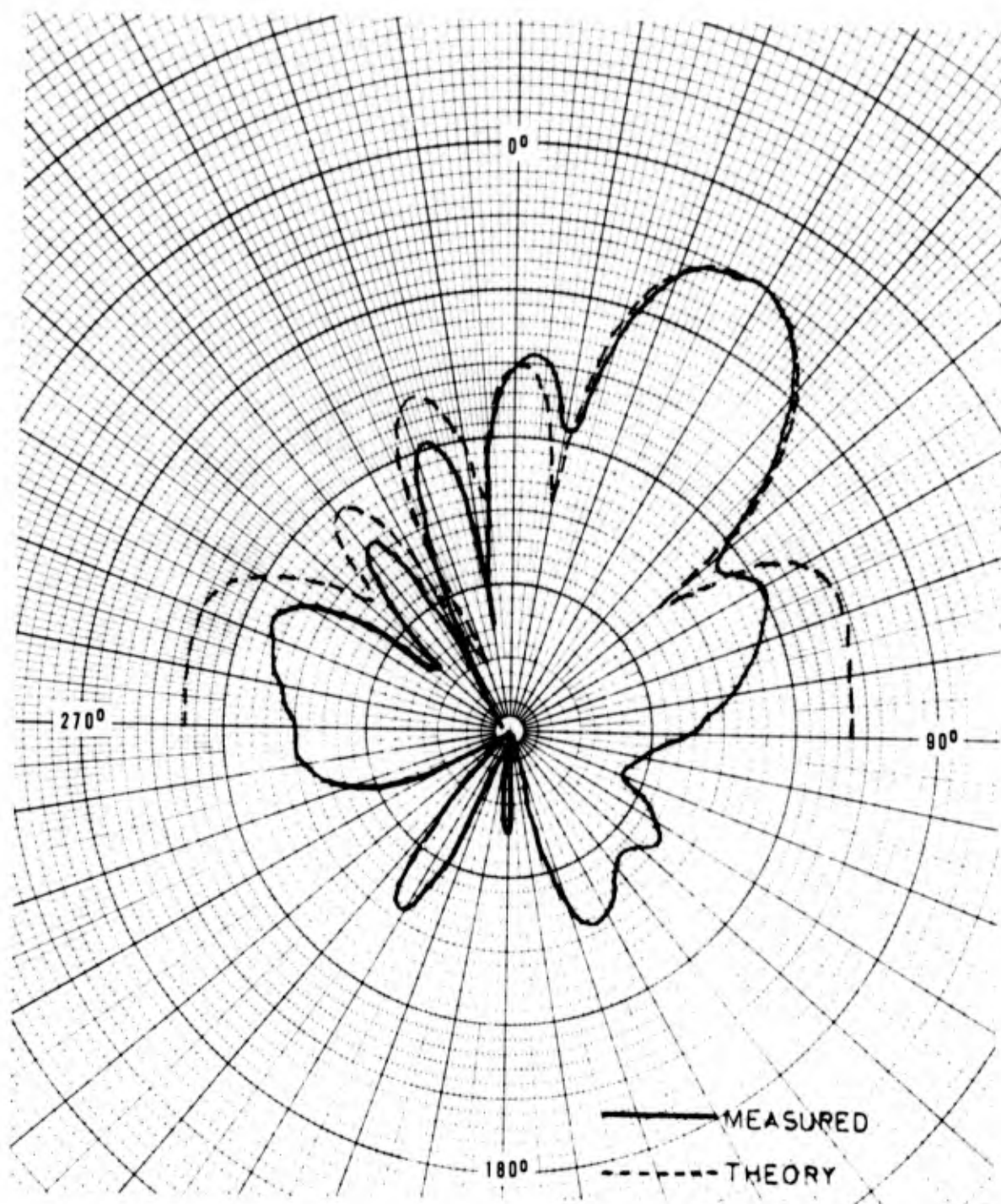


Figure 3-20. 30-Degree Beam Pattern, Hydrophones 1 Through 6 at 2.5 kHz  
With No Shading

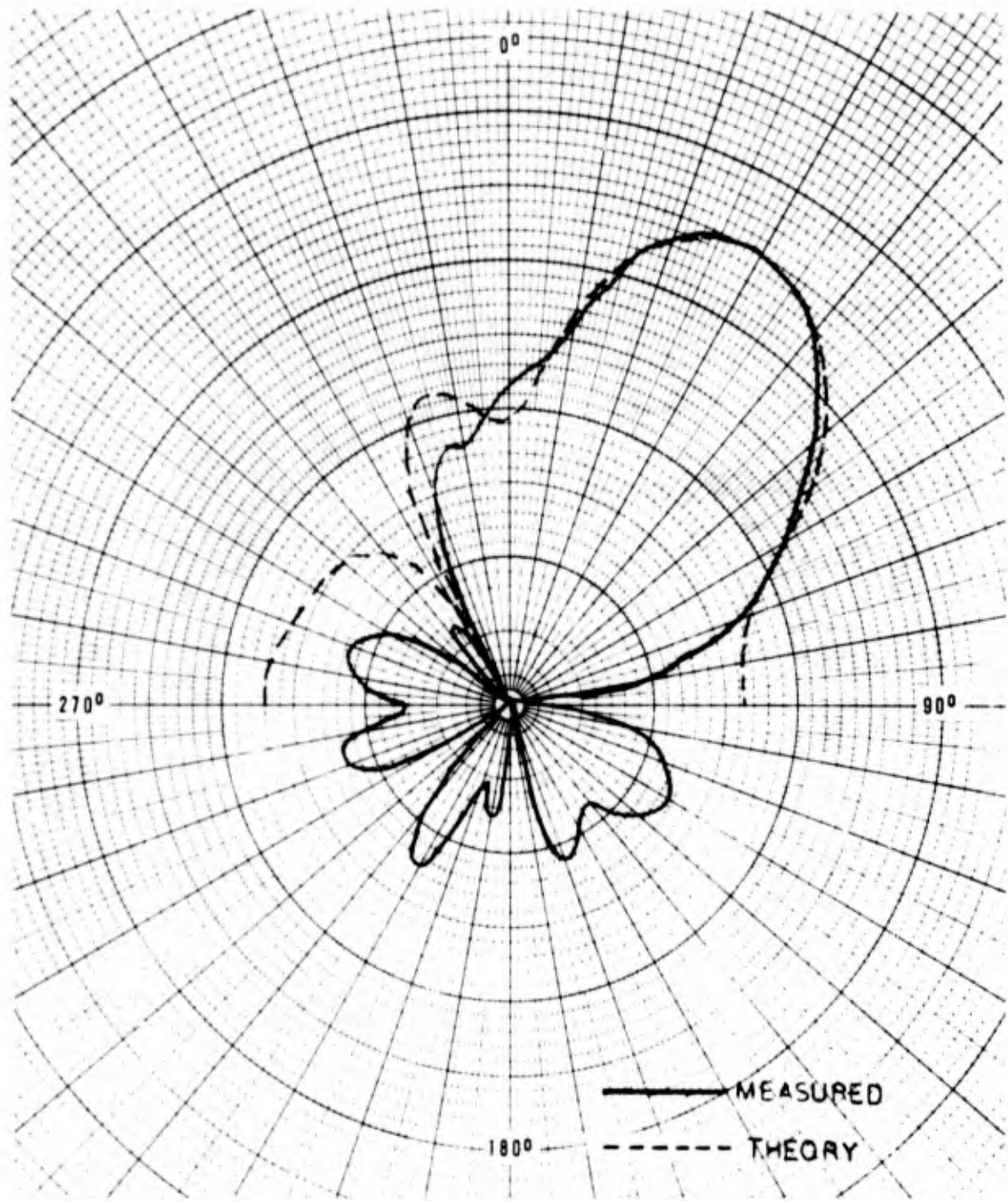


Figure 3-21. 30-Degree Beam Pattern, Hydrophones 1 Through 6 at 2.5 kHz with 20 dB Shading

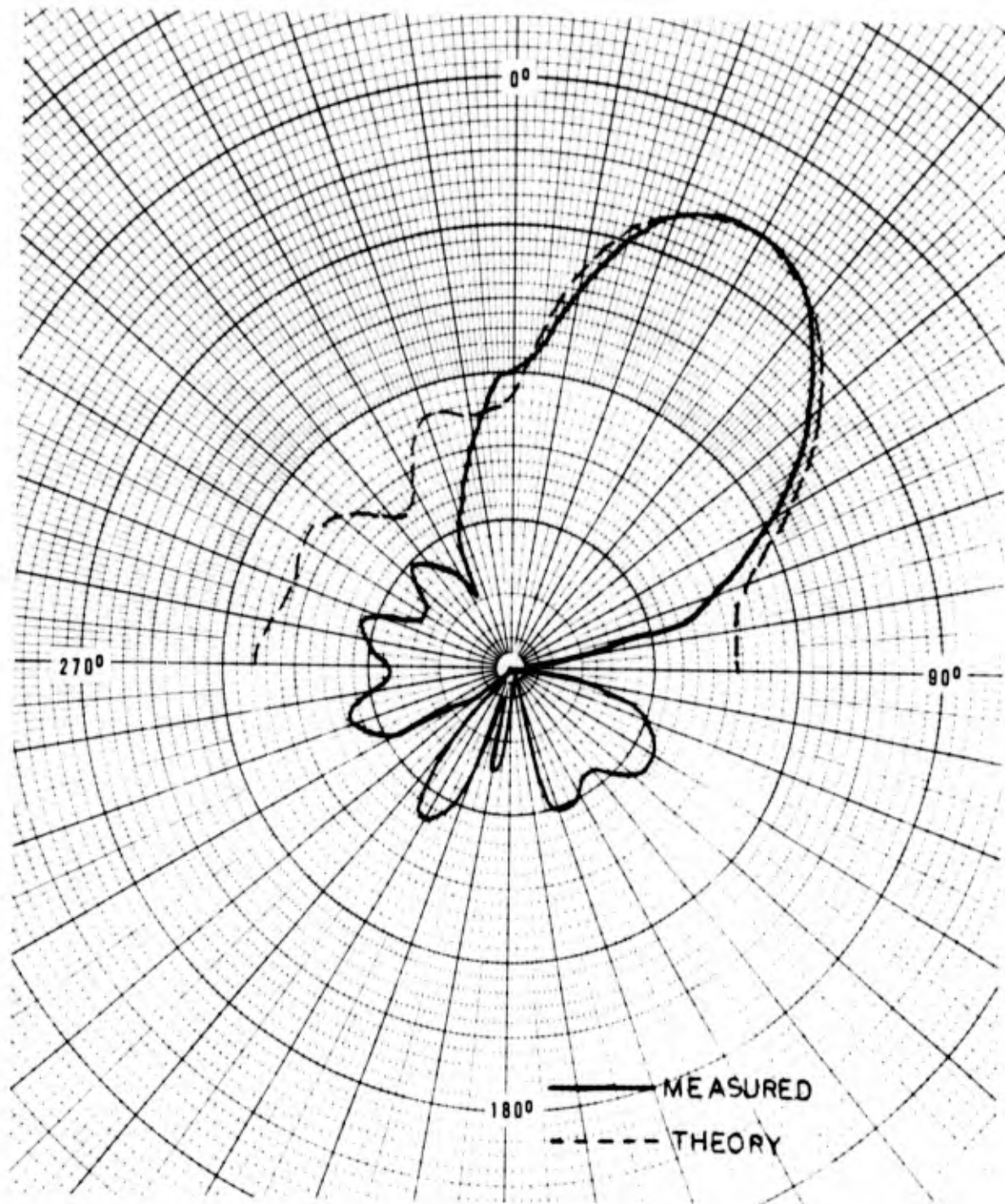


Figure 3-22. 30-Degree Beam Pattern, Hydrophones 1 Through 6 at 2.5 kHz with 30 dB Shading

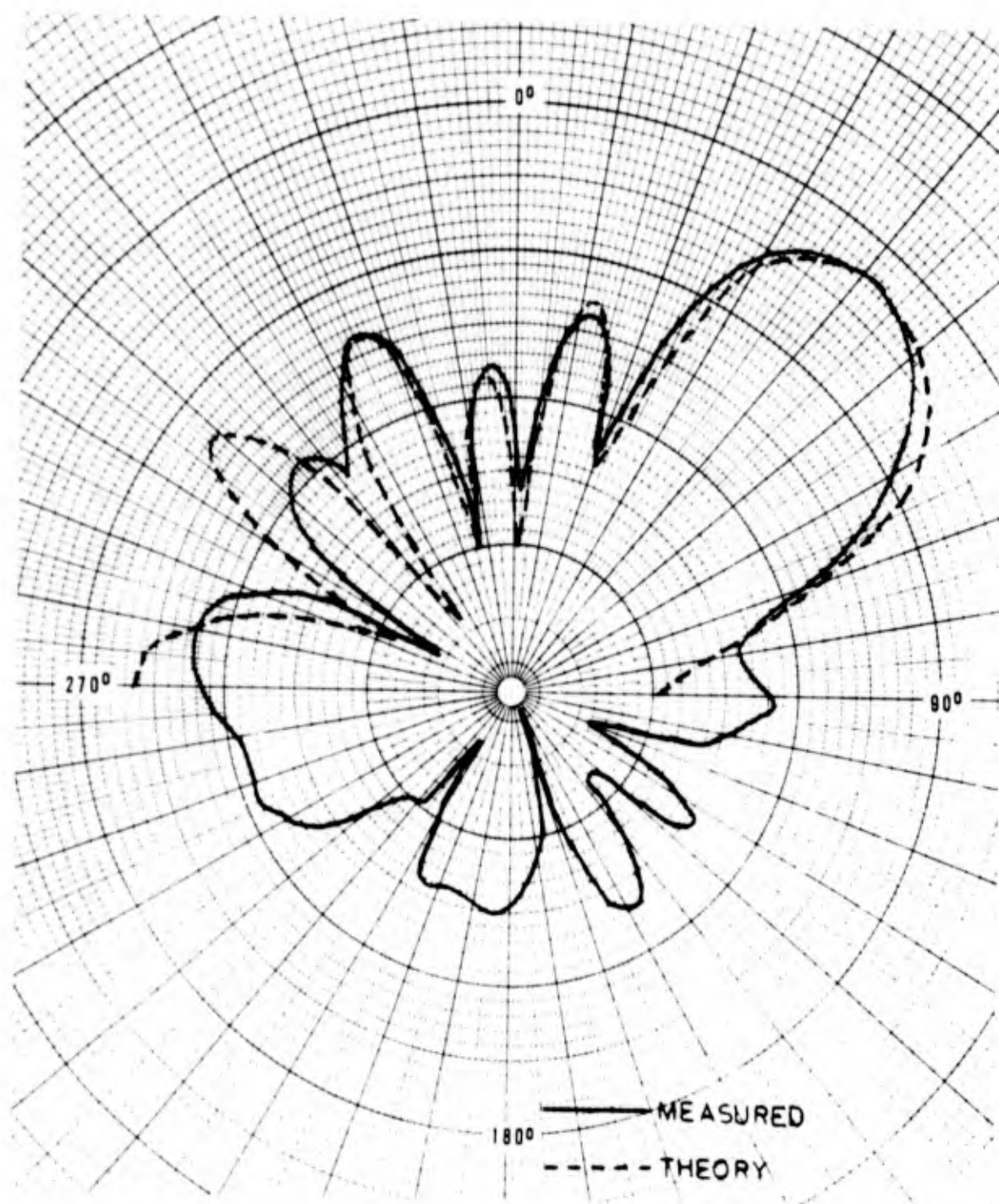


Figure 3-23. 45-Degree Beam Pattern, Hydrophones 1 Through 6 at 2.5 kHz  
With No Shading

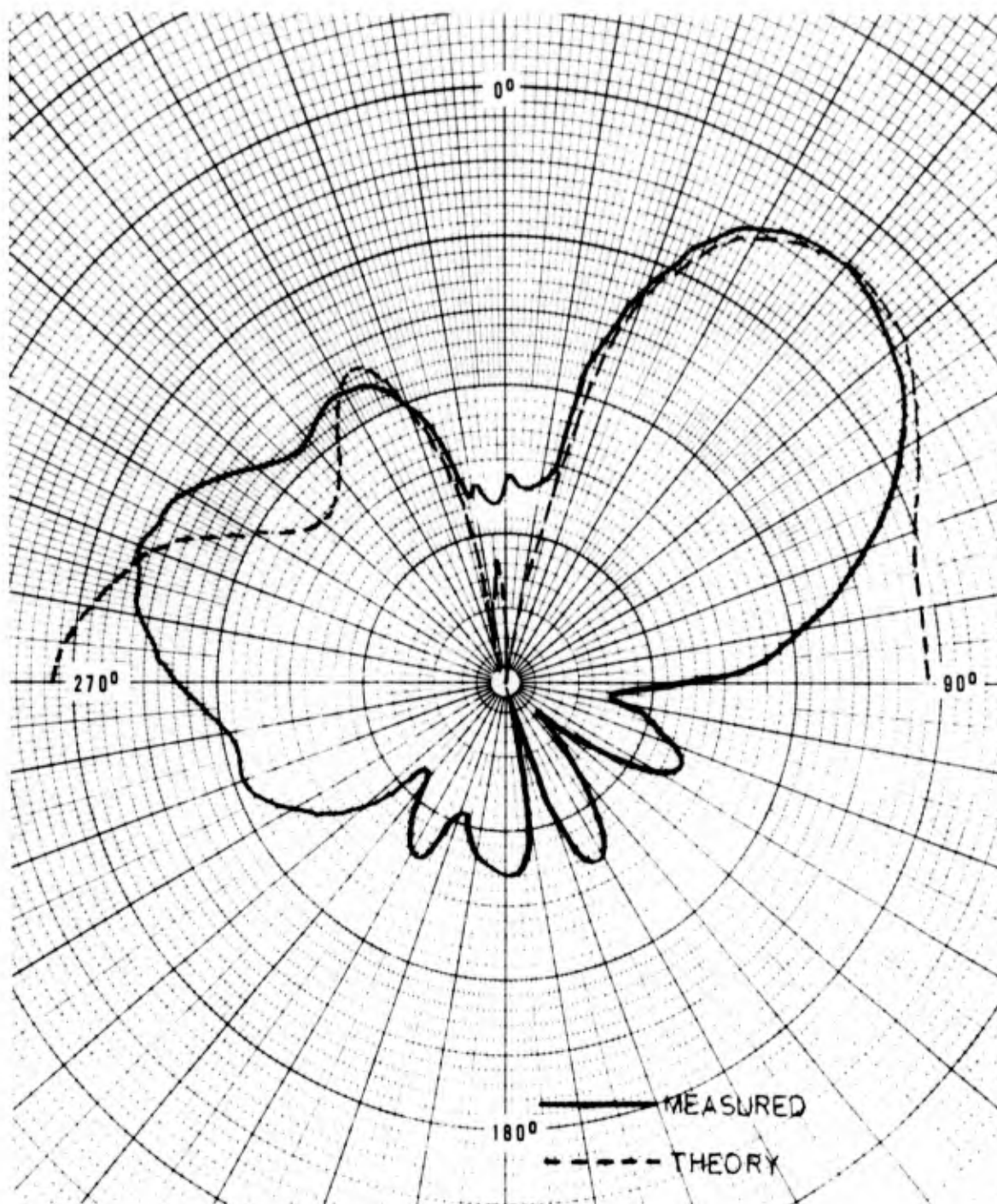


Figure 3-24. 45-Degree Beam Pattern, Hydrophones 1 Through 6 at 2.5 kHz with 20 dB Shading

## SECTION 4

### SONITE

#### 4.1 INTRODUCTION

Sonite is a highly porous, fiber-reinforced, ceramic material manufactured by the Johns-Manville Corporation. It was originally designed as a thermal insulation under the trade name MIN-K. According to the manufacturer, Sonite has been specifically formulated as a low acoustic impedance material over a wide pressure range for use in deep submergence applications.

During the manufacturing process, Sonite is compressed to yield initial densities ranging from 20 to 35 pcf. Under static pressure, such as would be encountered in an ocean environment, both the density of and speed of sound in Sonite increase. In order to give repeatable performance under pressure changes, the material must be prestressed through several cycles to the highest pressure it is expected to encounter. After being prestressed, Sonite exhibits elastic mechanical and acoustical properties up to the prestress limit. Its acoustic impedance increases linearly with pressure but remains low compared to water. Tests by Johns-Manville (reference 4) have shown that Sonite's major properties are unaffected by temperatures from 4 to 30 degrees Centigrade.

#### 4.2 THEORETICAL CONSIDERATIONS

The major component of Sonite is a microscopic particulate material. Small amounts of fiber and phenolic are added to stabilize its structure and increase handleability. Since the particulate material has an open cell structure, the cells tend to collapse under stress. However, if the Sonite is prestressed, the particles will not catastrophically collapse unless the prestress is exceeded. Up to this limit the individual particles undergo reversible deformation. As measured in reference 4, the properties of Sonite, under pressure cycling, become stable only after several cycles. This can be explained by realizing that during each stress cycle, the Sonite particles will rearrange themselves until an equilibrium position is reached. The reorientation process is believed to be exponential with a relaxation constant of two cycles.

Expressions for Sonite density and acoustic velocity as a function of prestress, initial density, and applied stress have been derived (reference 5) and are

$$\rho = \frac{\rho_0}{1 - \alpha \ln (P_m/P_{in}) - \frac{P}{B_{in} + \beta [\alpha \ln (P_m/P_{in})]^n}}$$

$$v = \left[ \frac{C_{in} + \gamma [\alpha \ln (P_m/P_{in})]^m + \delta P}{\rho} \right]^{1/2}$$

where

- $\rho$  = density
- $v$  = acoustic propagation velocity
- $\rho_0$  = initial density
- $P_m$  = prestress
- $P_{in}$  = initial stress supported by the sample
- $P$  = applied stress
- $B_{in}$  = initial compressive stiffness
- $B$  = compressive stiffness
- $C_{in}$  = initial stiffness
- $m, n$  = experimental parameters within the system related to detailed coupling mechanism
- $\alpha, \beta, \gamma, \delta$  = proportionality factors

It can be seen that the properties of Sonite can be changed to fit a particular requirement by applying the proper prestress,  $P_m$ .

The effects of the additional components used in the manufacture of Sonite are important. At low pressures, before Sonite has firmly compacted, the fiber and phenolic contribute to the material's mechanical behavior. At moderate pressures, because the load-bearing particles are much stronger, the effects become negligible. The phenolic also acts to increase the shear stiffness of Sonite by forming weak bonds between the microscopic particles locking them in place. Increasing shear stiffness, the dominant factor in Sonite, forces a corresponding increase in the sound velocity and thus raises the acoustic impedance. In general, anything that tends to bond the particles together will increase velocity; breaking the bonds will decrease velocity.

As a general guide to the use of Sonite, in order to avoid problems associated with its basic structure, it is recommended that the maximum applied stress be 20-percent less than the prestress and at least five cycles of prestress should be used to stabilize the material. To avoid contamination, which can form bonds between the particles and degrade Sonite's properties, the material must be carefully handled and encapsulated.

### 4.3 EXPERIMENTAL INVESTIGATION

Sonite is extremely porous and must be protected from direct contact with water. This fact complicates the problem of obtaining test data which reflects the acoustic properties of Sonite alone.

For the experiments conducted at the Sperry Sonar Test Facility, nine 12 x 12 x 1-inch panels were used. These panels were formed into one three-foot square structure by cementing thin (1/16 inch) aluminum panels to both sides and sealing the edges with cement. At the depths available for test purposes (12 feet) no problems with leaks were encountered.

The test configuration is shown in figure 4-1. Two series of runs were made, one with the reference hydrophone 1-5/8 inches from the baffle and the other at a distance of 3-1/4 inches. Frequency response data from 1 to 20 kHz were taken with the baffle and hydrophone located as shown in figure 4-1 and with the baffle and hydrophone rotated 180 degrees so that the baffle was between the hydrophone and projector. Horizontal patterns at various frequencies were also obtained with both hydrophone spacings.

Test results are shown in figures 4-2 through 4-4. Figures 4-2 and 4-3 are the frequency responses for hydrophone-to-baffle spacings of 1-5/8 inches and 3-1/4 inches, respectively. The responses at 180 degrees, compared to free field, are a measure of the baffle insertion loss. They indicate that 1 inch of Sonite can attenuate sound in the 1 to 20 kHz region by at least 10 dB. However, the relatively small size of the test baffle causes diffraction to limit the baffle performance. Figure 4-4 is a comparison between measured and predicted responses at a hydrophone spacing of 1-5/8 inches. Agreement is good over the 1 to 10 kHz frequency range. The predicted results, calculated by the Sperry multilayer baffled-hydrophone response computer program, include the effect of the two 1/16-inch aluminum panels cemented to the Sonite. However, another calculation, with a baffle composed of only Sonite, showed that this effect is negligible due to the small thickness of the aluminum. The acoustic impedance of Sonite (20 pcf) used in the calculations was 0.132 that of water. This is slightly lower than the more recent value of 0.145 (after 10 cycles of 0-1000 psi) reported by Johns-Manville in reference 4. However, the Sonite used in the tests had not been pressure cycled but had just been pressed to yield a density of 20 pcf.

Test results on Sonite to date are limited in scope but indicate its usefulness as a baffle material. Its light weight, coupled with an apparent ability to maintain a low acoustic impedance under high static pressures, makes it a good candidate for future investigation and experimentation.

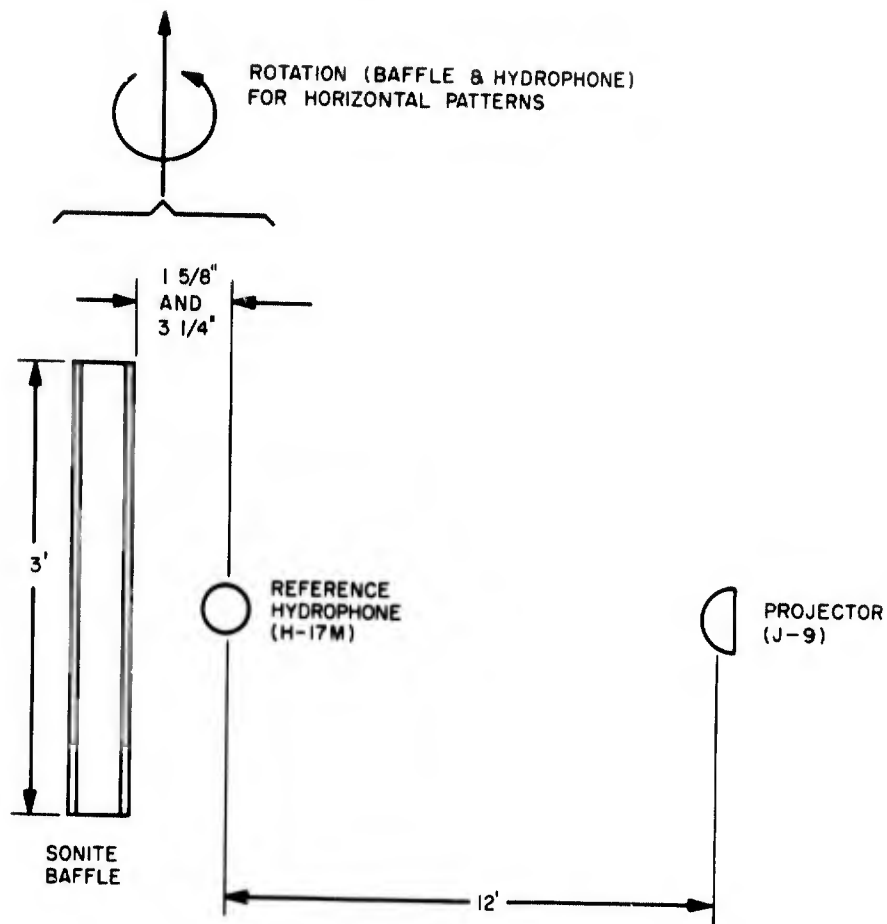


Figure 4-1. Sonite Test Configuration

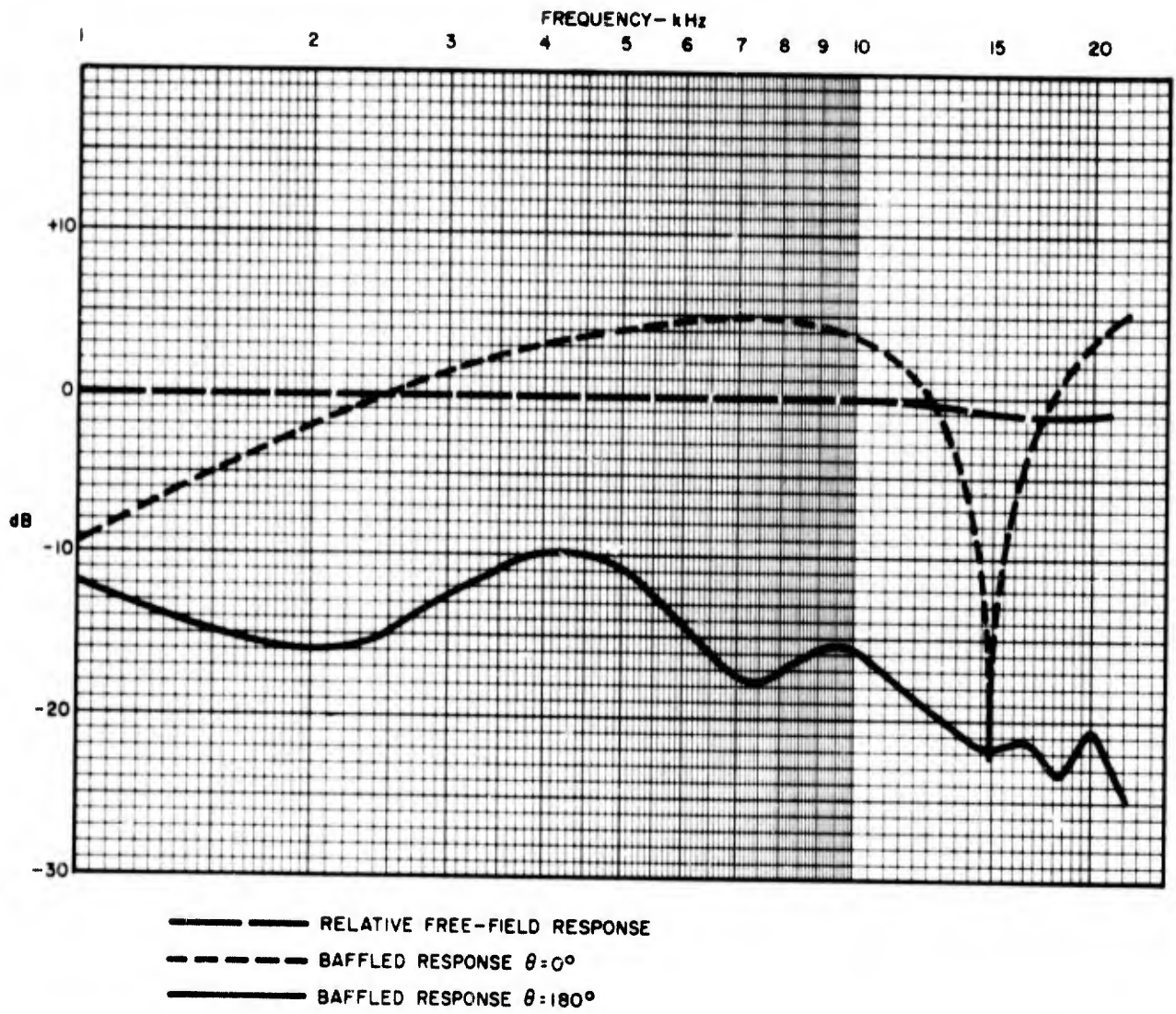


Figure 4-2. Relative Hydrophone Response In Presence of Sonite Baffle, Spacing 1-5/8 Inches

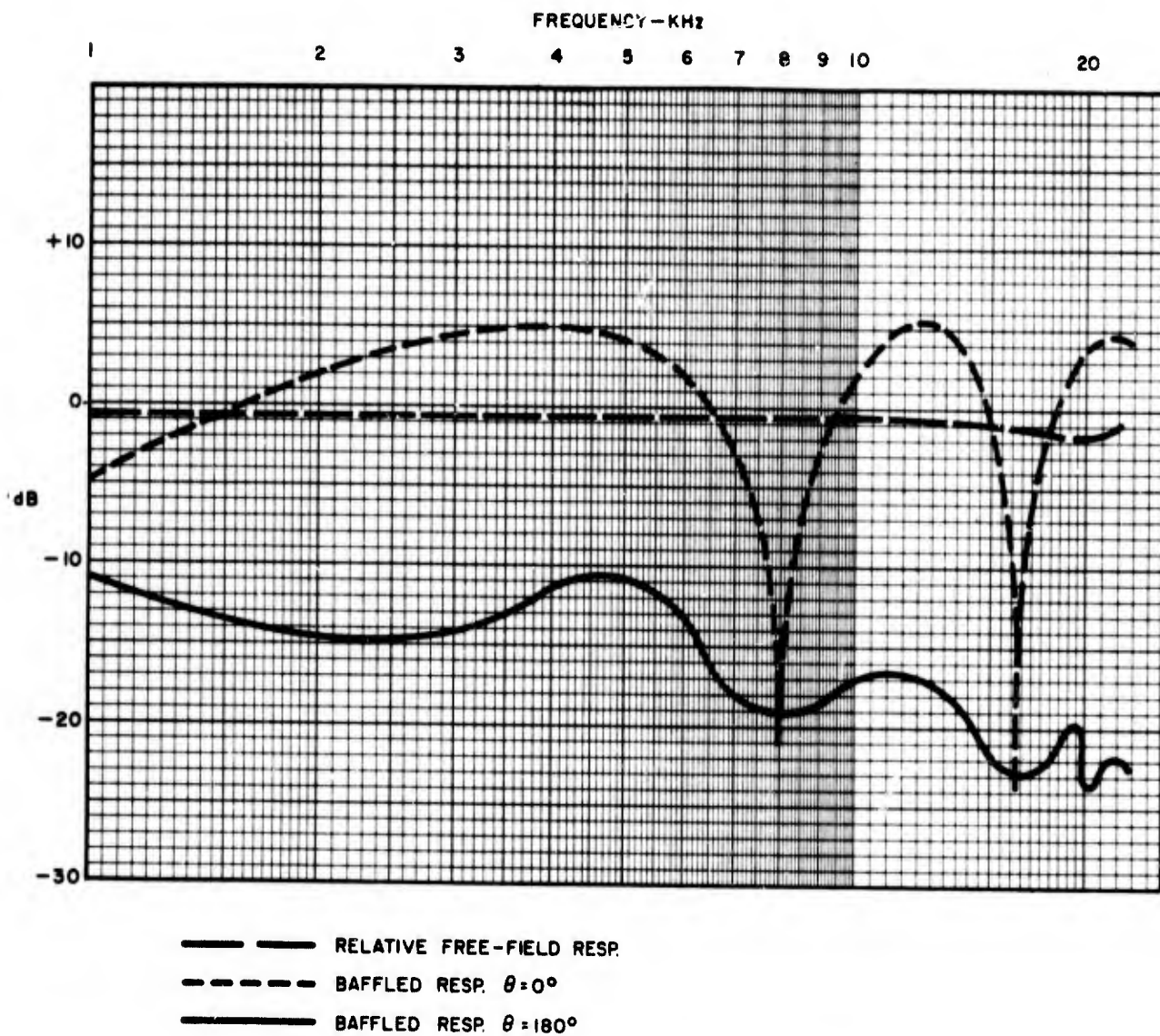


Figure 4-3. Relative Hydrophone Response In Presence of Sonite Baffle, Spacing 3-1/4 Inches

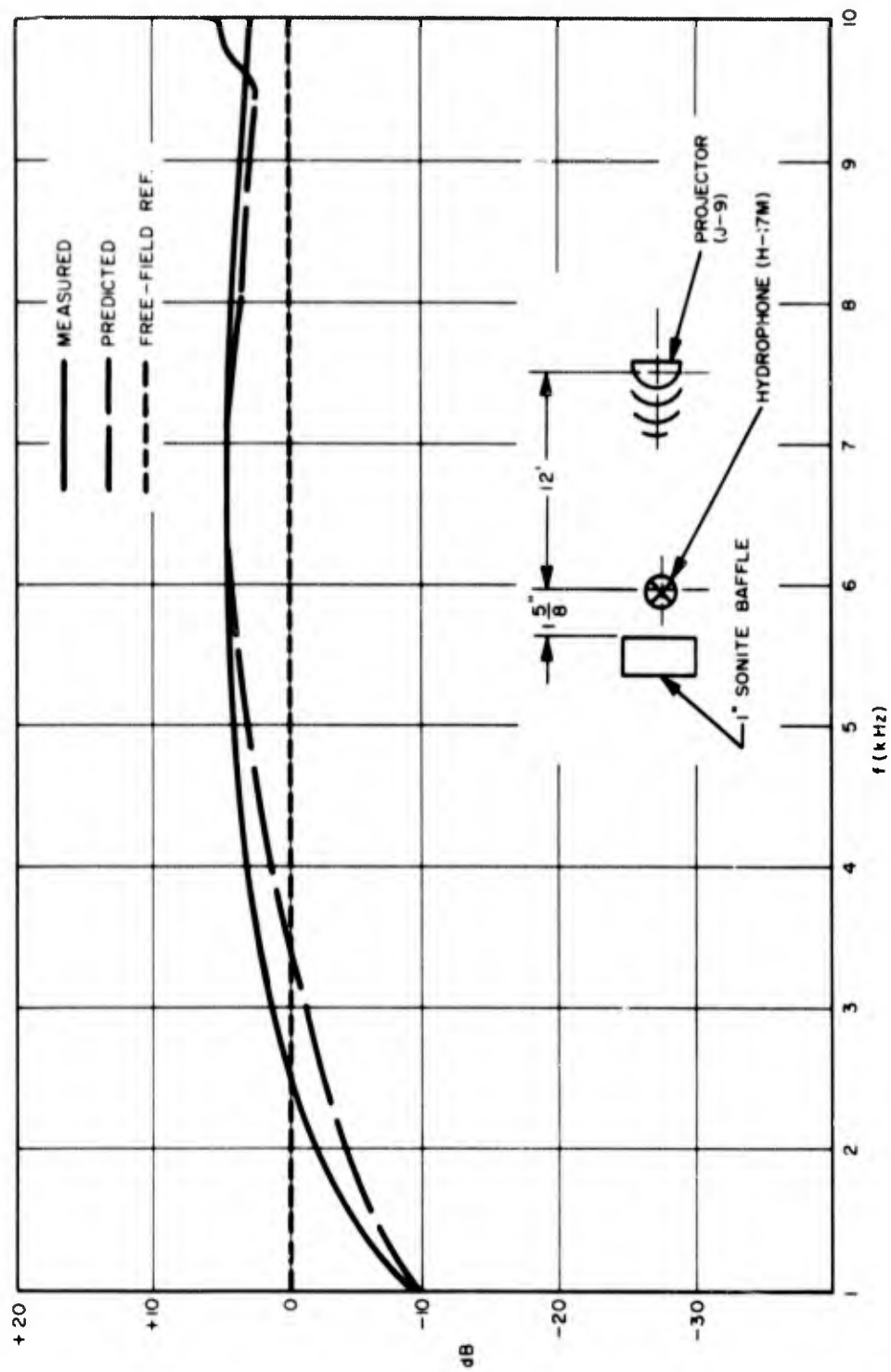


Figure 4-4. Comparative Response of Sonite Baffle

## SECTION 5

### SUMMARY

The following is a summary of the results of the investigations made during the period covered in this report.

- A baffle composed of an infinitely long cylinder, with walls made of layers of various materials, has been analyzed. Results of the analysis have been utilized in a computer program which calculates the response of a hydrophone placed anywhere outside the baffle. Limited comparisons between experimental and predicted data have shown extremely good agreement, although more work remains to be done.
- Studies were made to determine if a uncompensated spring-mass type of baffle could be designed to meet underwater noise reduction requirements. Lumped parameter models were used to calculate the performance of various configurations. Results of tests performed on a spring-mass baffle show that the lumped parameter models developed in this study are valid for predicting the performance when the effective thickness is small compared to one wavelength. Excellent agreement between predicted and measured data was obtained at the low frequencies. The tests further showed that good performance can be obtained with these spring-mass baffles over a wide range of frequencies and hydrostatic pressures.
- Sonite, a fiber-reinforced, ceramic material manufactured by the Johns-Manville Corporation, has been experimentally studied to learn about its performance as a low-impedance baffle element. Tests performed at the Sperry Sonar Test Facility on a Sonite panel, together with laboratory data concerning its behavior under pressure, indicate that this material shows promise for deep submergence noise reduction applications. Further experiments, especially at high hydrostatic pressures and using large baffle sizes, are need to fully characterize its performance.

## SECTION 6

### REFERENCES

1. Underwater Acoustic Noise Reduction Program-Interim Report, Sperry Gyroscope Division, SGD-4232-0014, April 1968.
2. Underwater Noise Reduction Study-Interim Report Phase II, Sperry Gyroscope Division, SGD-4232-0225, April 1969.
3. Philip M. Morse and Herman Feshbach, Methods of Theoretical Physics, McGraw-Hill
4. Physical Properties of Sonite-Final Report, Arnold E. Jabin, Report No. 3901-26, April 27, 1970, Johns-Manville Research and Engineering Center, Manville, New Jersey.
5. A Physical Model of Sonite Pressure-Release Material, Carl R. Johansen, NUC TN 387, Naval Undersea Research and Development Center, June 1970.